

**UCGE Reports  
Number 20175**

Department of Geomatics Engineering

**Development of a Low-cost GPS-based Attitude  
Determination System**

(URL: <http://www.geomatics.ucalgary.ca/links/GradTheses.html>)

**by**

**Chaochao Wang**

**June 2003**



THE UNIVERSITY OF CALGARY

DEVELOPMENT OF A LOW-COST GPS-BASED ATTITUDE DETERMINATION  
SYSTEM

by

Chaochao Wang

A THESIS

SUBMITTED TO THE FACULTY OF GRADUATE STUDIES  
IN PARTIAL FULFILMENT OF THE REQUIREMENTS FOR THE  
DEGREE OF MASTER OF SCIENCE

DEPARTMENT OF GEOMATICS ENGINEERING

CALGARY, ALBERTA

JUNE, 2003

© Chaochao Wang 2003

## **ABSTRACT**

This thesis describes an extensive investigation into the development of a low-cost solution for GPS-based attitude determination. Traditionally, high-performance GPS sensors have been used in multi-antenna attitude determination systems in order to achieve performance competitive with an Inertial Navigation System (INS). However, the high cost of hardware limits the wide usage of this system in general navigation applications. In this research, the employment of low-cost GPS and Dead Reckoning sensors are explored for attitude determination. The factors that affect the accuracy of attitude estimation are examined by using different GPS receivers and antennas along with a GSS simulator. The performance of a low-cost GPS attitude system using CMC Allstar receivers is investigated. Some reliability improvement strategies, namely high data rate measurements, angular constraints and a quality control algorithm in attitude estimation are implemented to enhance the overall performance of low-cost attitude determination. In order to overcome the limitations of the Allstar GPS-alone attitude system, three low-cost vibrating rate gyros have further been employed to build up a GPS/gyro integrated system. The integration methodology and the algorithm are explained at length. The advantages of integrating low-cost rate gyros are discussed in regard to accuracy, availability and reliability. A series of field tests were conducted to assess the performance of this low-cost integrated attitude system.

## ACKNOWLEDGEMENT

First of all, I would like to express my deepest appreciation to my supervisor, Dr. Gérard Lachapelle, for his continuous guidance and encouragement and for arranging for financial support. Without his help both in academics and finance, this thesis work is not possible for me.

I also wish to thank the members of my exam committee, Dr. Yang Gao, Dr. Susan Skone and Dr. Swavik Spiewak for their time and effort in reading my thesis and providing feedback. The help from Dr. Naser El-Sheimy during my graduate study is also highly appreciated.

Many thanks go to the graduate students in PLAN group, Glenn MacGougan, Oleg Mezentsev, Junjie Liu and Yan Lu, for their contributions in this research work. Helps from Mark Petovello is especially acknowledged for proof-reading my thesis and taking a lot of time for valuable discussions.

I would also thank many friends throughout my graduate study: Changlin Ma, Lei Dong, Xiaohong Zhang, Victoria Hoyle, Zhizhao Liu, Roland Rickborn, Kongzhe Chen, Wentao Zhang, Lichun Wei, Li Sheng, who make my life meaningful and enjoyable in Calgary.

Last but not least, I would like to thank my big family: my parents, grandma, three sisters and especially my wife, Na. Without your continuous support, encouragement and love for all these years, I can not complete this thesis work in Canada.

## TABLE OF CONTENTS

<b>ABSTRACT .....</b>	<b>iii</b>
<b>ACKNOWLEDGEMENT .....</b>	<b>iv</b>
<b>TABLE OF CONTENTS.....</b>	<b>v</b>
<b>LIST OF TABLES .....</b>	<b>viii</b>
<b>LIST OF FIGURES .....</b>	<b>ix</b>
<b>NOTATIONS.....</b>	<b>xii</b>
<b>CHAPTER 1</b>	
<b>INTRODUCTION.....</b>	<b>1</b>
1.1 BACKGROUND .....	1
1.2 OBJECTIVES.....	5
1.3 THESIS OUTLINE.....	6
<b>CHAPTER 2</b>	
<b>GPS ATTITUDE DETERMINATION.....</b>	<b>9</b>
2.1 COORDINATE FRAMES .....	9
2.1.1 Earth-fixed frame .....	9
2.1.2 Local level frame.....	11
2.1.3 Body Frame.....	12
2.1.4 Coordinates transformation from WGS-84 to local level frame.....	13
2.2 ATTITUDE PARAMETERIZATION.....	14
2.2.1 Euler Angles.....	15
2.2.2 Quaternion.....	16
2.3 BASICS OF GPS ATTITUDE DETERMINATION.....	19
2.3.1 GPS observables.....	19
2.3.2 Attitude determination using GPS.....	24
2.3.3 Ambiguity resolution.....	26
2.3.4 Cycle slip detection .....	29
2.4 HEADRT+™ ALGORITHM.....	31

<b>CHAPTER 3</b>	
<b>PERFORMANCE OF GPS ATTITUDE DETERMINATION.....</b>	<b>35</b>
3.1 MEASUREMENT ERRORS .....	35
3.1.1 Multipath .....	35
3.1.2 Antenna phase centre variation .....	43
3.1.3 Receiver Noise .....	45
3.2 OPERATIONAL FACTORS .....	47
3.2.1 Impact of satellite number and geometry.....	47
3.2.2 Antenna array configuration.....	50
<b>CHAPTER 4</b>	
<b>ATTITUDE DETERMINATION USING LOW-COST RECEIVERS.....</b>	<b>53</b>
4.1 INTRODUCTION OF CMC ALLSTAR RECEIVER .....	53
4.2 PERFORMANCE OF ATTITUDE ESTIMATION IN THE PRESENCE OF NOISE .....	55
4.3 GPS ANTENNAS.....	60
4.4 CARRIER PHASE DATA SYNCHRONIZATION .....	68
<b>CHAPTER 5</b>	
<b>RELIABILILTY IMPROVEMENT USING LOWCOST RECEIVERS.....</b>	<b>75</b>
5.1 RELIABILITY PROBLEM USING LOW-COST GPS SENSORS .....	75
5.2 AMBIGUITY RESOLUTION.....	76
5.2.1 High data rate .....	77
5.2.2 Fixed angular constraint scheme .....	79
5.4 KALMAN FILTER ESTIMATION.....	84
5.4.1 Attitude Estimation using Kalman filtering .....	84
5.4.2 Quality control.....	86
5.4.3 Kinematic Simulation Test.....	89
5.4.4 Field kinematic test .....	92
<b>CHAPTER 6</b>	
<b>DEVELOPMENT OF A LOW-COST GPS/GYRO ATTITUDE SYSTEM.....</b>	<b>102</b>
6.1 ADVANTAGES OF GPS/GYRO INTEGRATION .....	102
6.2 METHODOLOGY.....	104
6.3 RATE GYRO .....	105
6.4 SYSTEM DESIGN.....	109
6.5 FILTERING ALGORITHM .....	111
6.6 GYRO AIDING AMBIGUITY RESOLUTION.....	114

6.7 STATIC TEST .....	118
6.7.1 Test description .....	118
6.7.2 Static test results.....	120
6.8 KINEMATIC TEST .....	129
6.8.1 Kinematic test description.....	129
6.8.2 Determination of misalignment angle .....	131
6.8.3 Test results.....	133
<b>CHAPTER 7</b>	
<b>CONCLUSIONS AND RECOMMENDATIONS.....</b>	<b>142</b>
<b>REFERENCES.....</b>	<b>149</b>
<b>APPENDIX A:</b>	
<b>DOUBLE DIFFERENCE RESIDUALS OF SELECTED SATELLITE PAIRS .....</b>	<b>161</b>

## LIST OF TABLES

Table 2.1: Primary parameters of WGS-84.....	10
Table 3.1: Attitude estimation accuracy versus satellite number and geometry .....	50
Table 4.1: CMC Allstar Specifications .....	54
Table 4.2: Statistics of attitude estimates in static dual antenna simulation test.....	57
Table 4.3: Statistics of attitude estimates in kinematic dual-antenna simulation test.....	58
Table 4.4: Statistics of double difference residuals (PRN 24 -- PRN 4).....	71
Table 4.5: Statistics of attitude estimates using time-offset data .....	73
Table 5.1: Performance of ambiguity resolution using different data rate measurements.....	79
Table 5.2: RMS-Kalman filter versus least-squares (Unit: arc minutes) .....	91
Table 5.3 :Residual RMS (mm) for Beeline <sup>TM</sup> and CMC receivers .....	95
Table 6.1: Specifications of Murata ENV-05D-52 Gyroscope .....	108
Table 6.2: GPS attitude estimate statistics –Static test (Unit: degrees) .....	121
Table 6.3: Attitude rate estimate statistics using GPS only (Unit: deg/s).....	122
Table 6.4: Integrated system attitude estimate statistics in static test (Unit: degrees) .....	123
Table 6.5: Integrated system attitude rate estimate statistics (Unit: deg/s).....	124
Table 6.6: GPS outages during static test in GPS time (Unit: second) .....	128
Table 6.7: Attitude estimation error statistics - Kinematic test using Beeline <sup>TM</sup> units .....	135
Table 6.8: Integrated attitude estimation error statistics of kinematic test using Allstar units .....	140
Table A.1: Statistics of double difference residuals (PRN 24-- PRN 5).....	161
Table A.2: Statistics of double difference residuals (PRN 24-- PRN 6).....	162
Table A.3: Statistics of double difference residuals (PRN 24-- PRN 10).....	163
Table A.4: Statistics of double difference residuals (PRN 24-- PRN 30).....	164

## LIST OF FIGURES

Figure 2.1: Earth-fixed frame.....	10
Figure 2.2: Local level frame .....	11
Figure 2.3: Body frame .....	13
Figure 2.4: Ambiguity Resolution in HeadRT+™ .....	33
Figure 3.1: Attitude results in day-to-day test.....	41
Figure 3.2: Attitude parameters using 7 satellites .....	50
Figure 3.3: Attitude parameters using 6 satellites .....	50
Figure 3.4: Attitude parameters using 5 satellites .....	50
Figure 3.5: Attitude parameters using 4 satellites .....	50
Figure 3.6: Attitude estimation accuracy V.S. inter-antenna distance for medium performance receiver .....	51
Figure 4.1: System setup in dual-antenna hardware simulation test.....	57
Figure 4.2: Attitude estimates in static dual-antenna simulation test.....	57
Figure 4.3: Attitude estimation errors in kinematic dual-antenna simulation test .....	59
Figure 4.4: SNR V.S. Elevation .....	62
Figure 4.5: Attitude estimation using different antennas .....	64
Figure 4.6: RMS values of double difference residuals .....	65
Figure 4.7: Attitude estimates and satellite number using NovAtel 600 .....	67
Figure 4.8: Attitude estimates and satellite number using NovAtel 501 .....	67
Figure 4.9: Attitude estimates and satellite number using AT575-104.....	67
Figure 4.10: Double difference combination .....	70
Figure 4.11: Double difference residuals for PRN 24 -- PRN 4 .....	71
Figure 4.12: Attitude estimates using time-offset data .....	72
Figure 5.1: Time to fix ambiguity in hardware simulation .....	78
Figure 5.2: Time to fix ambiguity in field test.....	79
Figure 5.3: DOPs and SV number during simulation test.....	82
Figure 5.4: Effects of an incorrect ambiguity on an inter-antenna vector estimate .....	82
Figure 5.5: Effects of an incorrect ambiguity on attitude component estimates.....	83
Figure 5.6: Attitude results after implementing angular constraints in static simulation test.....	84
Figure 5.7: Type I/II Errors .....	89
Figure 5.8: Antenna configuration .....	90
Figure 5.9: True attitude parameters in hardware simulation test.....	90

Figure 5.10: Attitude estimation errors using different estimation methods.....	91
Figure 5.11: Cycle slip detection using Kalman filter .....	92
Figure 5.12: Test vehicle.....	92
Figure 5.13: DOPs and SV numbers during vehicle test.....	93
Figure 5.14: Residual RMS in vector solution using Beeline™ receivers.....	94
Figure 5.15: Residual RMS in vector solutions using Allstar receiver.....	94
Figure 5.16: Heading estimate using the Beeline™ system.....	96
Figure 5.17: Pitch estimate using the Beeline™ system.....	97
Figure 5.18: Roll estimate using the Beeline™ system .....	97
Figure 5.19: Heading estimate using the CMC system.....	98
Figure 5.20: Pitch estimate using the CMC system .....	99
Figure 5.21: Roll estimate using the CMC system.....	99
Figure 5.22: External reliability of the Beeline™ units .....	100
Figure 5.23: External reliability from the CMC units.....	101
Figure 6.1: Attitude estimation in the integrated system .....	105
Figure 6.2: Metallic triangular prism vibrator (Murata 2000) .....	107
Figure 6.3: Difference of the left and right detection signals (Nakamura 1990) .....	107
Figure 6.4: System design of low-cost GPS/gyro integrated system .....	110
Figure 6.5: Time tag of gyro data.....	111
Figure 6.6: Cubic search region method .....	117
Figure 6.7: Time to fix ambiguity using different search regions using 10 Hz data.....	118
Figure 6.8: Antenna configuration in static test .....	119
Figure 6.9: GPS/gyro attitude platform.....	119
Figure 6.10: Satellite number and DOPs in static test.....	120
Figure 6.11: GPS attitude estimates in static test .....	121
Figure 6.12: GPS attitude rate estimates in static test .....	122
Figure 6.13: Integrated system attitude estimates in static test.....	123
Figure 6.14: Integrated system attitude rate estimates in static test .....	124
Figure 6.15: Gyro bias estimation .....	125
Figure 6.16: External reliability in static test .....	127
Figure 6.17: Attitude estimates with GPS outages.....	128
Figure 6.18: Attitude differences .....	129
Figure 6.19: Antenna setup in kinematic test.....	130
Figure 6.20: Hardware layout in the vehicle .....	130
Figure 6.21: Trajectory of the kinematic test .....	131
Figure 6.22: Attitude reference in kinematic test.....	133
Figure 6.23: Integrated system attitude estimates -Kinematic test using Beeline™ units....	134

Figure 6.24: Attitude estimation errors –Kinematic test dusing Beeline™ units .....	135
Figure 6.25: Gyro bias estimation--Kinematic test using Beeline™ units .....	136
Figure 6.26: Integrated system attitude estimates - Kinematic test using Allstar units .....	139
Figure 6.27: Attitude errors using the integrated Allstar based attitude system .....	140
Figure 6.28: Gyro bias estimation from Allstar based integration system in kinematic test	141
Figure A.1: Double difference residuals for PRN2--PRN5 .....	161
Figure A.2: Double difference residuals for PRN2--PRN6 .....	162
Figure A.3: Double difference residuals for PRN24--PRN10 .....	163
Figure A.4: Double difference residuals for PRN24--PRN30 .....	164

## NOTATIONS

### i) Symbols

$\Delta$  single difference

$\nabla\Delta$  double difference

$\Delta E$  antenna vector component in East direction

$\Delta N$  antenna vector component in North direction

$\Delta V$  antenna vector component in Vertical direction

$B_n$  carrier loop noise bandwidth

$d_{ion}$  ionospheric delay

$d_{trop}$  tropospheric delay

$\delta\omega$  gyro bias

$\sigma_{PLL}$  standard deviation of PLL tracking error

$\sigma_t$  one sigma error in carrier phase due to thermal noise

$\sigma_v$  one sigma error in carrier phase due to vibration

$dT$  receiver clock error

$F_{Coriolis}$  Coriolis force

$L$  inter-antenna distance

$m$  quality

$N$  carrier integer cycle

$\Omega$  angular velocity

$p$	pseudorange measurement
$\mathbf{q}$	quaternion
$\mathbf{r}$	antenna vector
$\mathbf{R}$	rotation matrix
$s$	scale factor
$T$	integration time
$v$	linear velocity
$\Phi$	carrier phase measurement
$\dot{\Phi}$	phase velocity (Doppler)
$\rho$	satellite-receiver range
$d\rho$	satellite orbital error
$\lambda$	carrier wavelength
$\omega$	rate gyro measurement
$\psi$	yaw
$\theta$	pitch
$\phi$	roll
$\dot{\psi}$	angular rate in yaw
$\dot{\theta}$	angular rate in pitch
$\dot{\phi}$	angular rate in roll
$x_b$	x coordinate in body frame
$y_b$	y coordinate in body frame

$z_b$  z coordinate in body frame  
 $x_{ll}$  x coordinate in local level frame  
 $y_{ll}$  y coordinate in local level frame  
 $z_{ll}$  z coordinate in local level frame

**ii) Abbreviations**

ADOP Attitude Dilution of Precision  
AZ-DOP Azimuth Dilution of Precision  
C/A Course Acquisition  
DD Double Difference  
DLL Delay Lock Loop  
DOP Dilution of Precision  
EL-DOP Elevation Dilution of Precision  
GPS Global Positioning System  
MTTFA Minimum Time to Fix Ambiguity  
PLL Phase Lock Loop  
PPS Pulse per Second  
PRN Pseudorandom noise  
RMS Root Mean Square  
STD Standard Deviation  
SV Satellite Number  
WGS84 World Geodetic System of 1984

## **CHAPTER 1**

### **INTRODUCTION**

#### **1.1 Background**

Over the past twenty years, with the advance of satellite navigation technology, the Global Positioning System (GPS) has become widely used as an accurate sensor in many navigation and location systems. In some of these applications, not only the absolute positioning information, such as position and velocity, but also the attitude of mobile platforms is of interest to users. Traditionally, a guidance system is made up of different types of sensors: GPS sensors are used to provide position, velocity and time information, while the orientation of the platform is obtained from inertial navigation equipment. The inertial sensors can provide the high data rate attitude information with reasonable short-term stability. However, the high cost of INS, together with its long-term drift, restrains the employment of this sensor for attitude determination.

Although GPS was originally designed as a positioning and timing system, its usage in attitude determination for ship, aircraft and spacecraft has been heavily discussed in the past ten years (Cohen 1992, Lu 1994). This innovative technique is based on light-of-sight GPS interferometric observations to precisely estimate inter-antenna vectors in a specific navigation frame. The rotation of the antenna vectors from the body frame to the navigation frame is expressed as a rotation matrix parameterized by three Euler attitude angles. With

multiple closely-spaced GPS antennas, the GPS attitude system can precisely estimate the 3D attitude parameters of mobile platforms without error drift over time.

Although code measurements can be used in coarse attitude determination (Pruszyński et al 2001), the carrier phase measurements are preferable in estimating attitude parameters because of their cm-level measurement accuracy. The use of carrier phase measurements results in the ambiguity problem of carrier phase integer cycles. Most attitude determination techniques based on GPS carrier phase measurements involve two sequential steps, ambiguity resolution and attitude estimation.

As a first step, single (between receivers) or double difference ambiguities for the independent inter-antenna vectors (antenna baselines) are estimated in the local level frame. Many GPS attitude determination systems use dedicated GPS receivers that share a unique oscillator. In this circumstance, the single difference carrier phase combination between two receivers can effectively remove the satellite clock error. Nowadays, more and more attitude determination systems employ non-dedicated OEM GPS sensors for cost efficiency reasons and each receiver has an independent oscillator. In this case, the double difference combination is preferred as it can effectively cancel both receiver and satellite clock errors. In GPS attitude determination, fast and reliable on-the-fly (OTF) ambiguity searching methodology is always expected. Most ambiguity resolution strategies borrow ambiguity searching algorithms from static or rapid kinematic positioning, such as the fast ambiguity search filter (FASF) (Chen and Lachapelle 1994), the least squares ambiguity search

technique (LSAST) (Hatch 1989) and the fast ambiguity resolution approach (FARA) (Frei and Beutler 1990). Any of these ambiguity search techniques includes three main common phases: defining the ambiguity search region, forming the candidate ambiguity combination and identifying the correct ambiguities. With a closely spaced antenna configuration, the inter-antenna distance in GPS attitude determination systems can be easily determined by conventional surveying methods and used either as an observable or an extra constraint in ambiguity resolution. Once ambiguities have been correctly determined and the antenna vector has been transformed from WGS-84 frame into the local level frame, attitude parameters can be derived from the rotation matrix using least squares or Kalman filter estimation methods based on the known antenna coordinates both in the body and local level frames.

Apart from baseline estimation, another approach is to directly estimate attitude parameters from GPS observations (Cohen 1992). In this method, each single difference or double difference observable forms an independent observation equation. Compared with the baseline estimation method, the primary advantage of the direct method is more measurement redundancy, which improves the ambiguity resolution and overall reliability of the whole attitude system. However, the direct method relies on the rigidity of antenna arrays and the computation load of this method is much higher than that of the baseline estimation method.

Once single or double differencing has been done, many error sources in the carrier phase measurements, such as receiver and satellite clock errors, tropospheric delay and ionospheric effects are virtually removed for short inter-antenna distances. The remaining errors that affect the positioning accuracy come only from multipath, antenna phase centre variation and receiver noise. Of these, multipath is generally the dominant error source affecting attitude estimation accuracy (Cohen and Parkinson 1991). Much research has been done to mitigate the multipath errors in attitude determination, either by implementing new hardware technology or by estimating and removing low frequency multipath effect using a Kalman filter.

In GPS attitude determination, as well as in any other application based on GPS navigation and positioning, the expected accuracy is also related to the satellite distribution in the sky. The determination of receiver position is essentially a resection problem. The estimation accuracy is directly related to the geometric distribution and the number of known points. Even though only three satellite observations are needed for the attitude determination (El-Mowafy 1994), more observables and better satellite geometry lead to faster and more reliable ambiguity resolution and precise attitude estimation.

In short, the performance of GPS attitude determination systems is a function of estimation algorithms, receiver firmware, satellite geometry, antenna phase centre stability and multipath mitigation ability. Previous research mainly focused on algorithm development for attitude determination, and high performance receivers and antennas were employed to build

up the attitude system. More recently, low-cost GPS sensors that can output sufficiently accurate time synchronized carrier phase measurements are available on the market. The employment of such receivers in GPS-based attitude determination is very promising since the overall cost of hardware declines to a very competitive level. Due to some features of low-cost sensors, the reliability and accuracy of attitude determination is degraded accordingly when such hardware is implemented in an attitude system. Research work has to be done in developing cost-effective solutions for attitude determination using low-cost GPS receivers or other aiding sensors.

## **1.2 Objectives**

The overall objective of this thesis is to investigate a low-cost solution for a GPS attitude determination system alone and with Dead Reckoning sensor aiding. The feasibility of using low-cost GPS sensors in the GPS standalone attitude system is explored. The factors that affect the attitude accuracy and reliability in a GPS attitude determination system are thoroughly investigated. The main attitude errors introduced by employing low-cost GPS receivers and antennas in attitude determination, such as multipath, antenna phase centre variation and the receiver noise are extensively discussed. The potential problems caused by receiver clock misalignment in double difference carrier phase observables and attitude estimation are discussed. Due to the limitations of a low-cost GPS-only attitude determination system in kinematic conditions, some reliability improvement methods, such as using higher data rate measurements, angular constraint checks and quality control systems based on innovation sequences, are implemented in the attitude determination algorithm to detect and further eliminate the erroneous antenna vector solutions from attitude

estimation. Another objective of this research is to develop a low-cost GPS/gyro integrated attitude determination system. By employing three low-cost rate gyros, the angular velocity of the platform can be monitored. The introduction of dynamic measurements can bridge attitude outputs during GPS outages and improve the reliability of ambiguity resolution and attitude estimation as well. The low-cost integrated system will be tested both in static and kinematic conditions in order to evaluate its performance improvement in reliability, accuracy and availability.

### **1.3 Thesis Outline**

In Chapter 2, different coordinate frames, including earth-fixed, local level and body frames are defined and reviewed. The rotation matrix from one frame to another and attitude parameters are introduced. The concept of attitude determination using multiple GPS sensors is discussed. The On-The-Fly ambiguity resolution technique and the least squares attitude estimation method are discussed at length.

In Chapter 3, the factors that affect the performance of GPS attitude determination are examined respectively. The number of satellites and their geometric distribution on the attitude estimation accuracy are studied. The impact of multipath and antenna phase centre variation on attitude estimates are investigated. The effect of antenna array configuration on attitude estimation accuracy is also examined in this chapter.

Chapter 4 investigates the implementation of low-cost receivers for attitude determination. The low-cost CMC Allstar receivers and the corresponding OEM antennas are examined for

their feasibility in GPS attitude determination. Some static and kinematic test results are compared with the performance of high-end hardware in order to assess the advantages and limitations of using low-cost receivers for attitude determination. The impact of GPS measurement error sources, such as multipath, antenna phase centre variation and receiver noise on attitude estimation is examined in detail. There is also discussion of the effect of receiver clock misalignment when low-cost GPS sensors are involved.

In Chapter 5, some reliability measures, namely high data rate measurements, angular constraint schemes and Kalman filter dynamic estimation, are tested in attitude determination software to improve overall reliability performance using low-cost GPS sensors. Mathematical models of those techniques and corresponding formulations are described. Both simulated and field test results are presented to show the advantages and limitations of those methods.

In order to further improve the performance of the low-cost attitude determination system, piezoelectric vibration rate gyros are introduced into a GPS-based attitude determination system in Chapter 6. The advantages of employing rate gyros in GPS-based attitude determination system are discussed at length. Error sources of rate gyros are examined and evaluated. The methodology of integrating gyro measurements with GPS carrier phase data in the Kalman filter is given. System construction and test scenarios are described. Results of static tests are presented to indicate how the rate gyros can improve the noise level of attitude estimation and bridge attitude outputs during GPS outages. The kinematic test was done near

the University of Calgary. The accuracy and the reliability performance of the low-cost system are examined and compared with the results obtained from a high performance NovAtel Beeline™ system.

Chapter 7 contains conclusions based on the above work and other work that need to be done in the future.

## **CHAPTER 2**

### **GPS ATTITUDE DETERMINATION**

GPS attitude determination technology uses GPS sensors to determine the multi-antenna array in the local level frame and to derive the attitude parameters from the corresponding rotation matrix from the body to the local level frame. In this chapter, the concepts and definitions related to attitude, namely, coordinate systems, rotation matrix and attitude parameterization are reviewed. The attitude determination method, which includes ambiguity resolution and the attitude estimation, is also discussed.

#### **2.1 Coordinate frames**

Three different coordinate frames are commonly used in GPS attitude determination systems. GPS gives antenna coordinates in an Earth Centred Earth Fixed (ECEF) frame, namely WGS-84 frame. Such coordinates have to be transformed into the local level frame in order to derive the attitude parameters. The antenna array body frame should also be well-defined and precisely determined in order to achieve high accuracy attitude estimation.

##### ***2.1.1 Earth-fixed frame***

The earth-fixed frame is a non-inertial frame fixed to the Earth. It rotates with respect to the inertial frame at a rate of 15 deg/hr. As shown in Figure 2.1, the origin of the earth-fixed frame is the centre of the Earth mass. The X-axis is located in the equatorial plane and points toward the Greenwich zero meridian. The Y-axis is also located in the equatorial plane and

90 degree east of the zero meridian. The Z-axis coincides with the axis of rotation of the Earth. The most common of earth-fixed frame now in use is the WGS-84 coordinate frame, which is also used in GPS as the ECEF.

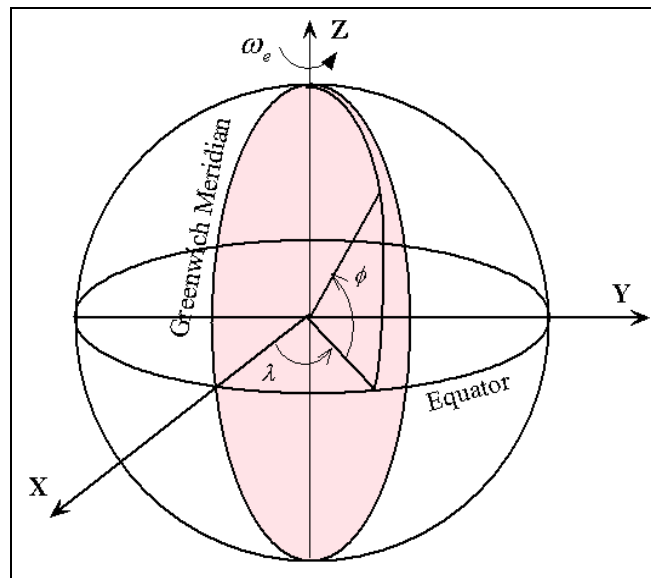


**Figure 2.1: Earth-fixed frame**

The WGS-84 is an earth-fixed global reference frame. The primary parameters given in Table 2.1 define the shape of the WGS-84 earth ellipsoid, its angular rate and Earth-mass which is included in the reference system.

**Table 2.1: Primary parameters of WGS-84**

PARAMETER	WGS-84
Semi-major axis	6378137.0 m
Flattening	1/298.25722563
Angular Velocity	$7.292115 \times 10^{-5}$ rad/s
Geocentric gravitational constant	$3.98600.5 \text{ km}^3/\text{s}^2$
Normalized 2 <sup>nd</sup> degree zonal harmonic coefficient of gravitational potential	$-484.16685 \times 10^{-6}$

### 2.1.2 Local level frame

The local level frame is a topocentric navigation frame and used as the reference to define the attitude of a mobile platform. Figure 2.2 depicts a local level frame with respect to the reference ellipsoid. The origin of the local level frame is selected as the phase centre of the primary antenna in the GPS attitude determination system. The Z-axis runs upward along the ellipsoidal normal. The X- and Y-axes are pointing towards ellipsoidal East and North respectively.

The local level frame is very similar to the local geodetic frame. As with the local level frame, the local geodetic frame is also defined with respect to the ellipsoid; the definitions of X- and Y- axes are also the same as in the local level frame. However, the Z-axis in the local geodetic system points downwards from the ellipsoidal normal and the three axes form a left hand coordinate system.

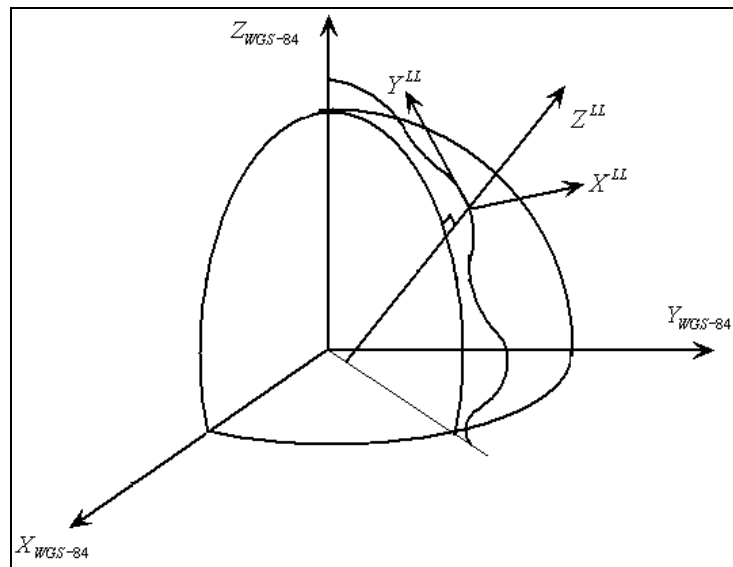


**Figure 2.2: Local level frame**

### ***2.1.3 Body Frame***

The antenna body frame is always formed by the configuration of the antenna array of the GPS attitude determination system. The antenna coordinates in this frame are considered free of error since the orientation and origin of the body frame are arbitrarily defined. In this research, the origin of the body frame corresponds to the phase centre of the primary antenna. The Y-axis follows the baseline from the primary antenna to the first secondary antenna. With another secondary antenna, the XY-plane can be determined and the X-axis is 90 degrees left of the Y-axis. The Z-axis, together with the other two axes, forms a right-hand Cartesian coordinate frame, as shown in Figure 2.3. If more than three antennas are involved in the system, the coordinates of other secondary antennas must be determined relatively to this user-defined body frame. Since the entire antenna array is considered a rigid body, the coordinates of the antennas in the body frame remain fixed during the dynamics of the platform in a single mission. The coordinates of the antenna array in the body frame can be obtained before the start of a mission by using a traditional surveying method or a GPS baseline determination method in static mode.

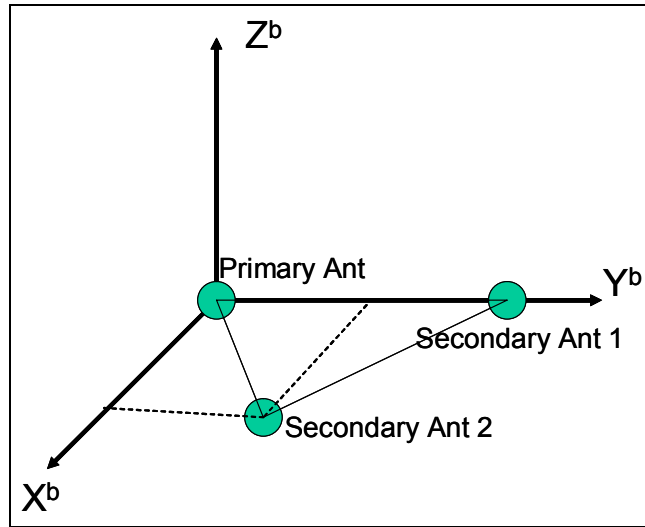


**Figure 2.3: Body frame**

#### ***2.1.4 Coordinates transformation from WGS-84 to local level frame***

Using GPS receivers, the inter-antenna vectors are accurately estimated in the WGS-84 frame. These coordinates have to be transformed into the local level frame in order to derive attitude parameters of the rotation matrix.

The transformation between the local level frame and WGS-84 as explained by Wong (1979) is given:

$$\begin{pmatrix} X^l \\ Y^l \\ Z^l \end{pmatrix} = \mathbf{R}_e^l \cdot \begin{pmatrix} X^e \\ Y^e \\ Z^e \end{pmatrix} = \begin{bmatrix} -\sin(\lambda) & \cos(\lambda) & 0 \\ -\cos(\lambda)\sin(\phi) & -\sin(\lambda)\sin(\phi) & \cos(\phi) \\ \cos(\lambda)\cos(\phi) & \sin(\lambda)\cos(\phi) & \sin(\phi) \end{bmatrix} \begin{pmatrix} X^e \\ Y^e \\ Z^e \end{pmatrix} \quad (2.1)$$

Since both the local level frame and WGS-84 are orthogonal, the rotation matrix ( $\mathbf{R}$ ) should be an orthogonal matrix and has the following property:

$$(\mathbf{R}_e^l)^{-1} = (\mathbf{R}_e^l)^T \quad (2.2)$$

Then, the rotation matrix from the earth-fixed frame to the local level frame can be expressed as

$$R_{ll}^e = (R_e^{ll})^{-1} = (R_e^{ll})^T = \begin{bmatrix} -\sin(\lambda) & -\cos(\lambda)\sin(\phi) & \cos(\lambda)\cos(\phi) \\ \cos(\lambda) & -\sin(\lambda)\sin(\phi) & \sin(\lambda)\cos(\phi) \\ 0 & \cos(\phi) & \sin(\phi) \end{bmatrix} \quad (2.3)$$

## 2.2 Attitude parameterization

The coordinate transformation from a three-dimensional Cartesian coordinate frame into another always involves three operations: scaling, rotation and translation. The mathematical expression of such conversion can be expressed as:

$$\mathbf{r}_b = s\mathbf{R}_a^b\mathbf{r}_a + \mathbf{r}_{a0}^b \quad (2.4)$$

where  $\mathbf{r}_a$  and  $\mathbf{r}_b$  are the coordinates of vector  $\mathbf{r}$  in different frames a and b

$s$  is the scale factor

$\mathbf{R}_a^b$  is the rotation matrix from coordinate frame a to another coordinate system b

$\mathbf{r}_{a0}^b$  is the position vector of the origin of coordinate frame a as expressed in the coordinate system b.

In an attitude determination system, only the rotation is of interest since both the local level frame (coordinate frame a) and the body frame (coordinate frame b) share the same origin and scale factor. The rotation matrix  $\mathbf{R}_{ll}^b$  is a 3-by-3 matrix that consists of nine parameters and defines the relative orientation of the two coordinate systems. However, the elements of the rotation matrix are not all independent, and each of them is the cosine of angles between

corresponding axes in two coordinate systems. Such a rotation matrix is also called the direction cosine matrix or the attitude matrix and is considered to be the fundamental quantity that specifies the orientation of the platform. The main advantage of direction cosine matrix is its potential to improve computational load and speed. However, the many correlated attitude parameters make it difficult to describe the platform orientation in a direct and simple manner. In specific applications, some other parameterization schemes, such as Euler angles, quaternions, Euler Axis/Angle and Gibbs vector, are used for their own suitability (Wertz 1978).

### ***2.2.1 Euler Angles***

In the attitude matrix  $\mathbf{R}$ , only three of nine elements are independent. The rotation of the body frame with respect to the local level frame consists of three successive rotations along the three axes. The three rotation angles around the axes are referred to as the Euler angles — yaw, pitch and roll. Yaw ( $\psi$ ) is defined as the rotation angle around the Z-axis counter-clockwise when seen from the positive end of the axis. Another parameter to describe this angle is heading (azimuth). It has the same value as yaw, but is different in sign and is measured in a clockwise direction. Pitch ( $\theta$ ) is the rotation around the X-axis in a counter-clockwise direction, while the roll angle ( $\varphi$ ) is the rotation around the Y-axis in a counter-clockwise direction. Using these three attitude parameters, any rotation matrix can be expressed as the matrix product of the three matrices for the individual rotation around the three axes. However, as any Euler angle refers to the orientation of the rotated body frame with respect to the local level in the current context, the changes of yaw (heading), pitch and roll depend on the rotation sequence around the three axes. In this research, the 3-1-2 rotation

sequence is applied with the first rotation along with Z-axis, the second around X-axis and the third rotation around Y-axis. The overall rotation matrix can be expressed as follows:

$$\mathbf{R}_I^b = \mathbf{R}_2(\varphi)\mathbf{R}_1(\theta)\mathbf{R}_3(\psi) \quad (2.5)$$

$$= \begin{bmatrix} \cos(\psi)\cos(\varphi) - \sin(\psi)\sin(\theta)\sin(\varphi) & \sin(\psi)\cos(\varphi) + \cos(\psi)\sin(\theta)\sin(\varphi) & -\cos(\theta)\sin(\varphi) \\ -\sin(\psi)\cos(\theta) & \cos(\psi)\cos(\theta) & \sin(\theta) \\ \cos(\psi)\sin(\varphi) + \sin(\psi)\sin(\theta)\cos(\varphi) & \sin(\psi)\sin(\varphi) - \cos(\psi)\sin(\theta)\cos(\varphi) & \cos(\theta)\cos(\varphi) \end{bmatrix}$$

The expressions for the three rotation angles in terms of the elements of the direction cosine matrix are

$$\psi = -\arcsin\left(\frac{R(2,1)}{R(2,2)}\right) \quad (2.6a)$$

$$\theta = \arcsin(R(2,3)) \quad (2.6b)$$

$$\varphi = -\arctan\left(\frac{R(1,3)}{R(3,3)}\right) \quad (2.6c)$$

Using Equations 2.5 and 2.6, the three Euler angles can easily be obtained once the rotation matrix is known, or vice versa. Although they are not convenient for numerical computations, the Euler angle representation is often used for computer input and output because of its ease for visualization and simplicity to generate a rotation matrix.

### 2.2.2 Quaternion

Quaternions, also called Euler symmetric parameters, are another useful representation of attitude parameterization. Given two Cartesian coordinate systems, there is always an invariant axis  $\mathbf{e}$ , along which the coordinates are the same in the two coordinate frames. It is possible to move one coordinate system into the other by the rotation around this axis with an

angle of  $\alpha$  (Schleppé 1996). This representation of attitude can be given by four mathematical parameters which are defined by

$$\mathbf{q} = \begin{pmatrix} q_1 \\ q_2 \\ q_3 \\ q_4 \end{pmatrix} = \begin{pmatrix} \mathbf{e} \sin \frac{\alpha}{2} \\ \cos \frac{\alpha}{2} \end{pmatrix} = \begin{pmatrix} e_1 \sin \frac{\alpha}{2} \\ e_2 \sin \frac{\alpha}{2} \\ e_3 \sin \frac{\alpha}{2} \\ \cos \frac{\alpha}{2} \end{pmatrix} \quad (2.7)$$

where  $e_1, e_2, e_3$  are the components of the unit direction vectors of the rotation axes..

However, these four parameters in quaternion representation are not all independent. In fact they satisfy the following constraint:

$$q_1^2 + q_2^2 + q_3^2 + q_4^2 = 1 \quad (2.8)$$

Quaternion representation has another feature that changing all the signs of quaternion parameters simultaneously does not affect the parameterization of the attitude.

$$\mathbf{q} = -\mathbf{q} \quad (2.9)$$

Using the quaternion parameters, the direction cosine matrix is given as shown by Wertz (1978):

$$\mathbf{R} = \begin{bmatrix} q_1^2 - q_2^2 - q_3^2 + q_4^2 & 2(q_1q_2 + q_3q_4) & 2(q_1q_3 - q_2q_4) \\ 2(q_1q_2 - q_3q_4) & -q_1^2 + q_2^2 - q_3^2 + q_4^2 & 2(q_2q_3 + q_1q_4) \\ 2(q_1q_3 + q_2q_4) & 2(q_2q_3 - q_1q_4) & -q_1^2 - q_2^2 + q_3^2 + q_4^2 \end{bmatrix} \quad (2.10)$$

The quaternion parameters can also be expressed in terms of direction cosine matrix elements in different methods. One of the expressions given by Wertz (1978) is as follows:

$$q_4 = \pm \frac{1}{2} (1 + R(1,1) + R(2,2) + R(3,3))^{1/2} \quad (2.11a)$$

$$q_1 = \frac{1}{4q_4}(R(2,3) - R(3,2)) \quad (2.11b)$$

$$q_2 = \frac{1}{4q_4}(R(3,1) - R(1,3)) \quad (2.11c)$$

$$q_3 = \frac{1}{4q_4}(R(1,2) - R(2,1)) \quad (2.11d)$$

Quaternions are much more compact than the direction cosine matrix, since only four parameters are needed. However, this parameterization scheme is not widely used in navigation systems with GPS mainly because they do not represent the physical qualities (El-Mowafy 1994).

Other kinds of attitude parameterization schemes are Euler Angle/Axis and the Gibbs vector. Due to instability at certain rotation angles, these two schemes are not generally used to parameterize attitude information. An extensive introduction to Euler Angle/Axis and Gibbs parameterization can be found in Wertz (1978) and El-Mowafy (1994).

In this thesis, the Euler angle parameterization has been chosen because of its wide popularity and its clarity in physical interpretation in attitude determination using GPS sensors. Many attitude determination algorithms have been developed based on Euler angles in the last ten years (Lu 1994, Cohen 1992). This representation has been proven to work well in GPS attitude determination for terrestrial applications.

## 2.3 Basics of GPS attitude determination

In the last twenty years, the Global Positioning System has been extensively investigated for many applications in geodesy, navigation and location. Using carrier phase measurements, GPS can achieve centimeter-level precision, provided that the initial integer ambiguity set is solved correctly. This level of accuracy allows for expansion into many other applications using GPS sensors, among which attitude determination using multiple closely space antennas has developed into an effective technology for many navigation missions. In this section, the principle of attitude determination using GPS is described at length. Different observables from GPS receivers are reviewed. The double difference combination and ambiguity resolution are introduced. Attitude estimation from vector measurements using least squares is also covered.

### 2.3.1 GPS observables

Two main kinds of measurements are simultaneously available from the GPS signals. The pseudorange measurement is estimated from the C/A random noise code while the carrier phase measurement is derived from the carrier waves of L1 or L2. In the next two sections, these two GPS range observables and their error sources are discussed briefly.

#### *A. pseudorange measurement*

The basic observation equation of the pseudorange measurement can be expressed as (Lachapelle et al 1992):

$$p_{\alpha}^i = \rho_{\alpha}^i + d\rho^i + d_{ion} + d_{trop} + c(dt^i - dT_{\alpha}) + \varepsilon(p_{mult}) + \varepsilon(p_{noise}) \quad (2.12)$$

where  $p_{\alpha}^i$  is the pseudorange measurement from satellite  $i$  to receiver  $\alpha$  in metres

$\rho_{\alpha}^i$  is the geometric range from satellite  $i$  to receiver  $\alpha$  in metres

$d\rho^i$  is the orbital error of satellite  $i$  in metres

$d_{ion}$  is the ionospheric delay in metres

$d_{trop}$  is the tropospheric delay in metres

$dt^i$  is the clock error of satellite  $i$  in metres

$dT_{\alpha}$  is the clock error of receiver  $\alpha$  in metres

$\varepsilon(p_{mult})$  denotes the pseudorange multipath errors in metres

$\varepsilon(p_{noise})$  represents the measurement error due to the receiver noise in metres

In GPS navigation and position mode, the satellite-receiver geometric range  $\rho_{\alpha}^i$  is used to determine the receiver location. However, the pseudorange  $p_{\alpha}^i$  is contaminated by different errors sources that are shown in Equation 2.12. The satellite orbital error is the discrepancy between the estimated satellite coordinates and the truth. According to Jefferson and Bar-Sever (2000), the magnitude of orbital error using the broadcast satellite ephemeris decreases to an average level of 4 m after Selective Availability (SA) was turned off. When GPS Radio Frequency (RF) signal travels through the atmosphere, the speed and the direction of the signal are affected by the ionized gases in the ionosphere and the nondispersive medium in the troposphere. The typical ionospheric error is around 5 metres at the zenith and it varies with satellite elevation and time of day (Skone 1999). The tropospheric error can be separated into two parts. The first part is the dry component which results from the dry troposphere and accounts for 90 % of the total error. The dry component is fairly stable and can be precisely estimated using certain measurements. As the second part, the wet

component varies with the temperature, pressure, humidity and satellite elevation. The measurement error due to the tropospheric delay is on the order of 2-25 metres depending on the elevation angle (Spilker 1996). Multipath is the phenomenon whereby a signal is reflected or diffracted from various objects and arrives at the receiver via multiple paths (Braasch and Van Graas, 1991). Multipath error in the pseudorange measurement is highly dependent on the conditions around the GPS antenna and on the type of GPS sensor (both receiver and antenna) that are used. The typical level of C/A code multipath error is about 3 m (Olynik 2002). Receiver noise includes the thermal noise caused by the electronic component in GPS receivers and the dynamics experienced by the receiver. The empirical level of measurement error due to receiver noise is less than 0.5 metres (Parkinson 1996).

### *B. Carrier phase measurement*

The carrier phase measurement is much more precise than the pseudorange measurement. Its mathematical expression can be given as follows

$$\Phi_{\alpha}^i = \rho_{\alpha}^i + d\rho_{\alpha} + c(dt^i - dT_{\epsilon}) + \lambda N_{\alpha}^i - d_{ion} + d_{trop} + \mathcal{E}(\Phi_{rx}) + \mathcal{E}(\Phi_{mult}) + \mathcal{E}(\Phi_{ant}) \quad (2.13)$$

where  $\Phi_{\alpha}^i$  is the carrier phase measurement from satellite  $i$  to receiver  $\alpha$  in metres

$N_{\alpha}^i$  is the carrier phase integer ambiguity

$\lambda$  is the wavelength of carrier in metres

$\mathcal{E}(\Phi_{noise})$  is the carrier phase measurement error due to the receiver noise in metres

$\mathcal{E}(\Phi_{mult})$  is the carrier phase multipath error in metres

$\mathcal{E}(\Phi_{ant})$  is the antenna phase centre variation in metres

Since a GPS receiver can only measure the fractional carrier phase and count the integer cycles after tracking, the initial integer cycle ( $N$ ) of the carrier remains unknown in the above equation. In order to accurately determine the satellite-receiver range, the ambiguous integer cycle of the carrier has to be solved. In the carrier phase measurement, a phase advance instead of group delay occurs when the GPS signal travels through the ionosphere and therefore the ionospheric error has a negative sign. The carrier phase measurement error due to receiver noise is usually less than 1 % of the wavelength (Misra and Enge 2001). The carrier phase multipath error is always within one quarter of the wavelength, approximately 5 cm for L1 and 6 cm for L2 (Ray 2000). The typical level of this error source on carrier phase measurement is about 0.5 cm. The antenna phase centre variation is the deviation of true phase centre location with respect to the nominal physical point on the antenna. GPS antenna phase centres may experience 1-2 cm variation in normal cases (Hofmann-Wellenhof et al 2001).

### *C. Observation Combination*

One way to effectively eliminate or reduce the error sources in the observation equations is to employ linear differencing combinations. Using single differencing between two receivers with respect to a common satellite, the satellite clock error can be cancelled out. However, double differencing between two satellites can entirely eliminate the clock errors both of the satellites and receivers.

The single differencing linear combination equations for carrier phase measurements are given in the following form:

$$\Delta\Phi_{\alpha\beta}^i = \Delta\rho_{\alpha\beta}^i + \Delta d\rho_{\alpha\beta}^i - c\Delta dT_{\alpha\beta} + \lambda\Delta N_{\alpha\beta}^i - \Delta d_{ion_{\alpha\beta}}^i + \Delta d_{trop_{\alpha\beta}}^i + \varepsilon(\Delta\Phi) \quad (2.14)$$

where  $\varepsilon(\Delta\Phi)$  represents the overall measurement errors due to receiver noise, multipath and antenna phase centre variation after single differencing.

Similarly, double difference carrier phase observations can be expressed as :

$$\nabla\Delta\Phi_{\alpha\beta}^{ij} = \nabla\Delta\rho_{\alpha\beta}^{ij} + \nabla\Delta d\rho_{\alpha\beta}^{ij} + \lambda\nabla\Delta N_{\alpha\beta}^{ij} - \nabla\Delta d_{ion_{\alpha\beta}}^{ij} + \nabla\Delta d_{trop_{\alpha\beta}}^{ij} + \varepsilon(\nabla\Delta\Phi) \quad (2.15)$$

In the double difference combination, both the satellite clock and receiver clock error have been cancelled out from the equation. For attitude determination, as the distance between the antenna pair is usually within 20 metres, the atmospheric effects and the orbital error ( $d\rho$ ) on the signals from the same satellite are almost identical on the carrier phase measurements of the two antennas. Therefore, after single or double differencing, either the phase advance ( $d_{ion}$ ) due to the ionosphere effect or the group delay ( $d_{trop}$ ) caused by the troposphere is virtually eliminated from the observation combination. The above two equations can be written concisely as follows:

$$\Delta\Phi_{\alpha\beta}^i = \Delta\rho_{\alpha\beta}^i - c\Delta dT_{\alpha\beta} + \lambda\Delta N_{\alpha\beta}^i + \varepsilon(\Delta\Phi) \quad (2.16)$$

$$\nabla\Delta\Phi_{\alpha\beta}^{ij} = \nabla\Delta\rho_{\alpha\beta}^{ij} + \lambda\nabla\Delta N_{\alpha\beta}^{ij} + \varepsilon(\nabla\Delta\Phi) \quad (2.17)$$

In attitude determination, both single difference and double difference combinations can be used as observables to estimate the antenna vectors in the navigation frame. In some multiple-receiver attitude determination systems, an external oscillator is employed to replace local clocks in the receivers. In this circumstance, the single difference combination is advantageous, since the noise level in this linear combination is smaller than in double

differencing. In the case that the attitude system is built up of non-dedicated GPS sensors without common oscillators, the double difference observables are preferable in that not only the receiver clock offset but also the line bias attributable to the different antenna cable lengths can be eliminated from the observation equations. In this research, as low-cost non-dedicated GPS receivers are investigated for attitude determination, double difference carrier phase combinations are used as observables to determine inter-antenna vectors in the local level frame.

### ***2.3.2 Attitude determination using GPS***

The utilization of differenced carrier phase measurements for three-dimensional attitude estimation has been discussed over the past decade (Cohen 1992, Lu 1994). The basic principle of attitude determination from GPS measurements follows previous work to determine spacecraft attitude using vector observations (Wahba 1965). This kind of technology has been extensively exploited by Shuster and Oh (1981) and by Markley (1993) for spacecraft attitude control. Using the double difference carrier phase measurements from GPS, the coordinates of inter-antenna vectors (baseline) are first determined in the earth-fixed WGS-84 frame. After coordinate transformation from the earth-fixed frame into the local level frame, the orientation of the body frame with respect to the local level can be estimated using vector observations in both coordinate systems. The general equation for attitude determination is:

$$\begin{pmatrix} x^b \\ y^b \\ z^b \end{pmatrix} = R(\psi, \theta, \varphi) \begin{pmatrix} x^l \\ y^l \\ z^l \end{pmatrix} \quad (2.18)$$

where

$x, y, z$  represent the components of the inter-antenna vector in the specific Cartesian coordinate and the superscripts  $l$  and  $b$  stand for the local level frame and body frame respectively

In Equation 2.18, the antenna coordinates in the body frame are known a priori and the inter-antenna vectors in the local level frame are determined by the GPS carrier phase measurements. The only unknowns here are the three attitude parameters in the rotation matrix  $R$  from the local level frame to the body. When the inter-antenna vector solutions are considered as the quasi-observables, the Euler angles can be determined using some estimation methods.

In land and marine attitude determination application, heading is more commonly used than yaw. Substituting heading to yaw by changing the sign of the yaw angle, the corresponding rotation matrix is given as follows:

$$R_{ll}^b = \begin{bmatrix} \cos(h)\cos(\theta) + \sin(h)\sin(\theta)\sin(\varphi) & \cos(h)\sin(\theta)\sin(\varphi) - \sin(h)\cos(\varphi) & -\cos(\theta)\sin(\varphi) \\ \sin(h)\cos(\theta) & \cos(h)\cos(\theta) & \sin(\theta) \\ \cos(h)\sin(\varphi) + \sin(h)\sin(\theta)\cos(\varphi) & -\sin(h)\sin(\varphi) - \cos(h)\sin(\theta)\cos(\varphi) & \cos(\theta)\cos(\varphi) \end{bmatrix} \quad (2.19)$$

As any Cartesian coordinate frame can be built up by at least two non-colinear vectors, at least three GPS antennas have to be involved to derive the three-dimensional attitude parameters. Therefore there are at least six observables (three quasi-observables per vector  $X$  2 vectors) in Equation 2.18. Three of them are redundant, since only three attitude parameters remain unknown at a single epoch. To make full use of all the observables and achieve

optimal estimates of those parameters, some estimation methods, namely least squares or Kalman filtering, are employed in the attitude estimation phase.

As shown in Equation 2.18, the inter-antenna vector components in the local level frame have to be precisely determined in order to derive accurate attitude parameters. Carrier phase measurements from GPS are by far the best measurements that can be used to estimate the antenna vectors, due to their cm-level positioning accuracy. However, the employment of carrier phase measurements inevitably brings forward another critical issue: the initial integer carrier phase cycles are still ambiguous and must be correctly determined.

### ***2.3.3 Ambiguity resolution***

As the most challenging part in GPS attitude determination, the techniques to resolve the integer carrier ambiguities have been intensively explored in the past ten years. The process to determine the correct integer ambiguity is conventionally called ambiguity resolution in GPS applications. Basically there are two different methods to estimate the carrier phase ambiguities for the inter-antenna vectors: motion-based ambiguity resolution (Cohen 1996) and vector-based ambiguity resolution (Lu 1994, Euler and Hill 1995). In this research, vector-based ambiguity resolution has been used since this method is independent of platform dynamics and suits both static and kinematic geomatic applications.

Vector-based ambiguity resolution was originally developed for rapid static or kinematic differential carrier phase positioning and allows for instantaneous ambiguity determination. In GPS attitude determination, the ambiguity resolution process should have the following

properties. The whole ambiguity search process should not involve too much computational load so that it can be completed within the data update interval; only the true ambiguity should be sorted out; the incorrect ambiguities should never be selected. In the real world, some of the criteria conflict between each other and compromises have to be made. In attitude determination, a desired ambiguity search method should have high computational efficiency and can be completed in a single measurement epoch and the correct ambiguity should be identified in normal circumstances. In cases where the wrong ambiguities have been selected, some quality control process should detect and identify the erroneous ambiguities.

For ambiguity resolution in attitude determination, the following three steps are always included: defining the ambiguity search region, forming the ambiguity combinations and distinguishing the correct ambiguity set. In a GPS attitude determination system, the multiple GPS antennas are closely spaced and the locations of the antennas are fixed with respect to each other during motion. Consequently the relative geometry of the antenna array can be determined using conventional surveying methods once the GPS attitude determination system has been set up. This can be used as prior information and redundant constraints to better determine the carrier phase integer cycles in ambiguity resolution.

A desired ambiguity search region should include the true ambiguity combination and have a small volume to save computation time. In GPS attitude determination, different kinds of search volumes, such as a sphere, a cube and an ellipsoid, can be defined based on specific

applications. In general, due to the known inter-antenna distances and the lack of attitude information, the sphere search region with the origin at the primary antenna is widely used to define the search space. With the radius of inter-antenna distance known, the potential location of secondary antennas should fall on the shell of this sphere.

Once the ambiguity search volume has been defined, the second step is to determine all the potential ambiguity sets that fall in the search zone. In a GPS attitude determination system, a modified Least Squares Ambiguity Search Technique (LSAST) introduced by Hatch (1991) was used for its computational efficiency. In this method, all the ambiguity combinations are formed using a set of three primary double differences at the same epoch, since only four satellite observations are needed to estimate a single inter-antenna vector. Using primary observations can significantly speed up computation and improve the efficiency in that most false candidate combinations can be quickly eliminated after checking the estimated antenna vector length with the known one and only a few of candidate ambiguity sets pass through this first length check. The double difference ambiguities for the remaining satellites can be directly calculated afterwards, as the antenna vector has been determined from the primary satellite measurements. The criteria to select the four primary satellites rely on the satellite distribution and the corresponding carrier phase measurement qualities. Herein, the four satellites that form the best PDOP have been selected in this case as the primary satellites in order to achieve optimal estimation of the antenna vector.

The most critical problem of ambiguity resolution is how to isolate the correct double difference ambiguity set from many potential combinations. In order to make sure only the correct ambiguity set is determined, different distinguishing tests based on antenna array constraints and the statistical properties of the true ambiguity set are used in this phase. The full geometry constraints, namely vector lengths and the angles between the antenna vectors, have been exploited by Euler and Hill (1995). The estimated inter-antenna distances from the true ambiguity set should be consistent with the known ones within a certain tolerance to cover carrier phase measurement errors. Once and if at least two antenna vectors have been determined using the candidate ambiguity set, the estimated vector angle can be checked with the known one to verify the ambiguity result. Another type of distinguishing test utilizes statistical properties to detect the true double ambiguity combinations. According to Hatch (1991), the sum of squares of double difference carrier phase residuals should be minimum for the correct ambiguity set and relatively smaller than the same quantity from the incorrect ambiguity sets. A ratio test recommended by Lu (1994) is also commonly used. It is pointed out that only when the ratio of the second smallest quadratic form of residuals to the smallest one is larger than the predefined threshold, the potential ambiguity with the smallest quadratic form should be selected as the correct ambiguity set.

#### ***2.3.4 Cycle slip detection***

Once the correct ambiguity set has been solved, it can be fixed and used permanently before cycle slip occurrence. A cycle slip is a sudden integer number of cycles jump in the carrier phase observable, caused by the loss of lock in the receiver phase lock loops (Leick 1995). It may be due to internal receiver tracking problems or an interruption in the ability of the

antenna to receive the satellite signals (Seeber, 1993). Once a cycle slip occurs, it has to be detected instantaneously, since the previous ambiguity is no longer valid. Therefore, a cycle slip detection process must be implemented in any carrier phase based positioning and navigation method.

In a GPS attitude determination system, several methods can be used to detect or further correct cycle slips, which include the phase prediction method, the residual check, the Chi-square test and the length constraint test. The methodology to detect cycle slips using phase rate is as follows:

$$\hat{\Phi}_k = \Phi_{k-1} + \frac{\dot{\Phi}_k + \dot{\Phi}_{k-1}}{2} \Delta t \quad (2.20)$$

where

$\hat{\Phi}_k$  is the predicted phase measurement at  $t_k$  (cycles),

$\Phi_{k-1}$  is the phase measurement at  $t_{k-1}$  (cycles),

$\dot{\Phi}_k$  is the phase rate measurement, Doppler, at  $t_k$  (cycles/s),

$\dot{\Phi}_{k-1}$  is the phase rate measurement, Doppler, at  $t_{k-1}$  (cycles/s), and

$\Delta t$  is the time difference between measurements (s).

The predicted phase at epoch  $k$  is then compared to the measured phase as follows:

$$\left| \hat{\Phi}_k - \Phi_k \right| < \tau \cdot \Delta t \quad (2.21)$$

where  $\tau$  is the tolerance criterion for the cycle slip detection capability and is a function of data rate, phase rate accuracy and the dynamics of platform. Using the phase prediction method, large cycle slip occurrences can be identified.

The residual check and the Chi-square test are based on the assumption that double difference carrier phase residuals have noise-like behaviour and the magnitude should always be within certain limits provided that the ambiguities are correctly solved. In the case of cycle slip occurrence, the residuals should grow dramatically and the sum of their squares does not follow a Chi-square distribution any more. Therefore, using a threshold to check residuals and giving a certain confidence region for the Chi-square distribution, cycle slips can be detected with these two methods. The limitation of the above methods is their inability to identify the satellite on which the cycle slip occurs.

When a cycle slip occurs, the solved inter-antenna distance will also jump from the true value. Therefore the computed inter-antenna length can be checked with the known distance to detect the cycle slip within a certain tolerance ( $\delta L$ ) to absorb measurement errors in the carrier phase. The length check for cycle slip detection can be expressed as:

$$|L_{est} - L_{known}| < \delta L \quad (2.22)$$

#### **2.4 HeadRT+<sup>TM</sup> Algorithm**

In this research, an open-architecture attitude determination software developed by the Department of Geomatics Engineering at the University of Calgary (Hoyle et al 2002), namely HeadRT+<sup>TM</sup>, has been used as the base for algorithm development and testing. All the methodologies discussed in this research work are implemented and realized in this software to assess the performance.

HeadRT+™ uses double difference carrier phase measurements to determine inter-antenna vectors, and can estimate the attitude parameters for an attitude system with at least two antennas. The ambiguity resolution in HeadRT+™, which is based on Hatch's LSAST algorithm, is shown in Figure 2.4. The entire search region of the double difference ambiguities is the sphere with the radius of known inter-antenna distance. After forming all double difference ambiguity combinations for four primary satellites, one coarse length check with a tolerance of 20 cm is conducted to reduce the number of candidate ambiguity sets. Then the ambiguities for the secondary satellites are calculated from the approximate vector solutions. After that a fine test is implemented to validate those ambiguity sets that satisfy the following two criteria: The inter-antenna distance for the correct ambiguity should be consistent with the known one with a tolerance of 5 cm; and the quadratic form of adjusted residuals should pass the Chi-squared test with a confidence level of 75 percent. If only one ambiguity combination passes the fine test, it will be identified as the correct one. In the case that at least two ambiguity sets get through the test, a ratio test is carried out to make sure that the quadratic form of residuals for the correct ambiguity set is significantly smaller than that of the wrong ones. The ambiguity fixing ratio threshold in this ratio test is normally selected as 2-3 in practice (Lachapelle et al 1993). The selected ambiguity combination is not used to solve the inter-antenna vector solution until it is verified by carrier phase measurements in the following epochs. The time to confirm the selected ambiguity set is dependent on the quality of carrier phase measurements and the variation of satellite geometry. In HeadRT+™, a user-input parameter, namely Minimum Time to Fix Ambiguity (MTTFA), is used to specify the time to double check the selected ambiguity.

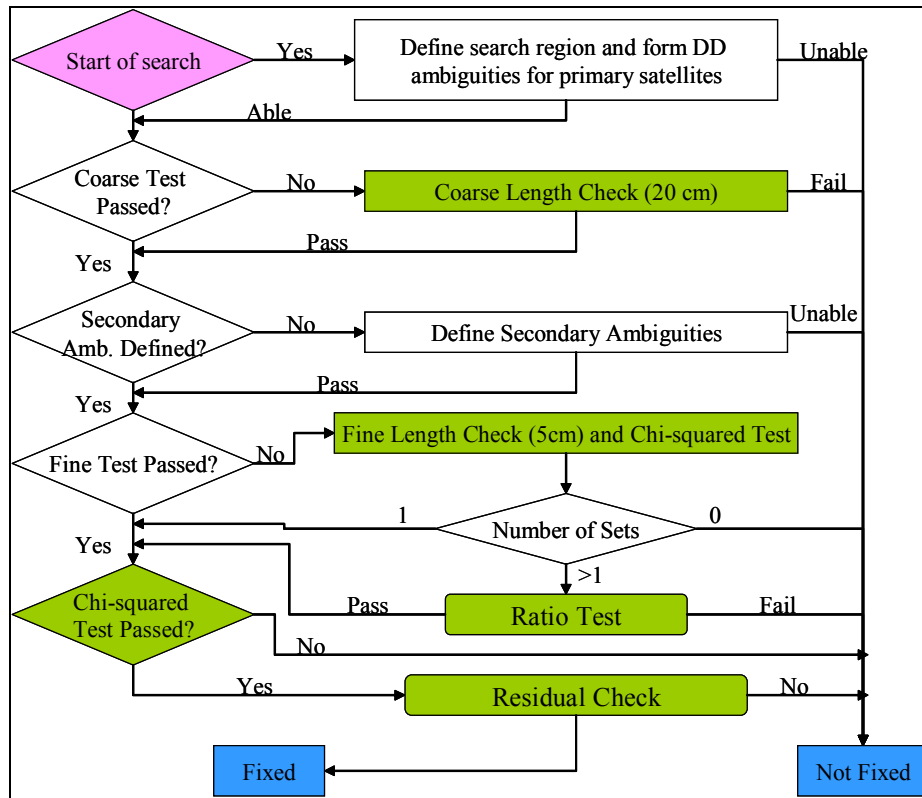


**Figure 2.4: Ambiguity resolution in HeadRT+™**

After fixing double difference ambiguities, the inter-antenna vector solutions are estimated from GPS carrier phase measurements until cycle slips are detected. The cycle slip detection methods used in HeadRT+™ include the phase prediction method, the inter-antenna length check, the Chi-squared test and the residuals test. Two kinds of criteria are used in the residual test to identify cycle slip occurrences. The first one is to check whether a single DD carrier phase residual is too large and exceeds the pre-determined tolerance. In the case when the small cycle slip occurs and the carrier phase error is absorbed by residuals of other satellite observables, a group test of three DD residuals is implemented. The two thresholds selected here are 5 cm for the single residual check and 3 cm for the group residual check to tolerate multipath and antenna phase centre variations.

If at least two inter-antenna vectors have been solved by GPS measurements, the three attitude parameters in the rotation matrix are estimated from vector components using an least squares method. If only one vector solution is available, only the heading and pitch can be computed. After outputting the attitude parameters both on the screen and into the specific file, the software moves to the next epoch. Currently, no dynamic constraints of the platform are implemented in the filtering process, which allows an epoch-by-epoch assessment of attitude estimation under any dynamics.

## **CHAPTER 3**

### **PERFORMANCE OF GPS ATTITUDE DETERMINATION**

In this chapter, the factors that affect GPS attitude determination performance are explored. The impact of carrier phase measurement errors, such as multipath, antenna phase centre variation and receiver noise, are extensively examined. In addition, the impact of visible satellite distribution and antenna array configuration on the performance of attitude determination are investigated.

#### **3.1 Measurement errors**

As mentioned in Chapter Two, using the differential technique, most carrier phase measurement errors, namely ionospheric and tropospheric errors along with clock errors are virtually cancelled out due to short inter-antenna distances in GPS attitude determination. The remaining measurement errors that affect the performance of attitude determination are multipath, antenna phase centre variations and receiver noise.

##### ***3.1.1 Multipath***

According to Cohen (1992), multipath is the most significant error source limiting the accuracy of GPS-based attitude determination. Multipath is the phenomenon whereby a signal arrives at a receiver via multiple paths attributable to reflection and diffraction (Braasch 1996). Reflection occurs when an electromagnetic wave hits the surface of an object. Reflected signals have two components depending on the roughness of the reflection

plane: if the surface is smooth, specular reflection occurs and the reflected wave is more deterministic; in the case of a rough surface, the diffusion of reflected signal happens. The roughness of the surface is quantified by the Rayleigh criterion (Ray 2000). Diffraction, on the other hand, occurs when an electromagnetic wave hits the edge of an object or a curved surface-like cylinder. Multipath affects both the code and carrier phase measurements in a GPS receiver. Code multipath can cause a range error as large as 150 m when using the wide correlator but is typically of the order of several metres in normal conditions. In recent years, many technologies have been developed to successfully mitigate or calibrate code multipath, such as MEDLL (Townsend 1995), Narrow Correlator (Dierendonck et al 1992), TrEC (Phelts and Enge 2000) and carrier-code smooth methods.

Carrier phase multipath, however, is much more difficult to isolate. A lot of research has been done to characterize and model carrier phase multipath in the past twenty years and some of the results can be found in the literature, e.g. Georgiadou and Kleusberg (1988), Ray (2000) and Braasch (1996).

According to discussions in the literatures, the receiver-generated signal correlated with the input signal in the in-phase and quadrature-arm for the prompt correlator in the ideal case can be given as follows:

$$IP = s_i(t)s_{IP}(t) \approx \frac{A}{2}R(\hat{\tau}_0 - \tau_0)\cos(\gamma_0 - \hat{\gamma}_0) \quad (3.1)$$

$$QP = s_i(t)s_{QP}(t) \approx \frac{A}{2}R(\hat{\tau}_0 - \tau_0)\sin(\gamma_0 - \hat{\gamma}_0) \quad (3.2)$$

where

$A$  is the satellite signal amplitude

$\tau_0$  is the satellite signal code delay (s)

$r_0$  is the satellite signal carrier phase (rad)

$\hat{\tau}_0, \hat{\gamma}_0$  are the estimates of the above two items

$R()$  is the correlation function

In order to achieve the best positioning accuracy, the estimated values for the code delay  $\hat{\tau}_0$  and the carrier phase  $\hat{\gamma}_0$  should be as close as possible to the corresponding true values. Such estimations are respectively done in the different tracking loops, namely the Delay Lock Loop (DLL), the Frequency Lock Loop (FLL) and the Phase Lock Loop (PLL). Extensive description of those loops can be found in the literature, such as Parkinson and Enge (1996) and Ray (2000).

With the existence of multipath, the actual incoming signal at the receiver part is the composite of a direct signal and (more than) one reflected signals. So the received signal in the in-phase and quadrature-arm for the prompt correlator can be expressed as:

$$IP = \sum_0^n \alpha_i \frac{A}{2} R(\hat{\tau}_c - \tau_i) \cos(\gamma_i - \hat{\gamma}_c) \quad (3.3)$$

$$QP = \sum_0^n \alpha_i \frac{A}{2} R(\hat{\tau}_c - \tau_i) \sin(\gamma_i - \hat{\gamma}_c) \quad (3.4)$$

where

$\hat{\gamma}_c$  is the receiver estimate of the incoming signal phase delay

$\hat{\tau}_c$  is the receiver estimate of the incoming signal code delay

The  $\alpha_i$  in the above equations represent the direct and reflected signal attenuation coefficients. For the direct signal, the corresponding coefficient  $\alpha_0$  is equal to one.

As mentioned above, the receiver estimated phase is determined from a Phase Lock Loop, such as the Costas loop. In the ideal case, the incoming carrier is the direct carrier from the satellite and the locally generated carrier can lock on it very accurately. When, however, the incoming signal carrier is contaminated by reflected signals, the locally generated carrier locks onto the composite carrier phase instead of onto the direct one. The difference between the composite carrier phase and the direct carrier phase is the phase measurement error generated by the multipath.

In much of previous research, it is assumed that there is only one dominant reflected signal carrier that contaminates the incoming signal. The numerical discrimination function in PLL can be expressed as:

$$D_r = \arctan(QP/IP) = \arctan\left(\frac{R(\hat{\tau}_c - \tau_0) \sin(\gamma_0 - \hat{\gamma}_c) + \alpha_1 R(\hat{\tau}_c - \tau_1) \sin(\gamma_1 - \hat{\gamma}_c)}{R(\hat{\tau}_c - \tau_0) \cos(\gamma_0 - \hat{\gamma}_c) + \alpha_1 R(\hat{\tau}_c - \tau_1) \cos(\gamma_1 - \hat{\gamma}_c)}\right) \quad (3.5)$$

In order to obtain the best estimate,  $D_r$  should be minimized in the carrier phase tracking loop. Assuming  $\tau_0$  and  $\gamma_0$  to be zero and defining  $\Delta\Psi = \hat{\gamma}_c - \gamma_0$ , Equation 3.5 can be transformed into the following expression:

$$\Delta\Psi = \arctan\left(\frac{\alpha_1 R(\hat{\tau}_c - \tau_1) \sin \gamma_1}{R(\hat{\tau}_c) + \alpha_1 R(\hat{\tau}_c - \tau_1) \cos \gamma_1}\right) \quad (3.6)$$

Since  $\Delta\Psi$  is the difference between the estimated incoming composite signal carrier phase and the direct carrier phase, it actually represents the phase measurement error caused by the multipath. It can be seen that the magnitude of the multipath carrier phase error is a function of the ratio of the direct signal power to the main reflected one, the path delay and the phase of the reflected signal. Stronger reflected signal power leads to a larger multipath error. The larger the multipath delay is, the smaller the correlation value, and so the phase multipath error is reduced. This conclusion indicates that in order to mitigate multipath error, the antenna should be placed far away from potential reflectors. The maximum multipath carrier phase error is one quarter of carrier phase wavelength, since the  $\Delta\Psi$  can only reach  $\pi/2$  in radian. The carrier phase multipath error becomes greatest when the reflected signal is perpendicular to the composite one. For the L1 carrier, the maximum multipath carrier phase error is limited to about 4.8 cm, while for the L2 carrier, the maximum phase multipath error can reach 6.1 cm.

In static mode, the receiver antenna is stationary and the environment is unchanged, therefore the multipath error varies due to satellite dynamics. The relatively slow change of satellite position leads to low-frequency variation of the carrier phase multipath errors. This property also explains the day-to-day repeatability of the carrier phase multipath error. As is known, the GPS satellite constellation has a period of one sidereal day (23 hours 56 minutes 04 seconds), and multipath errors (in both code and carrier phase measurements) therefore repeat after a sidereal day.

In order to show the effect of carrier phase multipath on attitude estimation, a static bi-antenna attitude test was carried out on June 17<sup>th</sup> and 18<sup>th</sup>, 2002 on the roof of the Engineering Building, which can be considered a high multipath environment. Two antennas were mounted rigidly on a metal bar with a separation of 0.92 m. The GPS antennas remained static during the test and the attitude parameters are constant from epoch to epoch. Therefore, it is possible to investigate the multipath effect on the attitude parameters. As mentioned above, satellite geometry repeats day to day and the multipath is closely related to the satellite motion and should have the same periodic repeatability in static mode. Since this research mainly focuses on low-cost solutions for attitude determination, two CMC Allstar receivers were used to collect the raw measurement data. The detailed information of these receivers will be described in the next chapter. The antennas used were NovAtel 501 antennas, which have very good antenna phase centre stability and a high gain at low elevation. Therefore, the antenna phase centre variations can be negligible in this test compared with the multipath effect.

Figure 3.1 shows the heading and pitch from epoch to epoch during the same time on two consecutive days. Most of the time, there were eight satellites visible in the sky. The blue lines show the estimated attitude parameters on the first day, which is intentionally offset by two degrees for clear comparison. The green lines illustrate the corresponding estimates on the second day. Clearly, the variations of the attitude parameters for the two days are quite similar. The computed standard deviations of heading and pitch for the first day are 15.5 and

29.5 arc minutes. For the second day, the standard deviations are 15.2 and 30.2 arc minutes. As the satellite geometry has little impact on low frequency variations in attitude estimation compared with multipath (as will be discussed in next chapter), the repeating patterns of attitude parameter variation stem mainly from the repetition of carrier phase multipath. The red lines in the plots indicate the differences of heading and pitch on the consecutive days. The differences in heading and pitch have zero means and an almost white noise behavior, which indicates that the effects of carrier phase multipath on the attitude estimates are almost identical and successfully cancel out after differencing. The poorer agreement in pitch estimates in the repeatability test is due to the poorer estimation in vertical direction due to geometry limitations.

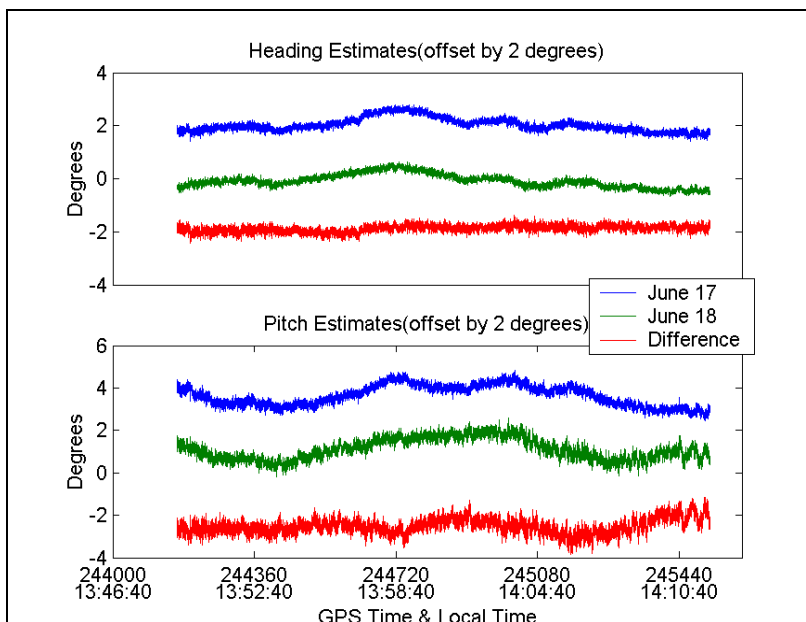


**Figure 3.1: Attitude results in day-to-day test**

In GPS-based attitude determination, the multipath error should be mitigated to as low a level as possible. The simplest approach to reducing the carrier phase multipath is to carefully select the location of antennas. It is always recommended that the GPS antennas be located

where there is no strong reflector nearby and no GPS signal shading or blockage exists. The use of the choke rings or ground plane antennas can reduce the multipath effect and improve the carrier phase measurement by about 30% (Lachapelle et al 1992). Good polarization discrimination and proper antenna gain pattern in high performance antennas can also effectively attenuate multipath effects (Braasch 1996). A direct GPS signal is right-hand circularly polarized electromagnetic wave and a single reflection leads to the signal polarization into the left-hand. Using the polarization discrimination technique, the antenna can largely reject the reflected left-hand circular polarized signal. Since GPS signals from low elevations are more susceptible to multipath, the rejection of GPS signals from near or below the horizon using a ground plane or well-shaped gain pattern, can also mitigate the carrier phase multipath errors.

Another scheme to mitigate carrier phase multipath errors is to estimate or model the multipath errors by using a filter. Ray (2000) used multiple closely-spaced antennas to calculate the parameters in a multipath model and further estimate carrier phase multipath errors. This approach was successfully implemented in static GPS attitude determination (Cannon et al 2000). The RMS of attitude estimates improved 47% after estimating the carrier phase multipath using six antennas with baseline lengths of 8-14 cm. However, the additional hardware cost and the fact that this technique is valid only in static mode limit its general application to attitude determination. Another approach to mitigate carrier phase multipath error in attitude estimation relies on optimal filters. Most filters estimate three angular rates around the attitude axes as well as three Euler angles so as to model the

platform dynamics. Then, an adaptive algorithm is applied to filter out variable multipath errors in carrier phase measurements (Campana and Marradi 1999, Bernelli-Zazzera and Campana 1999). This method is often used in spacecraft attitude determination, as predictable platform dynamics and repeatable multipath environment are obtainable. This method can not however be applied to most land and marine cases.

### ***3.1.2 Antenna phase centre variations***

When tracking RF signals from GPS satellites, the receiver can calculate the range between the satellite and the phase centre of the antenna, and then determine the coordinate of this phase centre in the WGS-84 frame. Conventionally, the GPS antenna phase centre is supposed to be a physical point, such as the geometric centre of the antenna. However, this is not in fact the case as the phase centre will change with the direction of incoming signals. This means that every signal with a different elevation and azimuth may result in a different antenna phase centre. The neglect of this phase centre variation may lead to a baseline error between millimetres and centimetres and it can reach up to 10 cm in vertical direction (Mader 1998). Due to the high accuracy required for GPS-based attitude determination, antenna phase centre variations should be taken into account when examining error sources and their impact on estimated attitude parameters.

The investigation of antenna phase centre variations is quite complicated. As the actual phase centre variation is related to the direction of satellite signals and has repeatability according to the satellite constellation, it is very difficult to isolate antenna phase centre variations from carrier phase multipath errors. Multipath errors should be mostly mitigated or removed from

the carrier phase measurement before exploring possible antenna phase centre variations. Furthermore, the actual phase centre is also a function of antenna type and design. Different antennas have different actual phase centres even for the same GPS signal. In precise GPS positioning, the most common approach is relative field calibration (Mader 1998), which means that the antenna phase centre variation results are relative to the reference one. A choke ring or ground plane is used on both antennas in order to mitigate the carrier phase multipath. An external oscillator is used as a frequency standard for both of the receivers. Since the two antennas are closely spaced, the atmospheric and satellite errors are cancelled out after single differencing of carrier phase measurements. The line bias is ignored when using the same cable type with same lengths at both receivers. The remaining measurement errors are only the relative antenna phase centre variations and the random receiver noise. After filtering the white thermal noise, the low frequency antenna phase centre variations can be easily obtained. Another method is the use of absolute real-time field calibration using a rotor (Schmitz et al 2002). It is assumed that during continuous measurement epochs, the multipath errors are identical. When the GPS antenna rotates with a rotor, only the antenna phase centre variation varies with time. After differencing carrier phase measurements in time, the antenna phase centre variation can be accurately estimated.

The antenna phase centre variations are dependent on the antenna type and internal design. The actual phase centre variations of two different antennas in a common type should be quite similar for this reason assuming a good construction quality. In GPS attitude determination, different types of GPS antennas are not usually used in the single attitude

system. The simplest approach to reducing the antenna phase centre variation effects might be to orient all the antennas in the same way if the non-isotropic effects reproduce from one unit to another. After carrier phase differencing, the impact of antenna phase centre errors can be significantly reduced from the carrier phase measurement in such a case.

### **3.1.3 Receiver noise**

Carrier phase receiver noise represents the measurement error in the phase tracking loops of a GPS receiver. It consists of PLL thermal noise, vibration induced oscillator jitter, Allan deviation induced oscillator jitter and dynamic stress (Ray 2002). As all of these errors are caused by the receiver hardware or algorithms and have a white noise behavior, they are conventionally called receiver noise in general. The empirical equation of the carrier phase tracking error budget can be expressed as (Raquet 2001)

$$\sigma_{PLL} = \sqrt{\sigma_t^2 + \sigma_v^2 + \theta_A^2} + \left| \frac{\theta_e}{3} \right| \leq 15^\circ \quad (3.7)$$

where

$\sigma_{PLL}$  is the standard deviation of PLL tracking error

$\sigma_t$  is the one sigma error due to thermal noise

$\sigma_v$  is the one sigma error due to vibration

$\theta_A$  is the error due to the Allan deviation

$\theta_e$  is the dynamic stress error

The thermal noise is a function of predetection integration time ( $T$ ), the carrier loop noise bandwidth ( $B_n$ ) and the carrier to noise density ratio ( $C/N_0$ ). The thermal noise error in PLL can be represented as (Ray 2002).

$$\sigma_t = \frac{\lambda}{2\pi} \sqrt{\frac{B_n}{C/N_0} \left(1 + \frac{1}{2T(C/N_0)}\right)} \quad (3.8)$$

Note that higher carrier to noise ratio reduces thermal noise error. As the  $C/N_0$  increases with the satellite elevation, the carrier phase measurement from a low elevation angle satellite is noisier than that from a high elevation angle satellite. Sometimes, the PLL thermal noise is treated as the only source of carrier phase tracking error, as the other sources of PLL jitter are transient and negligible (Raquet, 2001).

Addition to thermal noise, the vibration of the receiver oscillator introduces phase noise in the PLLs. The magnitude of this phase noise is proportional to the intensity of the vibration. In some severe environments, it is recommended that the receiver clock be mounted with vibration isolators. The Allan deviation induced phase error is inversely proportional to the bandwidth of the carrier loop noise bandwidth and is important for narrowband PLLs. This phase noise becomes the dominant source when the short-term stability of the oscillator is very poor. Carrier tracking errors due to the dynamics may be caused by real dynamics or dynamic stress due to the local oscillator. PLLs are more vulnerable to dynamic stress compared to code tracking loop; in the same dynamics, the change of loop bandwidth in the PLL is much larger than that in the code tracking loop.

After analyzing the different phase noise in the carrier tracking loops, it is found that receiver noise is closely correlated with receiver dynamics. If the GPS receiver is stationary, a very narrow carrier loop bandwidth is used in the PLL and there is no vibration and dynamics stress, the overall receiver noise is fairly low. When the receiver dynamics is high, the carrier tracking loop bandwidth automatically increases according to the dynamics, which eventually leads to large thermal noise. Together with the oscillator vibration and intensive dynamic stress, the phase noise becomes higher. The carrier phase noise level in static mode is less than 1 mm (Raquet 1998) but this value can reach several millimetres in high dynamics (Axelrad and Ward 1994).

### **3.2 Operational factors**

Besides GPS measurement errors in the carrier phase observables, there are also some operational features that affect attitude estimation accuracy. These factors are the number of satellites, their geometry, inter-antenna distance and antenna array configuration. The above-mentioned factors are discussed below.

#### ***3.2.1 Impact of satellite number and geometry***

In any GPS application, the number and distribution of observed satellites affect the accuracy of the solution. Each range measurement to a GPS satellite is treated as an observation when computing the coordinates of the antenna. An additional satellite observation increases the measurement redundancy by one. The addition of good observations inevitably improves the accuracy of GPS positioning since the accuracy level of unknown estimates can be increased with an increase in the number of good measurements. Meanwhile, the relative locations of

GPS satellites also affect the performance of GPS (Parkinson and Enge 1996). The satellite geometry is measured through the Dilution of Precision (DOP). By multiplying the standard deviation of carrier phase measurements with the DOP value, the estimation accuracy from GPS can be obtained. In GPS attitude determination, there are several types of DOPs to specify the estimated accuracy of attitude parameters. Hayward et al (1997) and Gomez (2000) used ADOP (Attitude Dilution of Precision) to define the solution accuracy using the direct attitude estimation method. When attitude parameters are estimated from vector observations using GPS, AZ-DOP (Azimuth DOP) and El-DOP (Elevation DOP) are commonly used to manifest the impact of satellite geometry on estimation of attitude parameters (Lu 1994, El-Mowafy 1994). Lower AZ-DOP leads to better azimuth determination. Similarly, the smaller El-DOP is, the more accurate the estimation of pitch and roll will be. AZ-DOP and El-DOP can be calculated from Relative Northing DOP (RNDOP), Relative Easting DOP (REDOP) and Relative Vertical DOP (RVDOP) in the local level frame. The explicit forms of these two DOPs are given as

$$AZDOP = \sqrt{\cos^2(\psi)RNDOP^2 + \sin^2(\psi)REDOP^2} \quad (3.9)$$

$$ElDOP = \sqrt{\cos^2(\theta)RVDOP^2 + \sin^2(\theta)AZDOP^2} \quad (3.10)$$

One hardware simulation test was carried out to show the impact of satellite number and geometry on the accuracy of GPS-based attitude determination. A two-antenna attitude determination system was simulated with the Spirent STR-4760 simulator. The advantages of using the hardware simulator are to isolate the multipath and antenna phase centre errors from the carrier phase measurements and to make it possible to investigate satellite constellation effects on attitude estimation accuracy. There are about 1800 epochs (30

minutes) of data and the accuracy is represented by the Root Mean Square (RMS) of the estimated attitude parameters. The true heading and pitch of the platform are set to zero during the test. The original satellite number was 7 during the test. After estimating the attitude parameters in HeadRT+™ using the full constellation, one satellite was intentionally removed and the attitude parameters were re-estimated in the software. Such procedure was repeated until the satellite number dropped to four.

The results in Figures 3.2 to 3.5 show that, with the decrease of the available number of satellites, the AZ-DOP and El-DOP values increase accordingly and the attitude estimates become poorer. The RMS of heading in Table 3.1 degrades 60% when the available satellite number drops from 7 to 4, while degradation in pitch is more than 150%. The difference of degradation in two dimensions is mainly caused by the distribution of the satellites and the geometry of the antenna array. The GPS positioning is essentially a resection problem and the solution accuracy is highly related to the distribution of known points (GPS satellites). The visible satellites may be evenly distributed in azimuth but their elevation angles are always positive. Therefore, the estimation in the vertical direction using GPS range measurements is therefore poorer than in the horizontal direction. Furthermore, when the platform is horizontally placed, the vertical uncertainty has the maximum influence on pitch estimation.

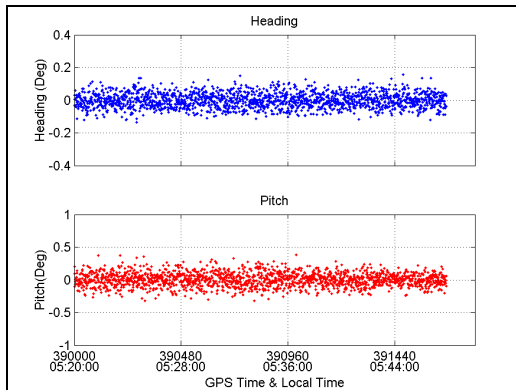


Figure 3.2: Attitude estimation using 7 satellites

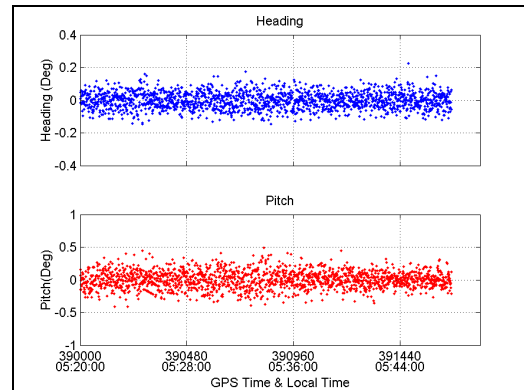


Figure 3.3: Attitude estimation using 6 satellites

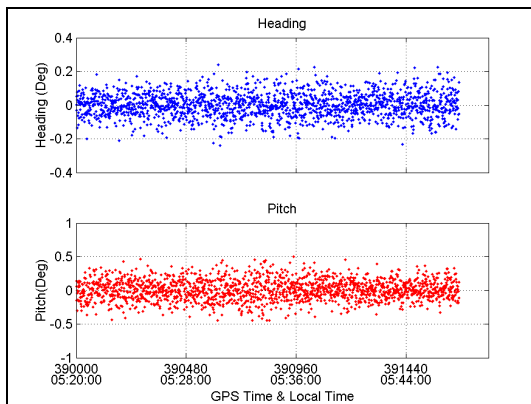


Figure 3.4: Attitude estimation using 5 satellites

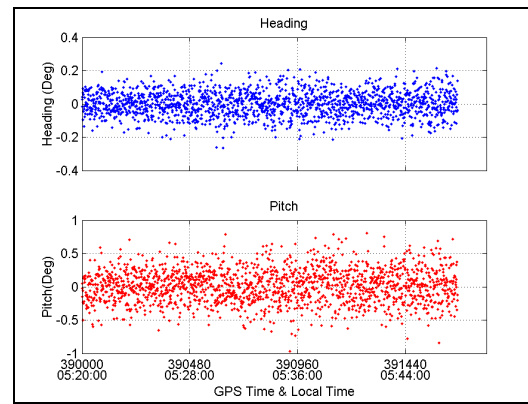


Figure 3.5: Attitude estimation using 4 satellites

Table 3.1: Attitude estimation accuracy versus satellite number and geometry

	Heading RMS (deg)	Pitch RMS (deg)	Average AZ-DOP	Average EI-DOP
7 SV	0.046	0.106	2.28	4.42
6 SV	0.051	0.131	3.24	5.56
5 SV	0.072	0.154	4.23	6.26
4 SV	0.074	0.251	5.79	10.61

### 3.2.2 Antenna array configuration

The accuracy of attitude parameter estimation is also related to the inter-antenna distance, the number of antennas and the geometry of the antenna array. The simplest way to dilute the

impact of ranging errors and thus to improve the accuracy of attitude estimation is to increase the inter-antenna distance. Figure 3.6 shows that the estimation accuracy of heading and pitch improves with the increase of inter-antenna distance using medium performance GPS receivers. It can also be found that when the antenna separation becomes larger the enhancement in pitch estimation is more significant than that in heading. However, the extension of inter-antenna distance has a negative effect on ambiguity resolution. The ambiguity search region expands dramatically with the extension of inter-antenna distance, which inevitably leads to an increased complexity in ambiguity identification as well as to a larger consumption of computational power.

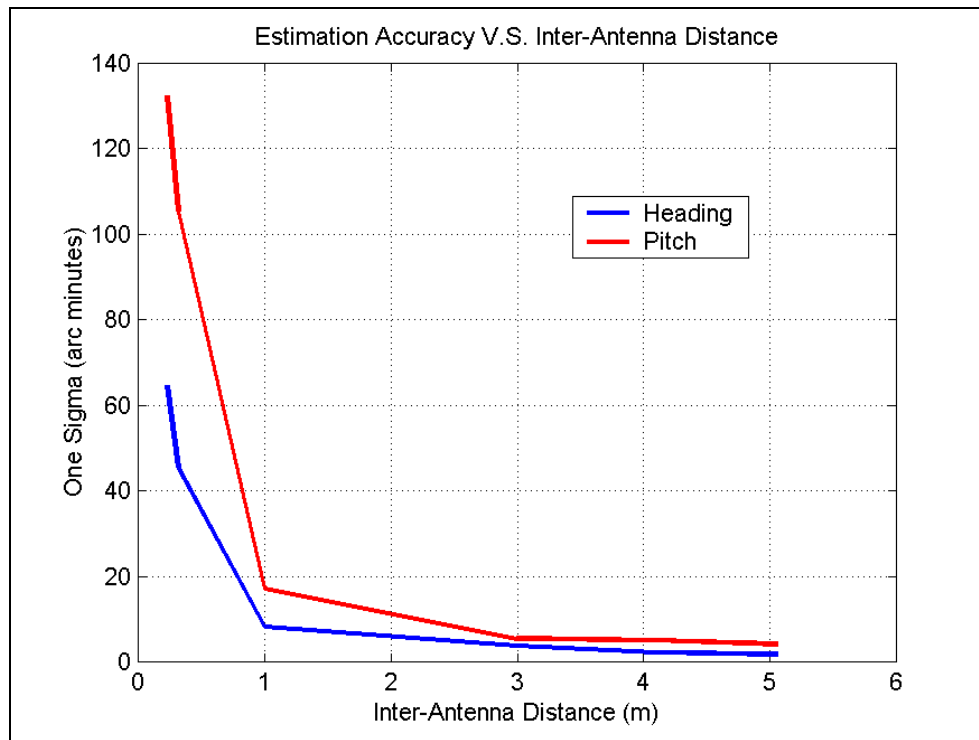


**Figure 3.6: Attitude estimation accuracy versus inter-antenna distance for medium performance receiver**

Another factor that affects the accuracy and reliability of attitude estimation is the number of GPS antennas. A bi-antenna system can only provide 2-D attitude parameters, namely heading (yaw) and pitch. A third antenna must be used if 3-D attitude parameters of the platform are required. Adding redundant antennas in the attitude system may significantly increase the availability and reliability of the attitude system. The improvement in estimation accuracy is found negligible compared to the additional hardware cost (Ueno et al 1997). A four-antenna attitude system has proven to be the best compromise solution to balance overall performance and hardware cost. Besides antenna number, the geometry of antenna array also influences the performance of attitude estimation. El-Mowafy (1994) pointed out that enlarging the height difference between antennas increases the accuracy of estimated attitude parameters. The optimal antenna configuration for attitude determination is discussed by Cohen (1992), Comp (1993) and El-Mowafy (1994). It is said that when the four antennas form a orthogonal triad, meaning that the three antenna vectors from the primary antenna to the secondary ones have the same length and are orthogonal to each other, the accuracy of three attitude parameters will be the best. In practice, this kind of optimal antenna configuration is very difficult to implement due to the location limitation of antennas on the platform, especially in vehicular kinematic navigation. It may only be useful as a prototype during the antenna setup and testing process.

## **CHAPTER 4**

### **ATTITUDE DETERMINATION USING LOW-COST RECEIVERS**

In this chapter, the feasibility of using low-cost CMC Allstar sensors for attitude determination is extensively investigated. The performance of attitude estimation using this kind of GPS receiver is examined in both hardware simulations and real field tests. Different types of low-cost GPS antennas are employed in the attitude system to show multipath and antenna phase centre variation effects on the accuracy of attitude estimation. The synchronization problem of carrier phase measurements from low-cost receivers is discussed. The impact of time offset on attitude estimation is also examined in detail.

#### **4.1 Introduction of CMC Allstar receiver**

The low-cost GPS sensor selected in this research is the CMC Allstar unit, a GPS OEM receiver card manufactured by Canadian Marconi Company. This is a 12-channel single frequency GPS receiver that offers competitive performance at a reasonable price (from 100 to 320 US dollars). This receiver can operate properly with signal levels from  $-165$  dBW to  $-120$  dBW. It can track the GPS signal with a minimum carrier to noise density ratio of 31dB-Hz. The complete position, velocity and time (PVT) solution is computed and output at a frequency up to 5 Hz. The compact size and low power consumption of the receiver make it appropriate for kinematic applications. The general specifications of this receiver can be found in Table 4.1 (Marconi Electronics 2000).

**Table 4.1: CMC Allstar Specifications**

<b>Specification</b>	<b>CMC Allstar</b>
Frequency	L1
Channels	12
Interface	RS232
WAAS Compatibility	Yes
PVT Data Rate	1 Hz / 2 Hz / 5 Hz
Raw Data Rate	1 Hz / 2Hz / 5 Hz / 10 Hz
Acquisition Sensitivity	34 dB-Hz
Tracking Sensitivity	31 dB-Hz
Operation Temperature	-30 °C to 75 °C
Size (OEM Board only)	10.2 cm X 6.7 cm X 1.4 cm
Weight (OEM Board only)	50 grams
Power Consumption	1.4 w
Maximum Velocity	514 m/s
Maximum Acceleration	4 g
Maximum Jerk	2 m/s <sup>3</sup>

The CMC Allstar receiver can output raw measurements up to 10 Hz through a RS232 port at a baud rate of 38400. The raw binary carrier phase measurement consists of PRN number, C/A code range and L1 carrier phase, carrier to noise density ratio and cycle slip counter. The noise level of code ranges was found to be about 0.5 m and the carrier phase noise is within 1 mm (Dumaine 1996). The high frequency accurate carrier phase measurements from the receiver and the low-cost of hardware allows for a wide application of the CMC Allstar receiver in precise GPS positioning and navigation. In recent years, the utilization of this low-cost GPS sensor in attitude determination has been investigated for vehicular and aircraft navigation (Vinnins and Gallop 1997, Hayward et al 1997, Alban 2002, Hoyle et al 2002, Wang and Lachapelle 2002).

As the CMC Allstar receiver does not output the raw Doppler measurement, the carrier phase velocity is calculated based on the carrier phase measurements from two previous epochs as.

$$\dot{\Phi}_k = \frac{\Phi_{k-1} - \Phi_{k-2}}{\Delta t} \quad (4.1)$$

The predicted Doppler measurement is not very accurate compared to the raw output, especially in kinematic conditions. Therefore, the phase prediction method for cycle slip detection is ineffective to detect small cycle slips for CMC receivers.

#### **4.2 Performance of attitude estimation in the presence of noise**

The performance of GPS is highly dependent on the hardware involved, the test environment and the receiver dynamics. In order to identify the effect of each error source, different tests were conducted to isolate them. First of all, The CMC-based attitude determination has been examined with the help of a Spirent STR-4760 (Global Simulation Systems 2000) hardware simulator. This hardware-in-loop test can be used to assess receiver noise and the impact of dynamics without the multipath and antenna phase centre variation errors.

The first hardware simulation test was carried out in static mode to test receiver noise effects on attitude estimation. In this test, a dual-antenna system was set up with an inter-antenna distance of 1 m and the true heading and pitch were fixed to zero. Another attitude system with high-quality NovAtel OEM4 receivers was used as the reference for performance comparison. The GPS RF signal from the hardware simulator was split and then fed into the NovAtel OEM4 attitude system and CMC Allstar attitude system simultaneously. The detailed setup of the test is illustrated in Figure 4.1. The attitude parameters were computed

with HeadRT+™ in real time. In this test, double difference ambiguities were correctly determined in a single epoch for both attitude systems. The attitude results and their statistics from the two systems are shown in Figure 4.2 and Table 4.2. The estimated attitude parameters using OEM4 receivers are intentionally offset by -40 arcmins for better visualization in Figure 4.2. It can be seen that compared with the high performance receivers, the carrier phase measurements from the CMC Allstar receiver have comparable noise level. The RMS of the attitude estimates from the Allstar system were 3.25 arc minutes for heading and 8.46 arc minutes for pitch. These values were only about 15% larger than the corresponding statistics using the OEM4 receivers. The low-cost Allstar receivers had fairly stable carrier phase measurements in this benign environment. Considering the short inter-antenna distance in this test and the fact that 1 mm measurement error leads to an attitude error of 3.4 arc minutes, the impact of receiver noise from the CMC Allstar receivers on attitude estimation can be considered negligible compared to other error sources. From the mean error values, one can see the attitude estimates from the Allstar system was a little biased from the true value. The main reason for that comes from the misalignment of receiver timing systems as discussed in Section 4.4.

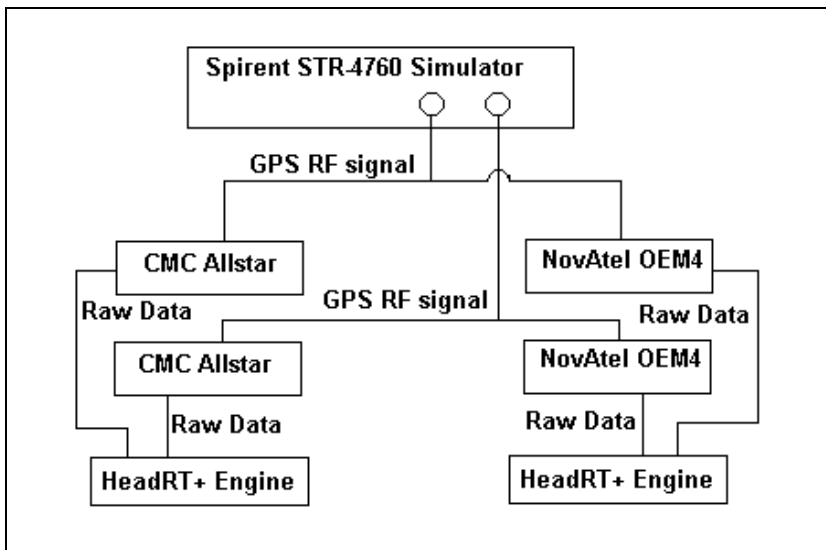


Figure 4.1: System setup in dual-antenna hardware simulation test

Table 4.2: Statistics of attitude estimates in static dual antenna simulation test

Statistics	Heading (arc minutes)		Pitch (arc minutes)	
	Mean	RMS	Mean	RMS
CMC Allstar	-0.7	3.2	-3.1	7.6
NovAtel OEM4	0.0	2.8	0.2	6.6

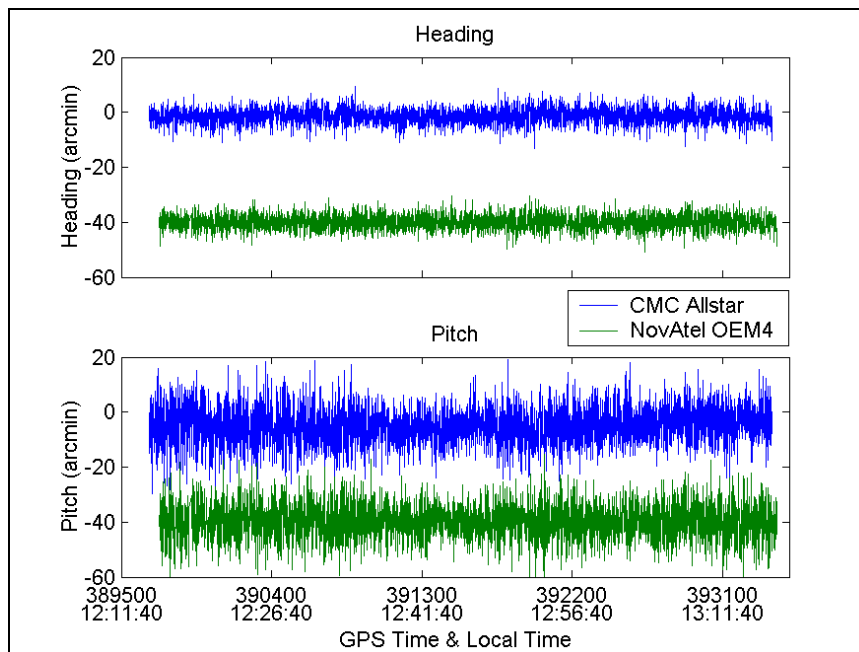
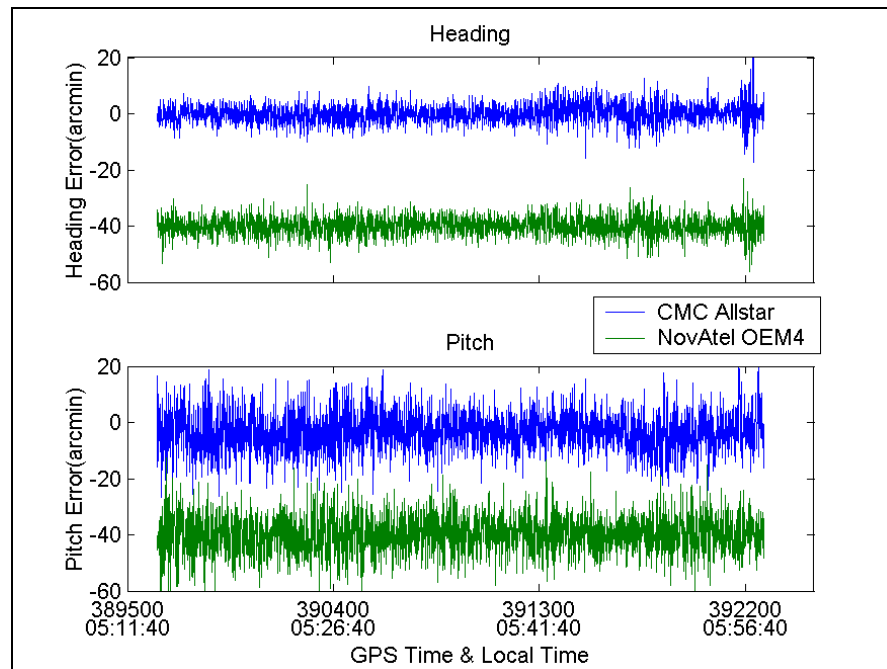


Figure 4.2: Attitude estimates in static dual-antenna simulation test

A similar kinematic test was carried out on the hardware simulator to examine the performance of tracking loops in dynamic mode. The setup was identical to that in the static one. The trajectory of the simulation test consisted of some straight and turning sections, with the velocity ranging from 30 km/h to 100 km/h. At the end of test, a downhill and uphill trajectory was simulated to introduce changes in pitch. The estimated attitude parameters could then be compared with true values and the estimation errors could be calculated. The test result in Figure 4.3 (the attitude estimates using OEM4 are offset by -40 arcmins for comparison as well) shows that attitude estimation errors due to receiver noise were quite small and have white-noise-like behavior for both receiver pairs. In vehicular dynamic conditions, the carrier tracking loops of the low-cost Allstar receivers can achieve performance similar to those of the NovAtel OEM4 receivers. No discernible degradation of attitude estimation could be observed in kinematic conditions. Still, the pitch estimate average using Allstar receivers was biased with a magnitude of 3.3 arc minutes in this kinematic test.

**Table 4.3: Statistics of attitude estimates in kinematic dual-antenna simulation test**

Statistics	Heading (arc minutes)		Pitch (arc minutes)	
	Mean	RMS	Mean	RMS
CMC Allstar	-0.1	3.5	-3.3	7.9
NovAtel OEM4	-0.1	3.4	0.2	6.9



**Figure 4.3: Attitude estimation errors in kinematic dual-antenna simulation test**

Some other kinematic hardware simulation tests were conducted to investigate the performance of the Allstar receivers in high dynamics with a linear velocity of up to 200 m/s and an acceleration of up to 3 g. The results indicate that the tracking loops have stable performance under these dynamics, and the accuracy and the reliability of the Allstar-based attitude determination system are fairly consistent.

Based on the results of the above tests, the following conclusions about the CMC Allstar receiver can be drawn: 1) Without multipath and antenna phase centre variations, the low-cost Allstar receivers performs similiarly to the high-end GPS receivers. 2) The carrier tracking loops have quite small noise levels and are not sensitive to the dynamics in vehicular-based applications. However, the impact of receiver vibration and jerk introduced by high dynamics on the receiver is unknown so far.

### 4.3 GPS antennas

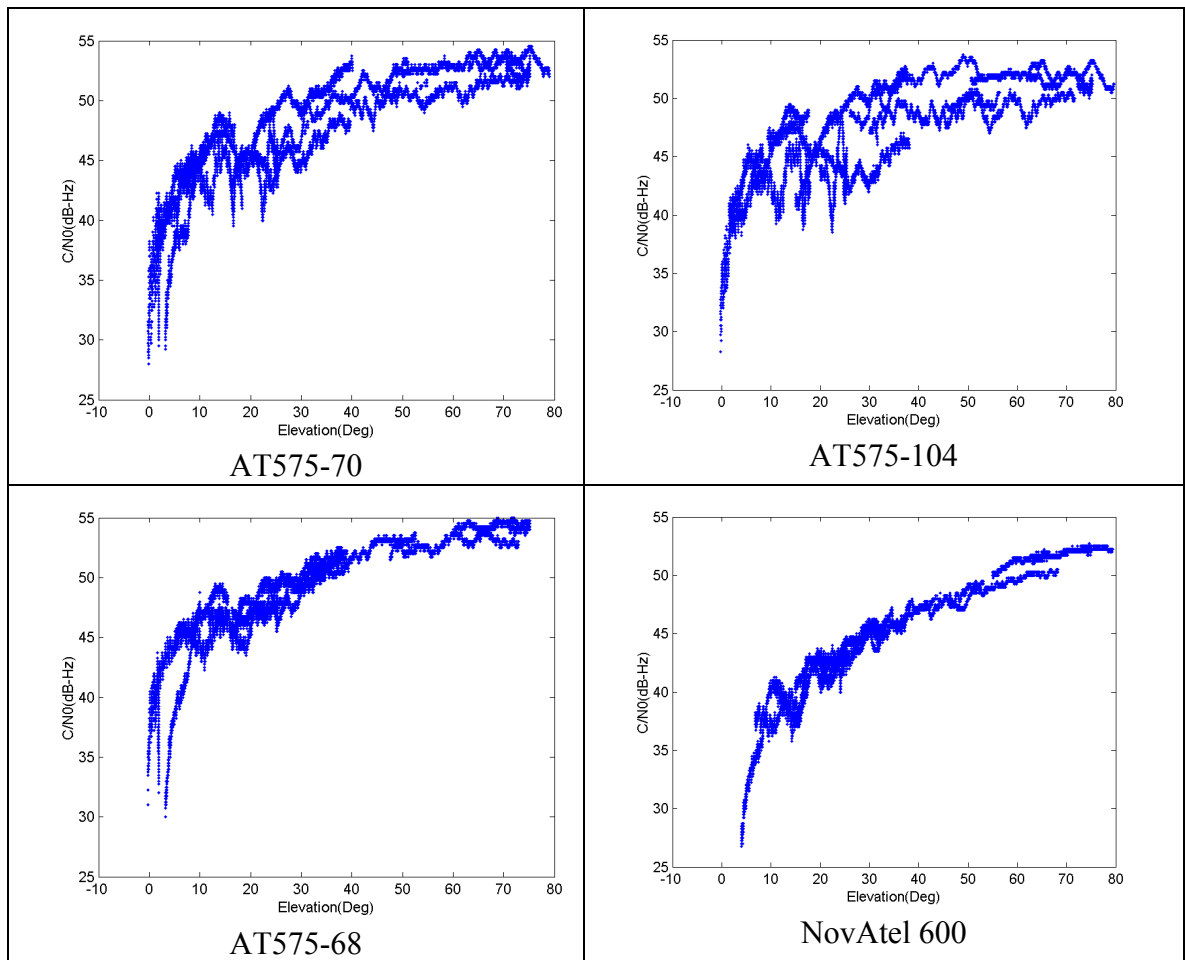
In addition to receiver hardware, the performance of GPS precise positioning and navigation relies heavily on the antenna at the receiver end. High performance antennas not only significantly mitigate the multipath effect on the carrier phase measurements, but also have a very stable antenna phase centre. It is always suggested that high-end antennas be used in GPS-based attitude determination systems in order to alleviate the carrier phase multipath and improve the accuracy of attitude estimates. In this research, however, a low-cost hardware solution is the ultimate objective and the high-end antennas are merely used as the reference for performance comparison. Consequently, only low-cost GPS antennas are of interest and employed to assemble the attitude system.

The CMC Allstar receiver supports a broad range of antennas, both active and passive. Some low-cost antennas recommended by the CMC Allstar manufacturer are investigated. These low-cost antennas are specially selected for different applications. The AT575-70 antenna is designed for vehicular-based usage. It is very compact in size (3 cm in diameter) and has a magnetic mount. The AT575-68 antenna is used for marine applications and its special design can effectively mitigate multipath from the sea surface. The diameter of this antenna type is about 5 cm. The AT575-104 antenna is the lowest-cost active antenna for Automatic Vehicular Location (AVL) with a diameter of 5 cm. The three antenna types used here are shown together with high performance NovAtel 600 antennas in Figure 4.4.



**Figure 4.4: Different antennas used in the test**

In order to examine these three low-cost antennas for attitude estimation, a day-to-day repetition test was carried out. During four consecutive days, one pair of each type of antennas together with high performance NovAtel 600 antennas were used with CMC Allstar receivers to collect static data at the same sidereal time on the roof of the Engineering Building at the University of Calgary. The locations of the two antennas in the four tests were fixed and the inter-antenna distance was 0.915 m. Therefore, it can be assumed that the test conditions of the four tests are more or less identical. Since the same GPS receivers were used in the tests, differences in the attitude estimation performance are dependent solely on the GPS antennas. As pointed out by Ray (2000), GPS signal power is highly correlated with the direction of satellite signals and antenna gain pattern, in which satellite elevation has the most significant impact on signal strength. With the existence of multipath, the measured signal power is the composite strength of direct and reflected signals, which attenuates the dependency of signal strength on satellite elevation.



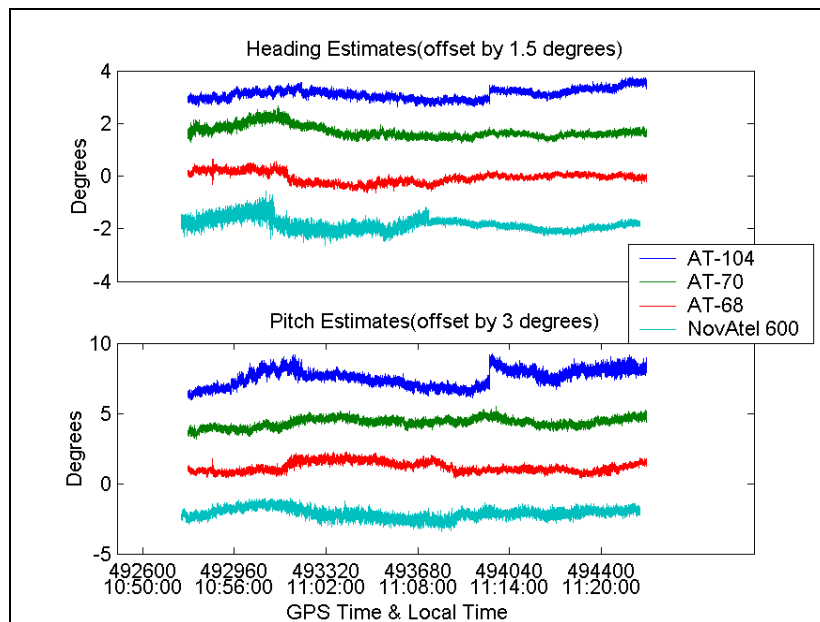
**Figure 4.5: SNR versus Elevation**

Figure 4.5 illustrates the carrier to noise density ratio ( $C/N_0$ ) of GPS signals with regard to satellite elevation using different antennas. The relatively low high frequency variations in the NovAtel 600 plot indicate that the carrier to noise density ratio depends heavily on satellite elevation and the multipath is effectively mitigated by the antenna. The AT575-68 marine-based antenna also has a satisfactory performance in alleviating the multipath effect. This may be due to its special design to reject multipath. As a vehicular based active antenna, the AT575-70 antenna has relatively poor performance in mitigating multipath in that the carrier to noise density ratio has a very loose correlation with the elevation angle, which

indicates that the multipath signal has contaminated the signal power of the direct one. Compared to the other three antennas, the AT575-104 antenna suffered severely from multipath, and the carrier to noise density ratio has a wide spread with respect to the elevation angle. Taking price into consideration, the performance of these antennas is quite reasonable.

Following the above analysis, the data was processed with HeadRT+<sup>TM</sup> to compute the attitude parameters in post mission. The performance of attitude estimation using different antennas is shown in Figure 4.6. The attitude parameter patterns vary with the antennas used. The difference in attitude estimation is mainly due to the differences in multipath effects, antenna phase centre variations and antenna gain pattern. The noticeable jump in the attitude parameters using AT575-104 antennas is caused by the change of satellites. The loss of low elevation PRN 30 at the epoch 493962 induces the jumps in both heading and pitch components. The drop of this satellite has two significant impacts. Since the GPS signal from a low elevation satellite is more subject to the multipath and antenna phase centre variations, the removal of this error-contaminated observation in the least squares estimation will inevitably lead to a change in estimated results. In addition, the loss of a redundant measurement may lead to a significant change of satellite geometry and distinctly affects the accuracy of estimation. Using the other antennas, however, no visible jumps can be found when PRN 30 drops below the mask angle, which indicates that the jump in attitude estimates with the AT575-104 antennas is mainly caused by multipath or/and antenna phase centre error in PRN 30. The attitude estimate patterns using the AT575-70 and AT575-68

antennas are similar compared to the others, since the number of tracked satellites and geometry are much more similar. The NovAtel 600 antenna has very good performance in multipath mitigation with its special gain pattern to reject the satellite signals from the horizon or with low elevation angles. This feature of the NovAtel 600 antenna however leads to fewer visible satellites in the first half of the test, and attitude estimates are noisier than in the second half.



**Figure 4.6: Attitude estimation using different antennas**

Figure 4.7 shows the RMS of double difference residuals at time series. These statistical values can be used as quantities to indicate the magnitude of measurement errors, such as multipath and antenna phase centre variations in the carrier phase. The RMS values of double difference residuals using AT575-104 antennas are fairly large and their mean during the test is 9.0 mm. Using AT575-104 antennas, poor antenna phase centre stability and multipath effects severely deteriorate the carrier phase measurements. The carrier phase measurements using the AT575-70 antennas have smaller errors and the mean of the double difference

residual RMS is only half of that using the AT575-104 antennas. The carrier phase measurement errors using AT575-68 antennas remain quite small and the RMS of double difference residuals are quite small during the test with a mean value of only 3.0 mm. This marine-based antenna can effectively alleviate multipath. The high performance NovAtel 600 antenna performs very well in the test and the RMS values of the double difference residuals are very small and stable. The above results show high consistency with the previous conclusions based on the  $C/N_0$ .

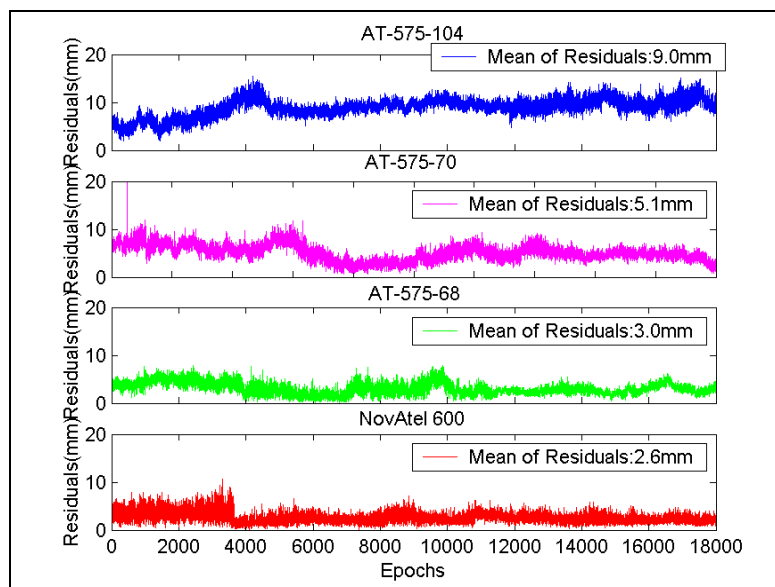


**Figure 4.7: RMS values of double difference residuals**

In order to identify the multipath and antenna phase centre variation effects on attitude estimation, the elevation mask angle has been increased from the default 7.5 degrees to 10 and 15 degrees respectively when processing these data sets here. The NovAtel 501 antenna, which has a stable antenna phase centre but limited multipath mitigation capability, was also used during the same sidereal time on another day for performance comparison. Among these antennas, the NovAtel 600 has a very good phase centre stability and a well-shaped gain

pattern to reject satellite signals with low elevation angles. With the increase of masking angle, the number of useful satellites decreases accordingly. However, there is no obvious change in attitude estimates shown in Figure 4.8, which indicates that the increase in satellite number and better geometry have an insignificant impact on attitude estimation with reasonable satellite distribution. The performance of attitude estimation using NovAtel 501 antennas is shown in Figure 4.9. The jumps in attitude estimates are related with the loss of PRN 30 accordingly at different epochs (GPS time 493944 s with a mask angle of 7.5 degrees and GPS time 493561 s with a mask angle of 10 degrees). Since this kind of antenna has a very good antenna phase stability, it can be concluded that the jumps are due to strong multipath effect on GPS signal from PRN 30. Figure 4.10 shows the attitude parameters as well as the satellite number using the low-cost AT575-104 antennas. It can be seen that with the increase of masking angles, carrier phase measurements from PRN 30 have been deleted from the attitude estimation at different epochs (GPS time 235470 s with a mask angle of 7.5 degrees and GPS time 235088 s with a mask angle of 10 degrees). These lead to the sudden jumps of attitude estimates happening at these epochs. When using the AT575-104 antennas, multipath, rather than antenna phase centre variations, is the dominant error source in carrier phase measurements. However, the antenna phase centre variations are highly antenna dependent. Previous research (Wang and Lachapelle 2002) shows that some very low-cost antennas are heavily affected by phase centre variations as well as multipath, and double differenced carrier phase measurement errors can reach up to 8 cm.

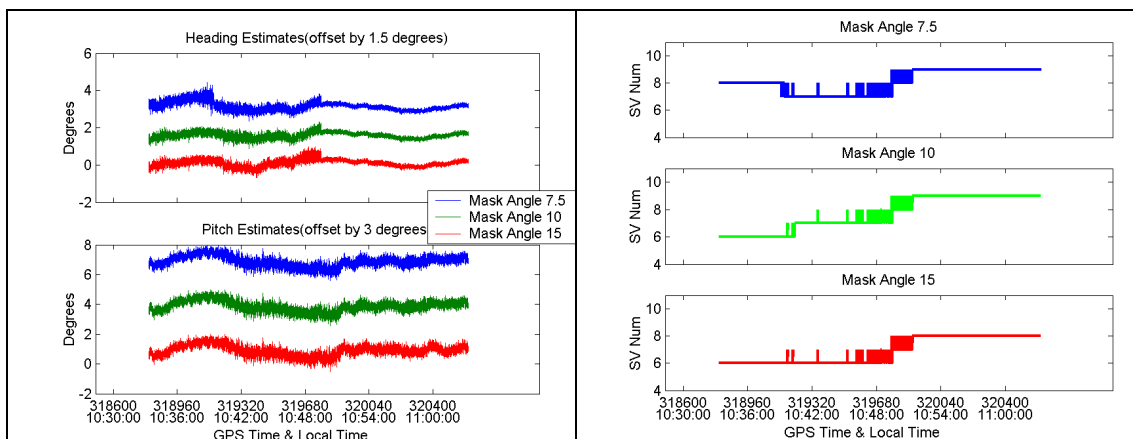


Figure 4.8: Attitude estimates and satellite number using NovAtel 600 antennas

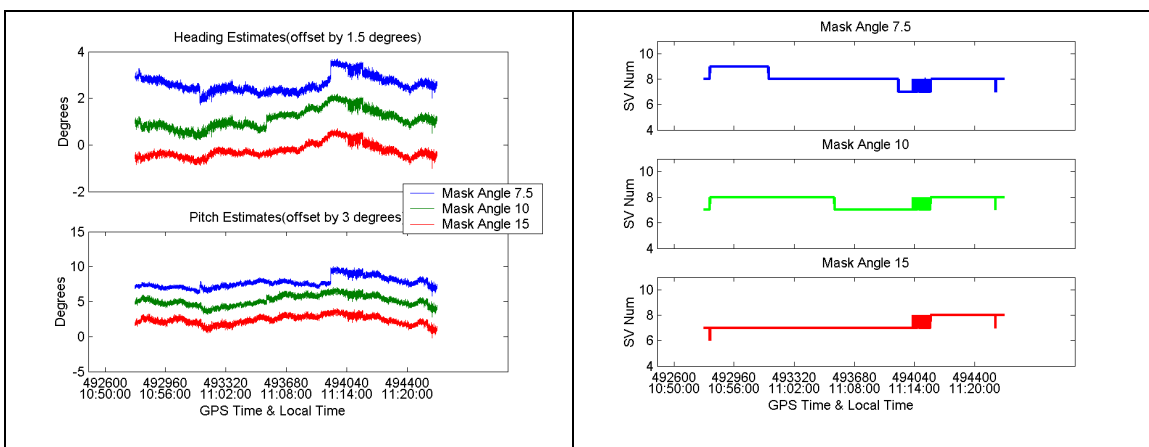


Figure 4.9: Attitude estimates and satellite number using NovAtel 501 antennas

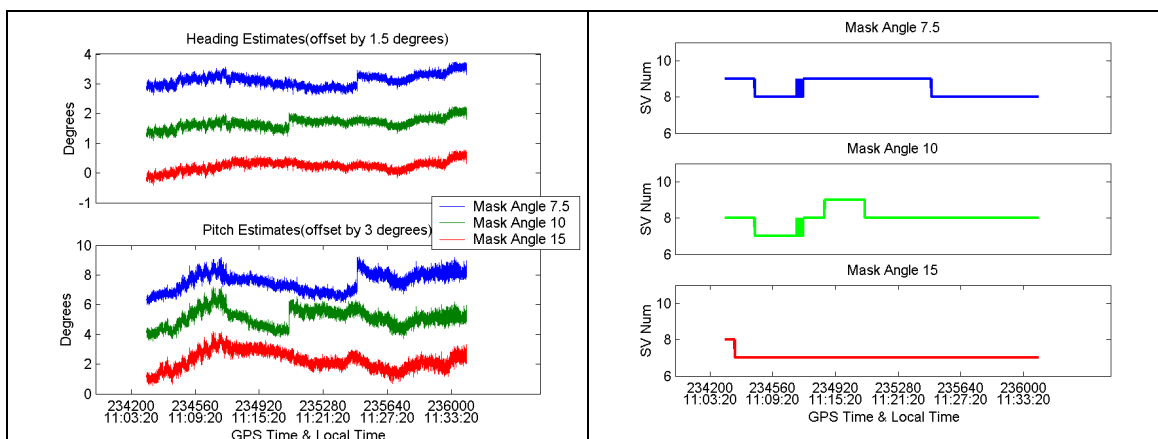


Figure 4.10: Attitude estimates and satellite number using AT575-104 antennas

From the above findings, one can conclude that the antennas play a vital roll in attitude estimation using low-cost GPS sensors. A good GPS antenna with a stable antenna phase centre and well-shaped antenna gain pattern can effectively mitigate measurement errors. With low-cost antennas, multipath and antenna phase centre variations may lead to large carrier phase measurement errors. In most cases, multipath is the dominant error affecting the performance of low-cost antennas.

#### **4.4 Carrier phase data synchronization**

When forming double difference observables, it is always assumed that carrier phase measurements are well time synchronized. Under this assumption, satellite clock errors can be entirely cancelled out. Using low-cost GPS hardware, however, the receiver clock misalignment can easily reach a few ms because the local oscillator of the receiver is not calibrated at every epoch unless the clock drift reaches a certain limit (Hoyle et al 2002). Consequently, some low-cost receivers do not maintain very accurate time synchronization of carrier phase measurements due to the heavy computation load required for calibration. If the misalignment between receivers is large, the high frequency variations of clock drift cannot be eliminated, and a bias occurs in the double difference carrier phase observables. In this section, the effect of receiver misalignment on double difference measurements and attitude estimation will be discussed at length.

A double difference observable is the linear combination of carrier phase measurements at a single epoch. The precise carrier phase time synchronization is a prerequisite in order to achieve high carrier phase positioning accuracy. The satellite clock errors in the

measurements from two receivers are identical at the same epoch and can entirely be removed after differencing between the receivers. For most high-performance GPS receivers, this is not a critical problem, as the local clock is slewed to the high-accuracy GPS time at every epoch. Using low-cost receivers, however, if the clock error is not calibrated at each epoch until drifting to a certain limit, the misalignment between two receivers may reach up to several ms. Then the scenario shown in Figure 4.11 occurs. During the time offset between two receivers, the satellite SV1 moves from Position 1 to Position 1A and the location of SV 2 changes from Position 2 to Position 2A. The change of the location will lead to two kinds of measurement errors in carrier phase observables. The first is an orbital error, as the receiver is still using the nominal epoch to calculate the satellite positions (Positions 1 and 2) while the actual locations of satellites are at 1A and 2A. As the GPS satellites fly on orbit with a linear velocity of about 4 km/s, 1 ms misalignment may result in a 4 m satellite orbit error. The second type of errors is the clock drift during this short interval. The magnitude of this error is highly related to the stability of clocks. In kinematic applications, the clock misalignment will also introduce errors in attitude estimation (Hoyle et al 2002).

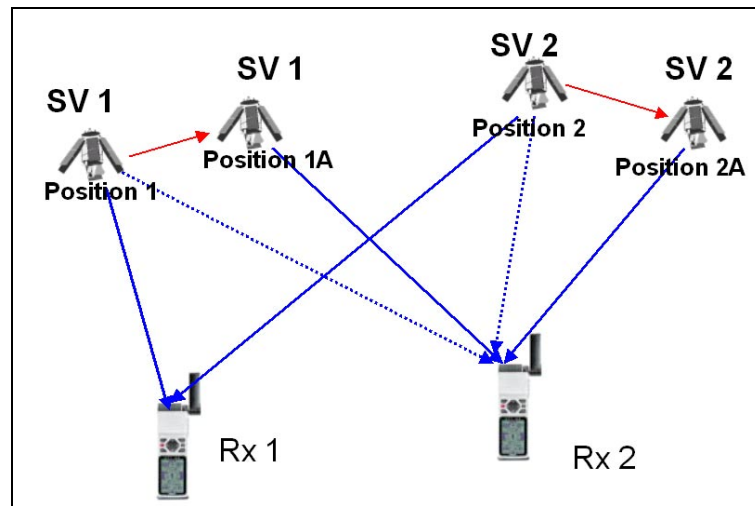


**Figure 4.11: Double difference combination**

In order to investigate the effect of receiver clock misalignment on attitude estimation, a static test was carried out. A dual antenna attitude system was set up with an inter-antenna distance of 0.92 m, using CMC Allstar receivers and AT575-70 antennas. The coordinates of the antennas were accurately determined by the traditional precise survey method. The raw measurements from the receivers was logged at 10 Hz. First, the time-synchronized data from the two receivers were processed in HeadRT+™ and the double difference residuals of satellite pairs were recorded. Then, the carrier phase measurements from one receiver were intentionally shifted by 0.1 second to simulate receiver clock misalignment when forming double difference observables. After the double difference residuals and the attitude estimates from HeadRT+™ were calculated, the above procedure was repeated with the time offset of 0.2 and 0.5 seconds. The double difference residuals for satellite pair PRN 24-PRN 5 are shown in Figure 4.12. The DD residuals for different receiver clock offsets are artificially offset by -1 cm to avoid overlapping each other. It can be seen in the figure that the residuals patterns are very similar to each other and the statistics of residuals in Table 4.4

have little variation between the four runs. However, the means of the DD residuals indicate that the residuals patterns shift downward with respect to the time offset in this plot. This shift is caused by the bias introduced by receiver misalignment in the DD carrier phase observables. Based on the results of DD residuals for other satellite pairs (see Appendix A), it is found that the offset of residuals varies with the satellite pairs.

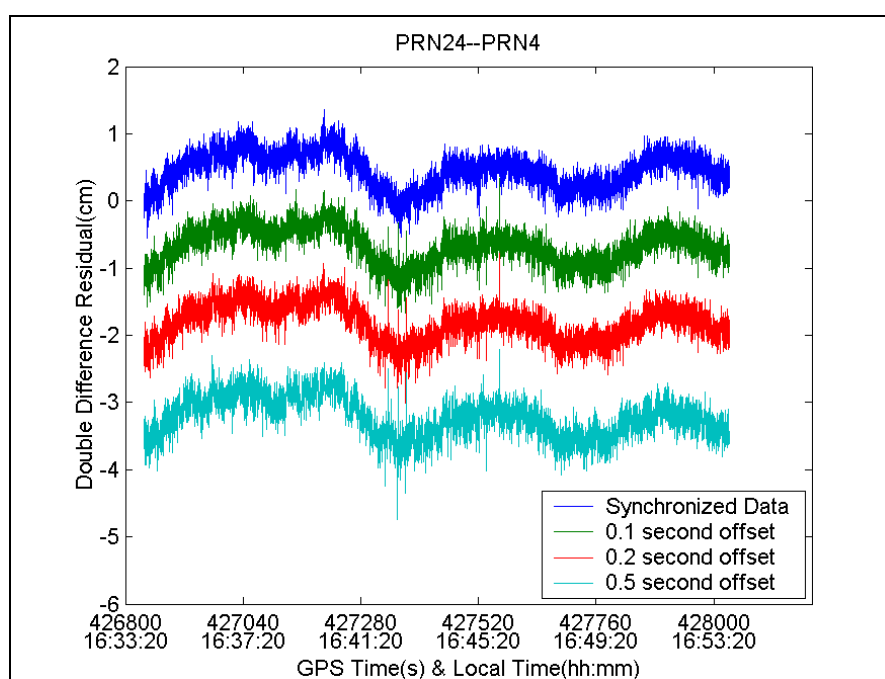


**Figure 4.12: Double difference residuals for PRN 24 -- PRN 4**

**Table 4.4: Statistics of double difference residuals (PRN 24 -- PRN 4)**

	Mean (cm)	STD (cm)	RMS (cm)	MIN (cm)	MAX (cm)
Synchronized	0.5	0.3	0.5	-0.6	1.4
0.1 s offset	0.3	0.3	0.4	-0.7	1.3
0.2 s offset	0.2	0.3	0.3	-1.0	1.2
0.5 s offset	-0.2	0.3	0.4	-1.7	0.8

The attitude results using the time-offset data are plotted in Figure 4.13 and the corresponding statistics are listed in Table 4.5. With the increase of time offset between

receivers, the variation patterns of attitude estimates are very similar with the synchronized results and the standard deviations of heading and pitch vary with the magnitude of 1-2 arc minutes. The mean values show that the bias introduced by the time offset is only up to 3 arc minutes in heading, and its impact on attitude determination can be negligible. However, the misalignment-induced bias in pitch is much more significant than in heading. It progresses to 0.46 degrees when the time-offset reaches 0.5 seconds. Since the measurement error has a much more severe impact on the vertical direction than on horizontal plane, and the pitch estimate totally depends on accuracy of the vertical component, pitch estimate is more sensitive to the bias induced by receiver misalignment.

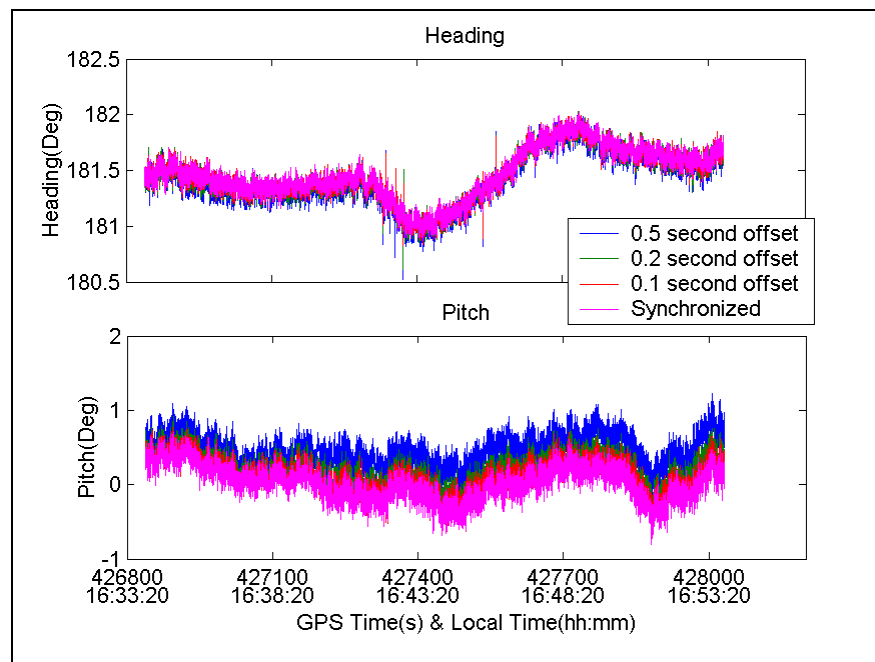


**Figure 4.13: Attitude estimates using time-offset data**

**Table 4.5: Statistics of attitude estimates using time-offset data**

	Heading		Pitch	
	Mean (degrees)	STD (arc mins)	Mean (degrees)	STD (arc mins)
Synchronized	181.47	13.57	0.02	14.14
0.1 s offset	181.46	13.74	0.11	13.63
0.2 s offset	181.45	13.88	0.20	13.24
0.5 s offset	181.42	14.29	0.48	12.60

Figure 4.14 shows the estimated local clock error of one of the CMC Allstar receivers. The receiver clock can be synchronized with GPS time with an accuracy of 3 ms. Therefore, the actual time misalignment between receivers should be at the ms level and is much smaller than the offset simulated above. Therefore, based on the above knowledge, one can conclude that the time synchronization problem in the low-cost receivers has insignificant effect on the accuracy of attitude estimation compared with the other measurement errors in static mode. But in the ideal case without multipath and antenna phase centre variation, which is shown in Tables 4.2 and 4.3 in the hardware simulation tests, this error lead to small bias in pitch direction. As for kinematic applications, the main problem comes from inaccuracy of timing in the low-cost attitude systems. Attitude estimation errors are then a function of the dynamics of the platform and the magnitude of the misalignment. If a large misalignment exists between the receivers, the locations of antennas change in kinematic condition during the time offset, which lead to a bias in the inter-antenna vector estimation. As a result of that, the attitude parameters deviate from the true orientation of platform. When the dynamics of the platform is very high, such as  $20^\circ$  per second, a 5 ms misalignment will cause a  $0.1^\circ$  attitude error (Hoyle et al 2002).

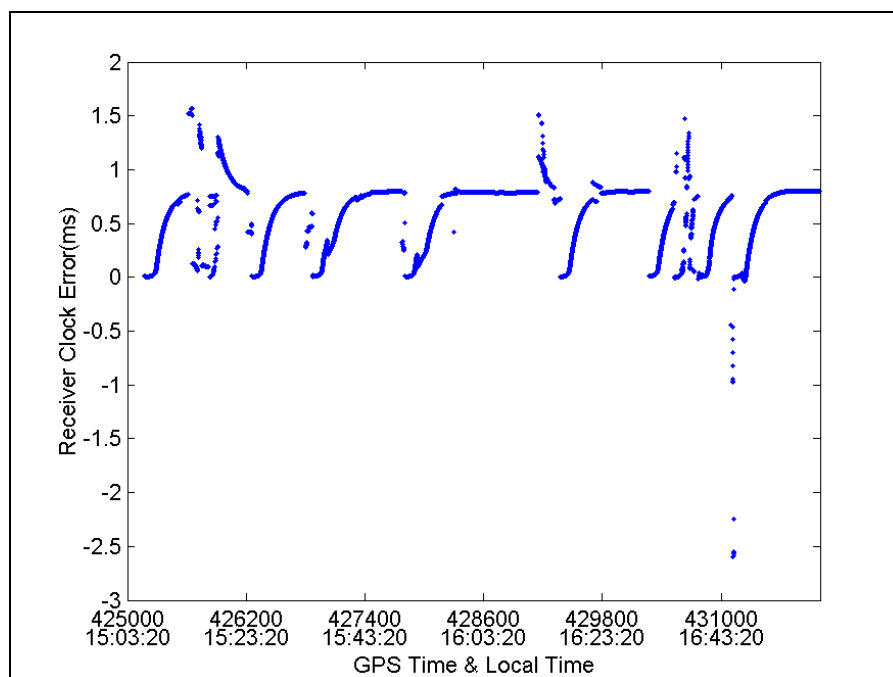


**Figure 4.14:CMC Allstar receiver clock error**

## **CHAPTER 5**

### **RELIABILILTY IMPROVEMENT USING LOWCOST RECEIVERS**

When using low-cost GPS sensors, measurement errors, namely multipath and antenna phase centre variations in carrier phase measurements are much more significant than such errors when high performance receivers are used. These error sources, together with frequent cycle slip occurrences, severely affect the performance of ambiguity resolution for inter-antenna vectors and lead to reliability problems in low-cost attitude determination systems, especially for kinematic applications. This chapter explores some methodologies to improve the reliability of low-cost attitude systems. Three different schemes, namely higher data rates, angular constraints, and Kalman filtering with quality control, are used interactively to improve reliability of the attitude system.

#### **5.1 Reliability problem using low-cost GPS sensors**

The previous chapter showed the advantages and limitations of using low-cost receivers and antennas such as the CMC Allstar for attitude determination. Without multipath and antenna effects, this receiver type can achieve attitude estimation performances comparable to those of high quality/high cost units during hardware simulations. This is because, under hardware simulation conditions, multipath and antenna phase centre errors do not have any impact. However, under field conditions, the low-cost receiver is more likely to suffer from multipath and antenna phase instability, as it has poor antenna phase stability and does not implement

any multipath mitigation. In some severe cases, these error sources, coupled with cycle slips, significantly deteriorate the carrier phase measurements and the wrong double difference ambiguities can be generated from the ambiguity resolution process. Incorrect ambiguities eventually lead to erroneous attitude estimates, which impair the reliability of the attitude determination system. In order to improve attitude estimation performance using low-cost receivers, some measures should be taken to enhance the reliability of attitude determination. Since the erroneous attitude output directly derives from the wrong double difference ambiguities, enhancing the integrity of ambiguity resolution is the simplest approach to improving the reliability of an attitude determination system. Once the wrong DD ambiguity set is determined after the search process, the attitude estimation process should have the capability to detect and identify the incorrect vector solution before estimating attitude parameters.

## **5.2 Ambiguity resolution**

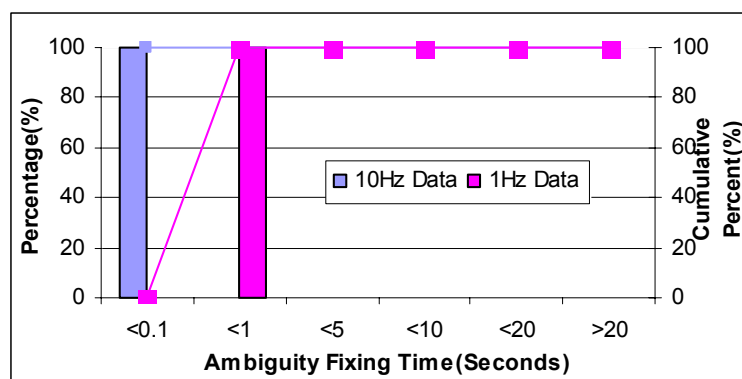
The reliability of attitude estimation rests heavily on the ambiguity resolution, because the attitude parameters are directly calculated using the estimated antenna vectors in the navigation frame. In order to enhance ambiguity resolution performance and further improve attitude estimation reliability, the following two measures, namely high rate measurements and angular checks, were implemented in HEADRT+<sup>TM</sup>.

### ***5.2.1 High data rate***

The CMC Allstar receiver can output raw time-synchronized carrier phase measurements up to 10 Hz. Compared with standard one Hertz data processing, the higher data rate can benefit the ambiguity resolution process due to the high availability of phase measurements. Also, platform dynamics can be precisely modeled and outlier estimates in the antenna vector lengths can be easily detected and further rejected using filtering of the high rate measurements. In this section, only the effect of the high data rate on ambiguity resolution will be investigated. The impact of the high data rate on Kalman filter estimation will be discussed in Section 5.4.2.

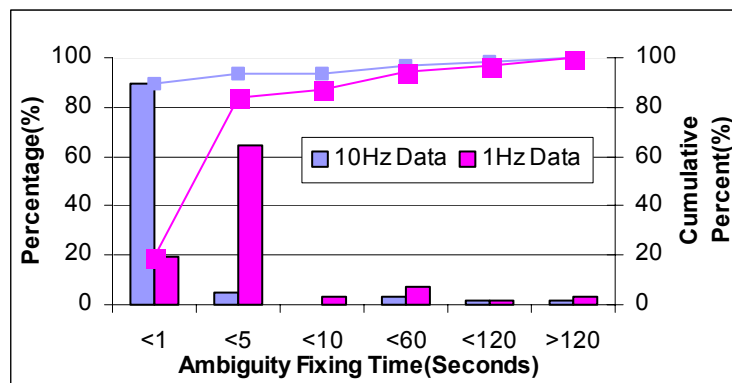
In order to evaluate the performance of ambiguity resolution, the time to fix ambiguities is utilized as the indicator. Two receivers were used, both for a hardware simulation and a field test. In the latter case, two AT575-104 low-cost antennas were employed. No errors were simulated during the simulator test and the only remaining error present was receiver measurement noise. The field test was conducted on the roof of Engineering Building at the University of Calgary. The inter-antenna distances were about one metre in both tests. The data was collected at a 10-Hz rate. The double difference ambiguities were intentionally reset every 120 seconds during the data processing to gather enough trials for a meaningful analysis. The Minimum Time to Ambiguity Fix (MTTAF) was set to zero and the fixing ratio was set to three in HEADRT+™.

Figure 5.1 shows the ambiguity fixing times for the case of the hardware simulation test. Without multipath and antenna phase centre variation, the integer ambiguities were successfully determined within a single epoch (1s or 0.1 s) during each trial, demonstrating that the CMC receiver measurement noise is not a significant factor affecting ambiguity resolution performance.



**Figure 5.1: Time to fix ambiguity in hardware simulation**

The corresponding field test statistics are shown in Figure 5.2. With the existence of multipath and antenna phase centre errors, only 19.6 % of the ambiguities were fixed in one second with 1 Hz data. The integer ambiguities were fixed in 5 seconds 84.9 % of the time. Meanwhile, with 10 Hz measurement rate, the corresponding values were 89.4 % and 93.4 % respectively. The time required to fix the ambiguities can be significantly reduced using high data rate during some trials. When fixing time was larger than 60 seconds, this is not the case due to the presence of time-correlated multipath and antenna phase centre variation errors.



**Figure 5.2: Time to fix ambiguity in field test**

Table 5.1 shows that the probability of resolving the correct ambiguities during the field test is 93% for 1 Hz data and 96% for 10 Hz data. With higher rate measurements, the ambiguity resolution reliability can thus be only slightly improved. Even though the incorrect ambiguities were selected occasionally, they can be easily rejected in the attitude software either by increasing the MTTAF in ambiguity resolution or by the reliability control in the attitude estimation phase.

**Table 5.1: Performance of ambiguity resolution using different data rate measurements**

Correctness (%)	10 Hz data	1 Hz data
Simulation Test	100	100
Field Test	95.5	92.9

### 5.2.2 Fixed angular constraint scheme

If one can assume that the antennas are mounted on a rigid platform, then their relative positions are fixed regardless of the platform motion. The full antenna frame geometry is known a priori and appropriate constraints can be used in the ambiguity resolution process to take advantage of this knowledge. Euler and Hill reported (1995) that besides the inter-

antenna length, the angle between two antenna vectors could also be measured and incorporated in the ambiguity processing scheme to assist in identifying the correct integer ambiguity values provided at least two inter-antenna vectors are solved. This a priori angular knowledge is especially useful when low-cost sensors are employed because the identification tests based on the DD residuals severely suffer from significant carrier phase measurement errors.

The implementation of the angular constraint is straightforward. First, the fixed planar angles ( $\theta$ ) between antenna vector pairs can either be measured a priori or calculated using the antenna coordinates in the body frame. Once the integer ambiguities of the antenna vector pairs have been determined, the angle between the inter-antenna vector pairs can be directly computed using the antenna vector coordinates in the local level frame:

$$\theta^E = \cos^{-1} \frac{\vec{b}_{AB}^{LL} \cdot \vec{b}_{AC}^{LL}}{\|\vec{b}_{AB}^{LL}\| \cdot \|\vec{b}_{AC}^{LL}\|} = \cos^{-1} \frac{\Delta E_{AB}^{LL} \Delta E_{AC}^{LL} + \Delta N_{AB}^{LL} \Delta N_{AC}^{LL} + \Delta V_{AB}^{LL} \Delta V_{AC}^{LL}}{b_{AB} \cdot b_{AC}} \quad (5.1)$$

where

$\theta^E$  is the estimated angle between the two antenna vectors

subscripts  $A, B, C$  represent the primary antenna and two secondary antennas

$\vec{b}_{AB}^{LL}, \vec{b}_{AC}^{LL}$  are the antenna vectors in local level frame

$b_{AB}, b_{AC}$  are the lengths of the antenna vectors

$\Delta E, \Delta N, \Delta V$  are three components of antenna vector in East, North, and Vertical directions.

Then, the estimated angle  $\theta^E$  is compared with the known angle  $\theta$ . If the ambiguities of two inter-antenna vectors are correctly solved, the two angles should be consistent within a certain tolerance:

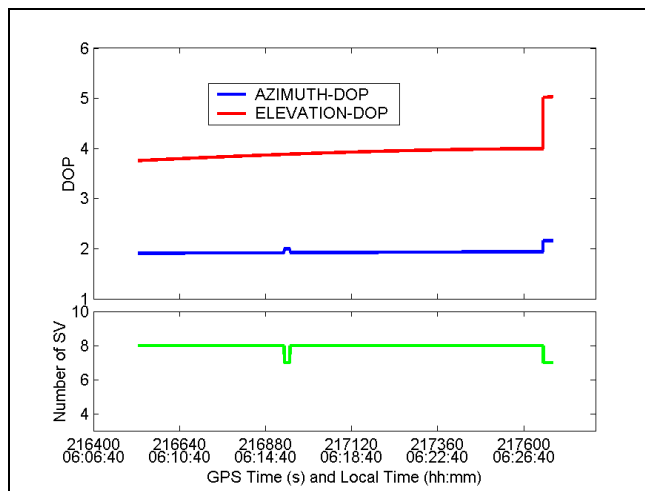
$$|\theta - \theta^E| < \delta \quad (5.2)$$

The numerical value of the angular tolerance  $\delta$  in Equation 5.2 depends on the inter-antenna distance and the quality of phase measurements, which are a function of measurement noise, multipath and phase centre stability. In the case of antenna vector lengths of 1-2 m and a moderate carrier phase measurement quality, a 5-degree tolerance is appropriate to detect the wrong ambiguities. If at least four antennas are used in the attitude determination system and only one vector ambiguity is wrong, this erroneous ambiguity combination can be detected and identified by checking all the angles between the inter antenna vectors.

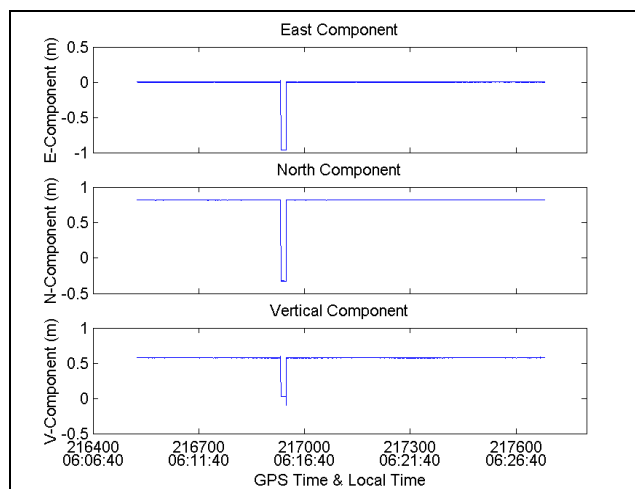
A hardware simulation was conducted to investigate the validity of the angular constraint scheme. An antenna body frame was simulated using inter-antenna distances of 1 m. The angles between the antenna vectors were intentionally set to 90 degrees.

Figure 5.3 shows the satellite's azimuth and elevation DOPs during the test. At GPS time 216932 s, the loss of SV27 in one of the secondary receivers caused the failure of the Chi-square test and the re-initialization of the double difference ambiguities for the corresponding inter-antenna vector. Unfortunately, the wrong ambiguities were determined due to the short MTTAF. When SV27 was re-acquired by the receiver, this wrong ambiguity set was

identified, with the true ambiguity obtained afterwards. The effect of this error on the vector solutions during this period is shown in Figure 5.4.



**Figure 5.3: DOPs and SV number during simulation test**



**Figure 5.4: Effects of an incorrect ambiguity on an inter-antenna vector estimate**

Since no quality control procedure was performed in the least squares attitude estimation, the erroneous inter-antenna vector solutions inevitably led to the wrong attitude parameters. The error effects on the attitude component estimates are shown in Figure 5.5.

After the angular constraint scheme was implemented in the software, the wrong ambiguity was easily detected and the erroneous vector solution was successfully detected and excluded from the attitude estimation. As shown in Figure 5.6, the correct attitude components were estimated in the least squares solution using the other two inter-antenna vectors. The small shift in the attitude estimates is due to the exclusion of SV27 and the slight change of satellite geometry.

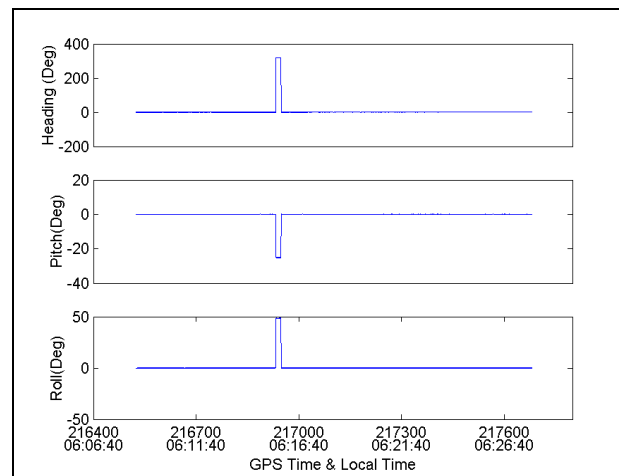


**Figure 5.5: Effects of an incorrect ambiguity on attitude component estimates**

By employing the angle consistency check in the ambiguity resolution, some incorrect ambiguity solutions can be effectively rejected, which significantly improves the reliability of multi-antenna attitude determination.

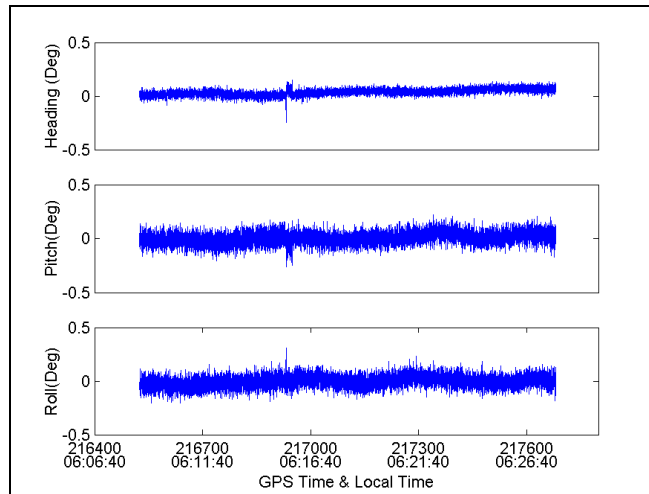


**Figure 5.6: Attitude results after implementing angular constraints in static simulation**

#### 5.4 Kalman filter estimation

So far, an implicit least squares method was used in HEADRT+™ to calculate the attitude parameters from antenna-vector components epoch by epoch, which entirely ignores the known dynamics of the platform. Compared with least squares estimation, Kalman filtering provides a recursive method for the determination of attitude components through a predicting and updating processes. The platform dynamics then can be modelled in a Kalman filter with the help of high rate measurements and be further used as a prior knowledge to detect the erroneous antenna vector solutions from ambiguity resolution.

##### 5.4.1 Attitude Estimation using Kalman filtering

The general formulas in Kalman filtering can be written as (Brown & Hwang 1992)

$$z_k = H_k \cdot x_k + v_k \quad (5.3)$$

$$x_k = \phi_k \cdot x_{k-1} + w_k \quad (5.4)$$

where

$z_k$  is the measurements vector at time  $k$

$H_k$  is the design matrix at time  $k$

$x_k$  is state vector at time  $k$

$v_k$  is measurement noise with covariance  $R$

$\phi_k$  is the transition matrix

$w_k$  is the process noise with covariance  $Q$

In attitude determination using vector components, the “measurements” are the antenna vector components in the local level frame. The design matrix consists of the partial derivatives of the rotation matrix with respect to the state vector.

$$H = \frac{\partial R}{\partial x} \quad (5.5)$$

The state vector includes the three Euler attitude parameters and their angular rates.

$$x = (\psi \ \theta \ \phi \ \dot{\psi} \ \dot{\theta} \ \dot{\phi})^T \quad (5.6)$$

A random walk process is used in the Kalman filter and the transition matrix  $\phi$  and the process noise can be expressed as follows

$$\phi = \begin{bmatrix} 1 & 0 & 0 & dt & 0 & 0 \\ 0 & 1 & 0 & 0 & dt & 0 \\ 0 & 0 & 1 & 0 & 0 & dt \\ 0 & 0 & 0 & 1 & 0 & 0 \\ 0 & 0 & 0 & 0 & 1 & 0 \\ 0 & 0 & 0 & 0 & 0 & 1 \end{bmatrix} \quad (5.7)$$

$$Q = \begin{bmatrix} \frac{\sigma_{\psi}^2}{3} dt^3 & 0 & 0 & \frac{\sigma_{\psi}^2}{2} dt^2 & 0 & 0 \\ 0 & \frac{\sigma_{\theta}^2}{3} dt^3 & 0 & 0 & \frac{\sigma_{\theta}^2}{2} dt^2 & 0 \\ 0 & 0 & \frac{\sigma_{\phi}^2}{3} dt^3 & 0 & 0 & \frac{\sigma_{\phi}^2}{2} dt^2 \\ \frac{\sigma_{\psi}^2}{2} dt^2 & 0 & 0 & \sigma_{\psi}^2 & 0 & 0 \\ 0 & \frac{\sigma_{\theta}^2}{2} dt^2 & 0 & 0 & \sigma_{\theta}^2 & 0 \\ 0 & 0 & \frac{\sigma_{\phi}^2}{2} dt^2 & 0 & 0 & \sigma_{\phi}^2 \end{bmatrix} \quad (5.8)$$

The numerical values of the angular rate variances in Equation 5.8 represent the tightness of the dynamic constraint of the Kalman filter. In vehicular attitude determination, the sigma of the angular rate in the Q matrix is empirically selected as 2 °/epoch in 10 Hz sampling in the present case. Using this model, the attitude parameters and their angular rates can be correctly estimated in the Kalman filter as long as all the measurements are free of errors.

#### 5.4.2 Quality control

As previously mentioned, the measurements used in the Kalman filter are the inter-antenna vector solutions after ambiguity resolution. In the case that the wrong ambiguity set is determined, these “quasi-measurements” are in error and the attitude estimates calculated from the Kalman filter will deviate from the truth. In order to reject the incorrect inter-antenna vector solutions from the Kalman filter and improve the reliability of the attitude estimates, a quality control system based on the filter innovation sequences is introduced herein.

The innovation sequence is the difference between the actual system observation and the predicted observation based on the predicted state (Teunissen & Salzman 1988):

$$\mathbf{v}_k^- = \mathbf{z}_k - f(\hat{\mathbf{x}}_k^-) \quad (5.9)$$

where

$\mathbf{v}_k^-$  is the innovation sequence at time  $k$

$\mathbf{z}_k$  is the actual observations at time  $k$

$\hat{\mathbf{x}}_k^-$  is the predicted observations at time  $k$

$f()$  is the function model, which is the rotation matrix multiplied by antenna vectors in the body frame

Under normal conditions, the innovation sequence is a zero-mean Gaussian white noise sequence with known variance. In the presence of erroneous measurements, such assumptions are no longer valid, and the innovation sequence deviates from its zero mean and white noise properties. Thus some statistical tests can be conducted to detect and identify outliers or faults in the measurements.

Firstly, an overall model test is conducted to detect the errors in the measurement vector. The test statistics in this global test are given as

$$T_k = \mathbf{v}_k^{-T} \mathbf{C}_{\mathbf{x}_k^-}^{-1} \mathbf{v}_k^- \sim \chi_a^2(m, 0) \quad (5.10)$$

where

$m$  is the number of observations taken at time  $k$ ,

$\mathbf{C}_{\mathbf{x}_k^-}$  is the covariance matrix of the innovation sequence and

$\chi_a^2$  is the Chi-squared probability with a significance level of  $\alpha$ .

If the global test is rejected, the system error can be identified with the one-dimensional local slippage test:

$$w_{ik} = \frac{l_i^T C_{v_k}^{-1} v_k^-}{\sqrt{l_i^T C_{v_k}^{-1} l_i}} \sim N(0,1) \quad (5.11)$$

where

$$l_i = (0, \dots, 0, 1, 0, \dots, 0)^T \text{ for } i=1, \dots, m$$

The suggested significant level  $\alpha$  in the local test is 0.999, which leads to a boundary value of 3.29. Thus the  $i$ -th measurement is flagged for rejection when

$$|w_i| > 3.29 \quad (5.12)$$

When implementing statistical tests to identify outliers in the measurements, two types of errors may be made. The first type (Type I) is rejecting a good measurement. The probability associated with this type error is denoted by  $\alpha$ . If a bad measurement is accepted by the test, a Type II error occurs. The probability of a Type II error is expressed as  $\beta$ .

Given the probability values of Type I and Type II errors, the Minimum Detectable Blunder (MDB) can be calculated as the ability to detect errors in the system as

$$|\nabla z_i| = \frac{\delta_0}{\sqrt{l_i^T C_{v_k}^{-1} l_i}} \quad (5.13)$$

where  $\delta_0$  is a function of  $\alpha$  and  $\beta$  (see Figure 5.7).

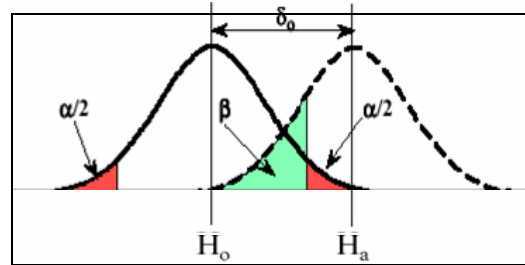


**Figure 5.7: Type I/II Errors**

In GPS kinematic applications,  $\alpha$  and  $\beta$  are commonly selected to be 0.001 and 0.2 respectively and  $\delta_0$  is then 4.13.

In the presence of strong multipath, the identification test (Equation 5.13) may be too sensitive and will sometimes lead to a false alarm. In order to alleviate this problem, a further step is introduced by comparing the innovations with the MDB. If the innovation is larger than the MDB, the measurement is considered erroneous; otherwise it is considered a false alarm (Lu 1991).

#### ***5.4.3 Kinematic Simulation Test***

The modified Kalman-filter-based attitude determination software was tested with the data collected with the hardware simulator using four CMC receivers. A vehicle trajectory was simulated with the antenna configuration is shown in Figure 5.8. The maximum attitude rates were about 20 degree/s in heading and several degrees per second in pitch. The true attitude during the test is plotted in Figure 5.9.

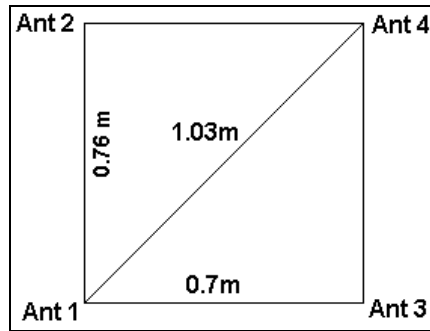


**Figure 5.8: Antenna configuration in hardware simulation**

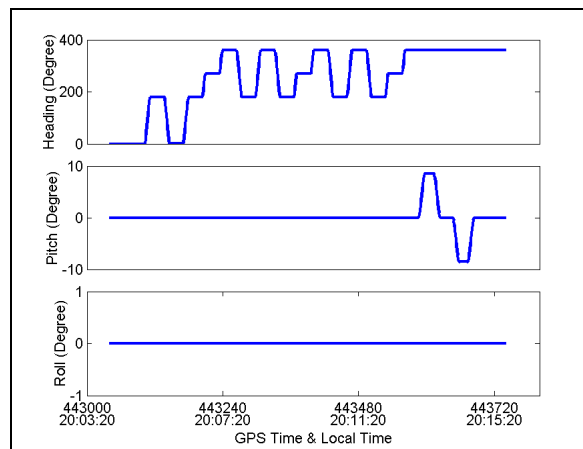


**Figure 5.9: True attitude parameters in hardware simulation**

The results, summarized in Figure 5.10 and Table 5.2, show that the Kalman filter method did not work well with tight dynamic constraints using a 1-Hz data rate, as over-smoothing effects occur. However, if loose dynamic constraints are used, the performance of the quality control system based on innovation sequence degrades significantly. With a 10-Hz data rate, the performance of the filter is excellent, the attitude parameter estimates being slightly better than those of the least squares estimates. The filtering process has better performance in pitch and roll, as the dynamics in these two dimensions are quieter than in heading and the dynamics constraints can better compress the estimation noise.

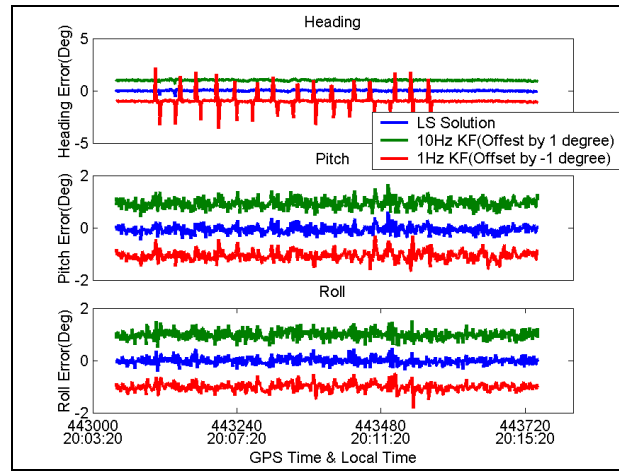


**Figure 5.10: Attitude estimation errors using different estimation methods**

**Table 5.2: RMS-Kalman filter versus least-squares (Unit: arc minutes)**

RMS	Heading	Pitch	Roll
10 Hz LS	3.9	11.7	9.9
10 Hz KF	3.9	9.8	7.9
1 Hz KF	31.9	11.8	9.0

In order to test the performance of cycle slip detection using the quality control method implemented by the Kalman filter, 80 cycle slips were introduced in the carrier phase measurements on different receivers with a magnitude ranging from one to eight cycles. Using the traditional phase prediction detection and inter-antenna length consistency check, all the cycle slips but one were either detected or recovered. The remaining cycle slip was removed only when the Kalman filter was used, as shown in Figure 5.11.

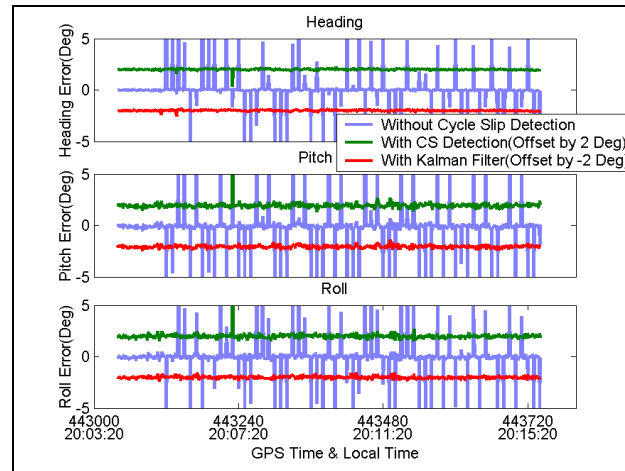


**Figure 5.11: Cycle slip detection using Kalman filter**

#### **5.4.4 Field kinematic test**

In order to assess the reliability improvement method in real dynamic conditions, a field test was carried out using two grades of GPS receivers. The high-end system consisted of two NovAtel Beeline<sup>TM</sup> receivers and four NovAtel 501 antennas, while the low-grade system consisted of four CMC Allstar receivers and four AT575-70 antennas. Two antenna frames were mounted with similar geometry on the roof of a minivan, to create the mobile platform in this test, as shown in Figure 5.12. The antenna configuration used was the same as in the above simulation test (Figure 5.8). The raw GPS measurements from both attitude systems were logged using a 10-Hz data rate.



**Figure 5.12: Test vehicle**

The test field was carried out on the major streets near the University of Calgary. The selected roads usually included trees and houses on the either side, which caused some GPS signal blockage during the test. The azimuth and elevation DOPs and the number of satellites tracked are shown in Figure 5.13. During the test, the number of satellites tracked was mostly around six to seven, except in some cases where there was heavy foliage near the road, and the satellite numbers dropped to five or less.

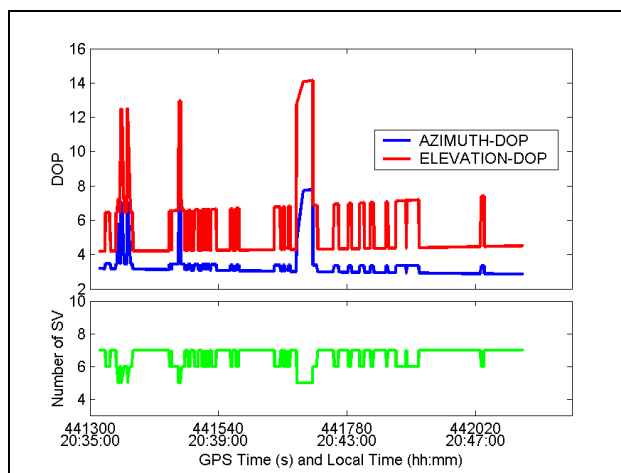


**Figure 5.13: DOPs and SV numbers during vehicle test**

During data processing with the standard version of HeadRT+<sup>TM</sup>, it was found that the Chi-square test in the ambiguity resolution was too sensitive with the presence of large measurement errors using low-cost CMC units in kinematic mode. Most of times, false alarms for cycle slips resulted from this check led to very low availability in the attitude estimation. Therefore when estimating the attitude parameters using low-cost sensors, this Chi-square test was deactivated to allow for the high availability of attitude output. As a result, the attitude system may be insensitive to the small cycle slips in carrier phase measurements.

Figures 5.14 and 5.15 show the RMS values of the double difference residuals at every epoch in the inter-antenna vector solutions. The means of the RMS values are given in Table 5.3. The CMC units have larger double difference residuals since their carrier phase measurements are more affected by multipath and antenna phase centre errors than those of the Beeline™ units.

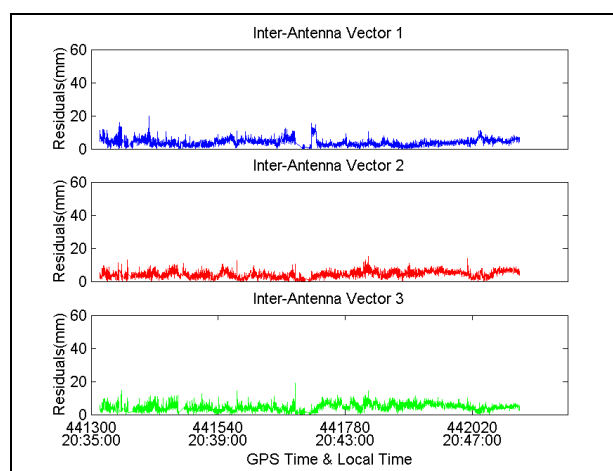


**Figure 5.14: Residual RMS in vector solutions using Beeline™ receivers**

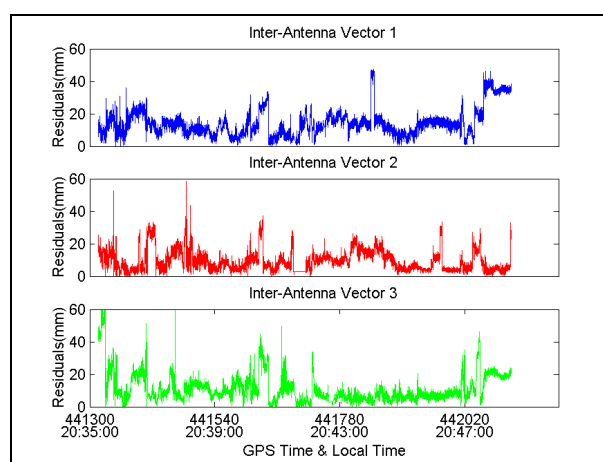


**Figure 5.15: Residual RMS in vector solutions using Allstar receivers**

**Table 5.3 :Residual RMS (mm) for Beeline™ and CMC receivers**

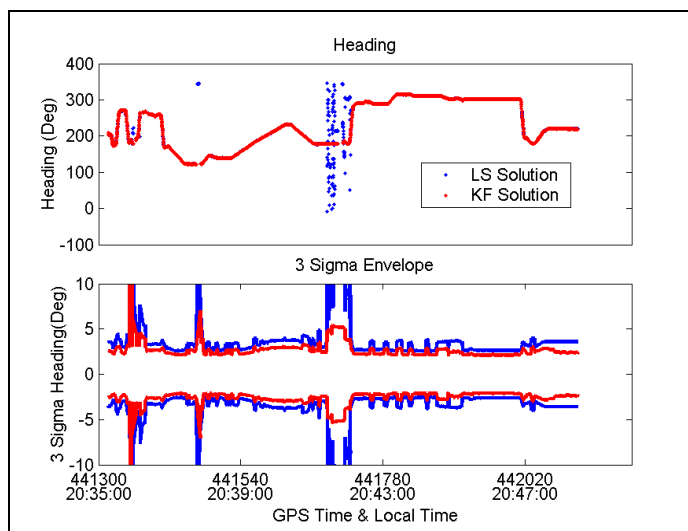
Vector	Beeline™ Units	CMC Units
1	5	17
2	5	12
3	5	15

The three Euler attitude parameter estimates using the Beeline™ units are shown in Figure 5.16, 5.17 and 5.18. The blue dots are the least squares attitude estimates and their 3-sigma standard deviation envelopes, while the red dots are the corresponding estimates from the Kalman filter with the quality control method turned on.

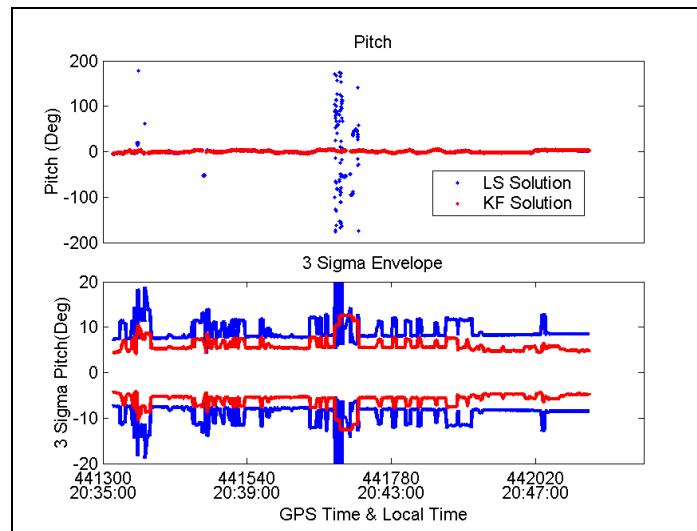
Using least squares estimation, wrong attitude parameter estimates were output when heavy satellite blockages occurred. The reason for this is that the least squares estimation was severely affected by incorrect vector solutions in such circumstances. Once the base satellite was lost, the double difference ambiguities had to be resolved at the next epoch. The performance of ambiguity resolution is highly correlated to the number of visible satellites and their geometry. In a heavy signal blockage area with strong multipath and phase centre variations, ambiguity resolution is more likely to produce an incorrect solution, which leads to erroneous attitude parameter estimates. The large 3-sigma standard deviation envelopes show the errant performance of least squares estimation due to these incorrect inter-antenna vector solutions and can be discreetly used to indicate the quality of attitude estimates.

Then the angular constraint scheme was implemented in the ambiguity resolution and Kalman filtering with the quality control replaced the least squares method to estimate the attitude

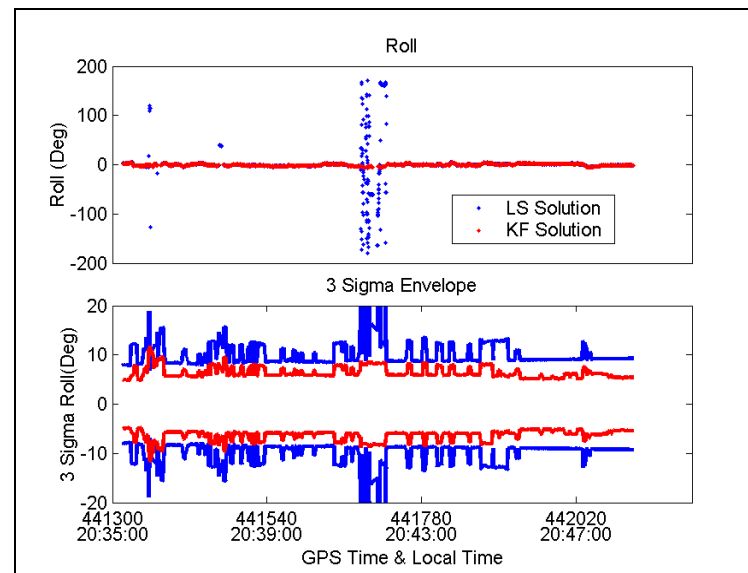
parameters. Using these reliability improvements, the wrong inter-antenna vector solutions were detected and excluded from the solution. This eliminated erroneous attitude parameters from the output. The Kalman filter 3-sigma standard deviation envelopes are slightly smaller than those from the least squares method due to the filter constraints. As can be seen in the figures, the standard deviation improvement was more significant in pitch and roll than in heading.



**Figure 5.16: Heading estimates using the Beeline™ system**



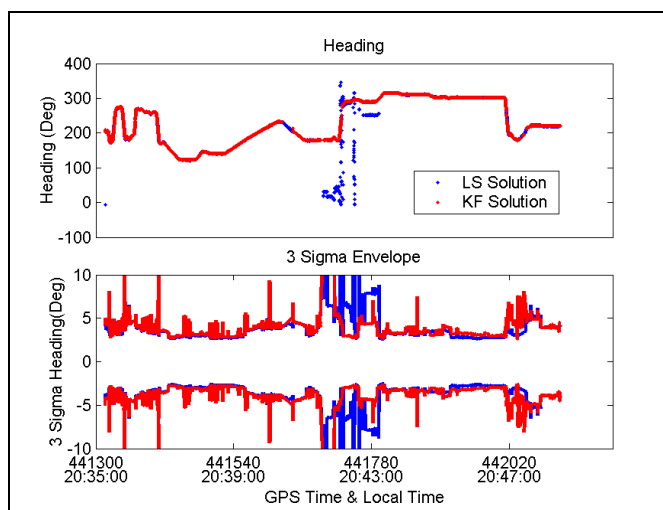
**Figure 5.17: Pitch estimates using the Beeline™ system**



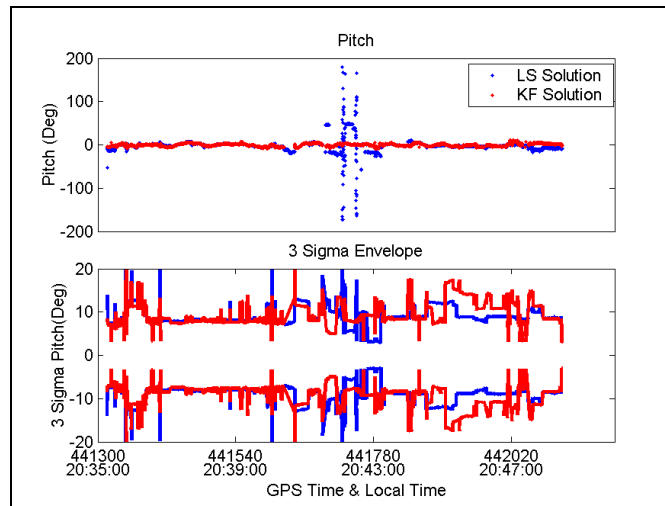
**Figure 5.18: Roll estimates using the Beeline™ system**

The CMC data was then processed with the two different versions of HeadRT+™ to examine the reliability improvements. As the carrier phase measurements from the low-cost CMC receivers are inferior to that from high-performance Beeline™, the sigma of CMC carrier phase observation was increased from 4 cm<sup>2</sup> to 6 cm<sup>2</sup> to represent larger multipath, antenna phase centre variations and receiver noise. The attitude results are shown in Figures 5.19,

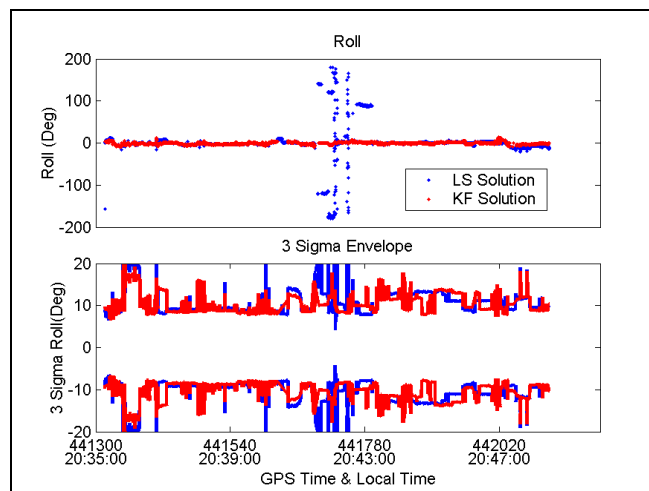
5.20 and 5.21. The overall attitude estimation accuracy was slightly lower than that obtained with the Beeline™ units. Using the Kalman filter augmented with the quality control method, erroneous vector solutions, which caused wrong attitude estimates in the least squares approach, were successfully identified and rejected from the attitude estimation. As the phase measurements are more vulnerable to multipath, phase centre errors and cycle slips, erroneous inter antenna vector solutions were frequently determined. When the incorrect solutions were rejected by the Kalman filter, the availability of attitude estimates degraded due to the reduction of correct “quasi-observables”. The lower number of vector solutions involved in attitude estimation, coupled with the larger carrier phase errors, caused large variations in the estimation accuracy of the Kalman filter.



**Figure 5.19: Heading estimate using the CMC system**



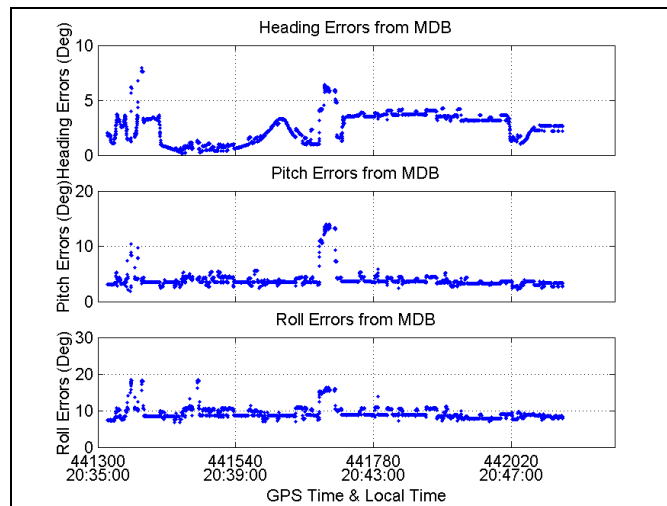
**Figure 5.20: Pitch estimate using the CMC system**



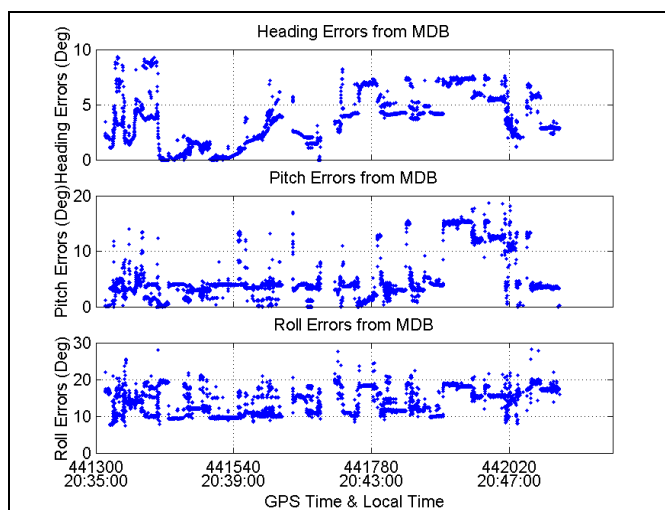
**Figure 5.21: Roll estimate using the CMC system**

Figure 5.22 and 5.23 show the external statistical reliability, that is the impact of the maximum measurement errors that could occur and go undetected, on the attitude estimates, for both systems. This statistical reliability measure is a function of the quality of carrier phase measurements and of the number of valid estimated inter-antenna vectors in the Kalman filters. The external statistical reliability of the Beeline<sup>TM</sup> system is fairly consistent during the test except during times of poor geometry. The corresponding statistical reliability

of the CMC system is much lower due to changes in the number of estimated inter-antenna vectors and the larger sigma of carrier phase observations in the Kalman filtering, which represents the higher multipath and antenna phase centre variations. This relatively low statistical reliability indicates that the quality control in the Kalman filter is insensitive to small cycle slips with the presence of large measurement errors using low-cost GPS sensors. Thus, one can conclude that the CMC units have reached their limit in term of accuracy performance, if one assumes that the choice of antennas is limited to current low-cost units. In order to increase attitude component estimation performance, higher performance, but more expensive antennas could be used. The use of longer inter-antenna distances would also improve accuracy, but at the cost of a lower portability. Aiding with external sensors is another alternative.



**Figure 5.22: External reliability of the Beeline™ system**



**Figure 5.23: External reliability from the CMC system**

## CHAPTER 6

### DEVELOPMENT OF A LOW-COST GPS/GYRO ATTITUDE SYSTEM

As discussed in the previous chapter, high data rate measurements, angular constraints as well as the implementation of a quality control system in a Kalman filter can effectively improve the reliability of attitude estimation using low-cost GPS sensors. However, large carrier measurement errors, namely multipath, antenna phase centre variations and cycle slips, result in some limitations in reliability performance using the above techniques. In order to overcome such problems, low-cost rate gyroscopes are integrated in the GPS-based attitude system. The performance of this low-cost GPS/gyro attitude determination system is probed both in static mode and under kinematic conditions in this chapter.

#### **6.1 Advantages of GPS/gyro integration**

The performance of a GPS-based attitude determination system is highly related to carrier integer ambiguity resolution. For the case when low-cost GPS sensors are employed in the attitude system, large carrier phase measurement errors may lead to incorrect ambiguity resolution as well as false alarms of cycle slips when the tolerance selected is too small. The erroneous ambiguity result and the large amounts of time required for ambiguity search deteriorate both the reliability and availability of attitude estimation.

The gyroscope is an instrument used to measure the rate of rotation and integrated attitude change of a platform in a single dimension (Savage 1978). With a triad of gyros that are orthogonally mounted, the 3D rotation of the platform can be continuously measured. The attitude increments and Euler angles can be obtained by integrating the gyroscope angular velocity measurements and the initial attitude angle. Based on operation principles, the gyroscope types are spinning mass gyro, optical gyro and vibrating gyro. For this research, the piezoelectric vibrating rate gyro has been selected for its low-cost (\$10 - \$20 per unit in large quantities) and reasonable performance.

With the introduction of low-cost rate gyroscopes, the overall performance of GPS-based attitude determination can be significantly improved. From the accuracy aspect, vibrating gyros have good accuracy for short intervals, so the platform dynamics can be precisely sensed by gyro rates and the filtering process in the Kalman filter is enhanced with the angular rate data. The noise behavior of attitude estimates can then be effectively decreased by integrating the angular rate data into attitude estimation. During GPS outages, the attitude parameters can be directly computed from gyro measurements until the GPS antenna vector solutions recover. The availability of the integrated attitude system can theoretically increase to 100% accordingly. With continuous attitude results, the search region for a secondary antenna can be specified as a small cube near the estimated position from the attitude information. With fewer candidate ambiguity combinations, the identification in the ambiguity resolution process becomes much simpler and faster. Furthermore, with the introduction of direct angular rate measurements, the Minimum Detectable Blunder (MDB)

of the quality control system can be diminished and the Kalman filter attitude estimation is strengthened as well. These two improvements in ambiguity resolution and attitude estimation enhance the overall reliability of the integrated attitude determination system.

## 6.2 Methodology

As discussed in Chapter Two, the attitude estimation in HeadRT+™ is carried out in two phases: antenna vector estimation and attitude determination. Since the vector estimation process is nothing more than ambiguity resolution and coordinate transformation, and no attitude information (except the ambiguity search space definition) is involved in this phase, the data fusion of GPS/gyro system is implemented in the attitude determination phase after the antenna vector estimation. As the rate gyros can only provide the relative angular rates of rotation, the absolute orientation of the platform has to be calculated from carrier phase measurements when GPS is available. When the GPS antenna vector solution is not obtainable, the rotation of the platform since the last GPS outage can be obtained by integrating the estimated attitude rate over time. Figure 6.1 depicts the integration scheme of the attitude system using GPS and rate gyro sensors. After data synchronization, the antenna vector components are estimated in the local level frame, provided the double difference ambiguities are correctly determined. Then the antenna vector solutions from GPS are fused with rate gyro measurements in a Kalman filter to estimate the attitude parameters as well as attitude rates and gyro biases. If the ambiguities are not fixed, the search process has to be triggered to determine the true ambiguity set for the antenna vectors before attitude estimation. If the ambiguities cannot be correctly determined within the current epoch, the attitude angles and their angular rates are estimated from angular rate data only.

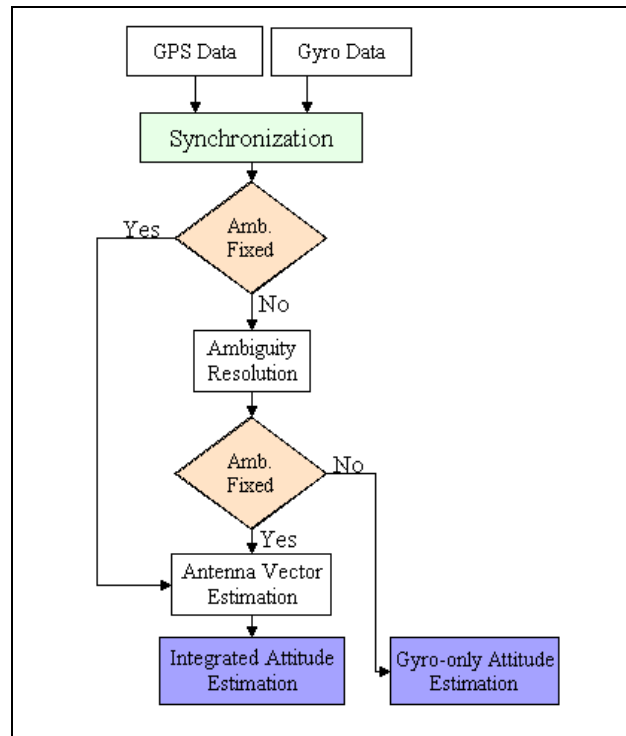


**Figure 6.1: Attitude estimation in the integrated system**

### 6.3 Rate gyro

The low-cost gyroscope type selected in this research is the Murata ENV-05D-52 Gyrostar. This sensor is designed to measure the angular rate using the Coriolis force. The Coriolis force is a fictitious force exerted on a body when it moves in a rotating reference frame (Motta 2000). For example, if we create a resonant motion with a velocity of  $v$  in a direction (X) perpendicular to the axis of rotation (Z), the Coriolis force induces motion in the third direction(Y). Given a mass of  $m$  and the angular velocity of  $\Omega$ , the expression for the Coriolis force is (Motta 2000):

$$F_{Coriolis} = 2m(\mathbf{v} \times \boldsymbol{\Omega}) \quad (6.1)$$

Note that the Corliolis force in the above equation is proportional to the angular velocity of  $\Omega$ . If this Corliolis force is converted to a voltage by the detector element and signal

conditioning circuitry, the angular velocity is easily derived since the mass of the structure and the vibration velocity of the bar are both known quantities.

Inside the Murata piezoelectric rate gyro, there is a triangular metal prism (Figure 6.2), which is forced to vibrate by a piezoelectric ceramics with the feedback loop at a frequency of 7 kHz. In the case of no rotation around the axis, the other two ceramics detect equal signals. When the prism is turned, the ceramics detectors are excited and receive different signals as shown in Figure 6.3. The signal difference is compared and examined by the internal analogue circuits and output as a voltage proportional to the angular velocity. This equilateral triangle design of this piezoelectric gyroscope greatly simplifies the circuit, makes frequency adjustment easier, and provides the highest sensitivity among vibrators having the same volume (Murata 2000). These features account for its widespread use in the car navigation system and video movie markets. In this project, three Murata ENV-05D-52 rate gyros are used to sense the angular rates around three axes of the platform body frame. These gyroscopes were chosen for their low-cost (around \$50 for single quantity and \$15 with a large quantity purchase) and their satisfactory performance compared to other MEMS gyro sensors within this price range. The specifications of this vehicular version of the gyroscope can be found in Table 6.1.

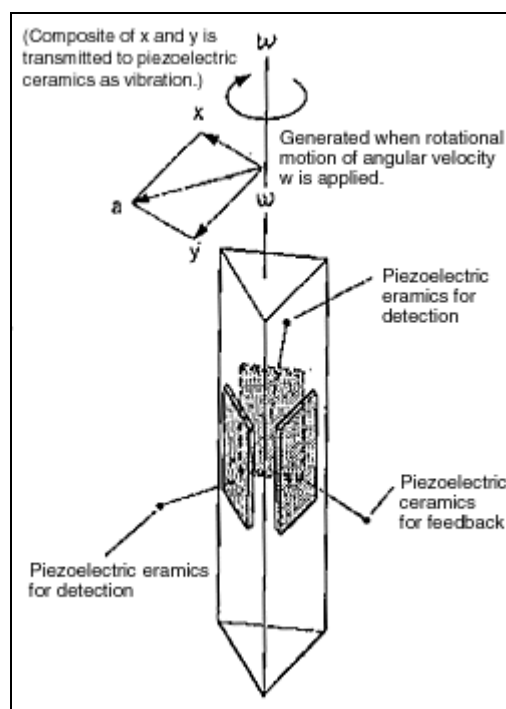


Figure 6.2: Metallic triangular prism vibrator (Murata 2000)

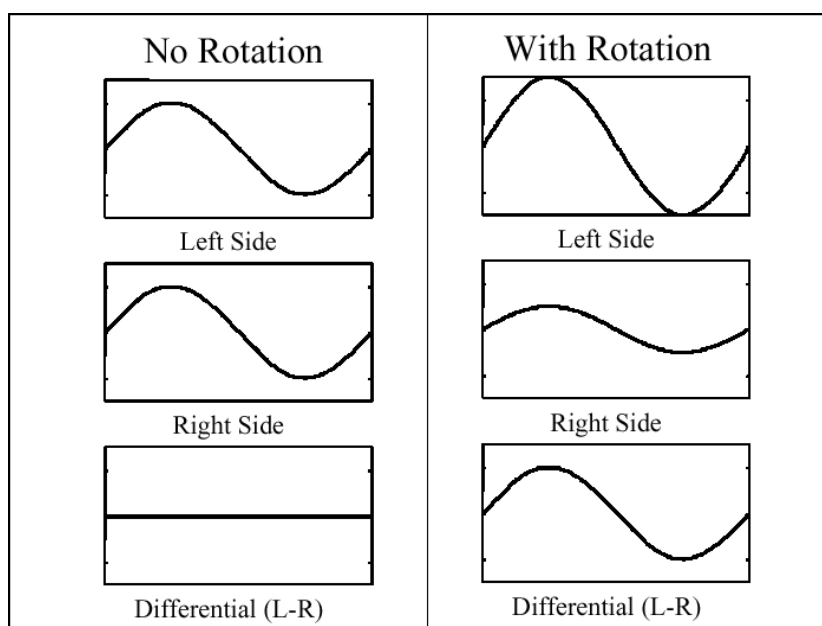


Figure 6.3: Difference of the left and right detection signals (Nakamura 1990)

**Table 6.1: Specifications of Murata ENV-05D-52 Gyroscope**

Characteristic	ENV-05D-52 Gyroscope
Gyro type	Piezoelectric vibratory
Resolution	0.1 deg/sec
Bias Stability	9 deg/sec
Scale Factor	$22.2 \pm 1.8$ mV/deg/sec
Angular Velocity	-80 +80deg/sec
Supply Voltage	4.5-5.5 v
Output Voltage at Zero Rate	2.2-2.8 v
Raw Data Rate	2K Hz
Dimension	18X30X41 mm

The output from the Murata piezoelectric gyroscope is the analog voltage proportional to the sensed angular rate at the frequency of 2 kHz. The voltage output at the zero rate is unit-dependent and ranges from 2.2 to 2.8 V with a mean of 2.5 V. With the increase of angular velocity, the variation of the voltage can reach 1.5 V in each direction.

The performance of the Murata piezoelectric gyroscope suffers from its limited stability in gyro bias drifting and the scale factor as well as the high frequency noise. Previous research (Stephen 2000, Hayward et al 1997) has shown that the magnitude of the first two error sources is related to the external temperature and it is very difficult to calibrate them simultaneously in navigation mode. The gyro bias drifts over time due to self-heating in the hardware. In this work, the biases are estimated and updated online in the filter when GPS measurements are available. During GPS outages, the bias estimates remain fixed and are used to compensate their effects on angular rate output. Compared with the gyro bias, the scale factor is not so sensitive to temperature and the values are very close to 22 mV/°/s

within a range of 30 degrees. For this reason, it can be determined once and used for the entire navigation mission, since the temperature does not usually change greatly over several hours. The high frequency noise in the angular velocity data can be easily suppressed when averaging the high frequency gyro data to 10 Hz for data synchronization. The gyro has also shown limited endurance to shock and vibration. In vehicular attitude determination mode, the vibration of the platform varies significantly depending on the engine velocity, temperature and many other factors (Stephen 2000) and it is very hard to develop a valid model to compensate for the angular rate measurement errors caused by the vibration of the platform.

#### **6.4 System design**

Figure 6.4 shows the system setup of the low-cost GPS/gyro integrated attitude determination system in detail. The sensors used include CMC Allstar receivers and Murata ENV-05D-52 gyroscopes. At least three Allstar sensors and corresponding AT575-70 antennas are used to set up a multi-antenna attitude system. Raw carrier phase measurements from the receivers are logged into the computer with a data rate of 10 Hz. Three orthogonally-mounted rate gyros are rigidly mounted in a box to sense the rotations around three axes in the platform body frame. The misalignment between the axis of the rate gyro and that of body frame is within one or two degrees due to alignment errors. This small misalignment can be considered negligible due to the poor estimation accuracy of the rate gyros. The output from the rate gyros is the voltage pulse with a sampling rate of 2 kHz. It is digitized in an Analog to Digital converter, namely DAQPad-MIO-16XE-50. As the measurement data is post-processed, time tagging of the gyro data is necessary for data synchronization. Precise GPS

time is provided by a NovAtel OEM receiver temporarily for convenience. At the start of the data logging, a pulse from the A/D converter is sent to the time mark pin of OEM4 to record the GPS time as shown in Figure 6.5. The rate gyro data is then tagged with the 1 PPS generated by the OEM4 receiver. The precise GPS time of the PPSs can be obtained by estimating the time interval ( $\Delta T$ ) between the startup and the first PPS. Since the time-tags generated by the PPS by GPS receiver are co-incident with each 2000<sup>th</sup> sample, the gyro data is then time tagged with the GPS time with the use of PPSs.

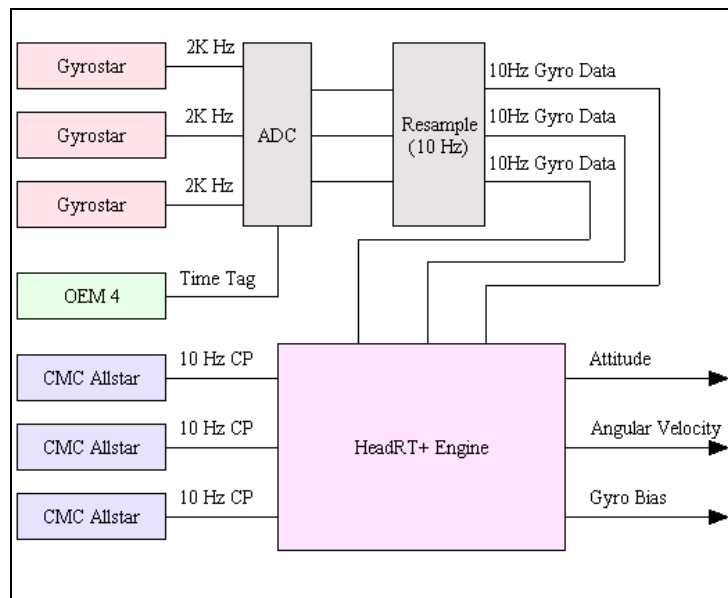


**Figure 6.4: System design of low-cost GPS/gyro integrated system**

After the data digitization, the 2 kHz angular rate measurements are averaged into 10 Hz for synchronization with GPS carrier phase measurements. The high measurement noise in gyro data is thus effectively suppressed throughout the averaging process. The time tagged GPS/gyro data is then input into the modified HeadRT+<sup>TM</sup> to estimate the attitude parameters.

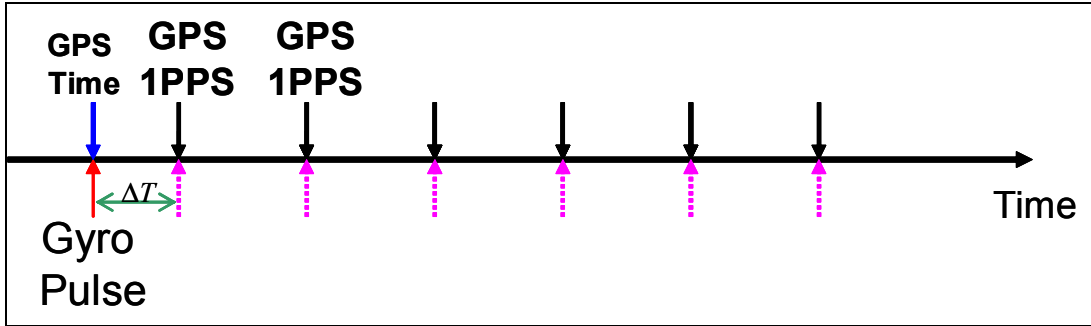


Figure 6.5: Time tag of gyro data

### 6.5 Filtering algorithm

The data fusion for the GPS/gyro integrated attitude system is realized in an extended centralized Kalman filter similar to the one described in Chapter Five. The advantages of using the centralized Kalman filter instead of the de-centralized one are the tight data fusion and the better error detection. As mentioned above, after determining the double difference ambiguities and the inter-antenna vectors, the observables from GPS are the inter-antenna vector components in the local level frame. The measurements from the rate gyros are the angular rates around the three axes in the body frame  $(\omega_x, \omega_y, \omega_z)$ . The state vector in Kalman filter consists of three gyro biases, three Euler attitude parameters and their angular rates.

$$X = (\psi \ \theta \ \varphi \ \dot{\psi} \ \dot{\theta} \ \dot{\varphi} \ \delta\omega_z \ \delta\omega_x \ \delta\omega_y)^T \quad (6.2)$$

Similar to that in the GPS alone Kalman filter, the design matrix for the GPS vector components are the partial derivative of the rotation matrix with respect to the state vector:

$$\mathbf{H}_{3n \times 9_{gps}} = \frac{\partial \mathbf{R}}{\partial \mathbf{X}} \quad (6.3)$$

where  $n$  is the number of antenna vectors estimated from the GPS measurements.

The relation of the angular rates, the attitude angles and the gyro biases is given below, in which  $s()$  and  $c()$  denote the sine and cosine functions.

$$\begin{pmatrix} \omega_z \\ \omega_x \\ \omega_y \end{pmatrix} = \begin{pmatrix} c(\varphi)c(\theta) & -s(\theta) & 0 \\ s(\varphi)c(\theta) & c(\varphi) & 0 \\ -s(\theta) & 0 & 1 \end{pmatrix} \cdot \begin{pmatrix} \dot{\psi} \\ \dot{\theta} \\ \dot{\varphi} \end{pmatrix} + \begin{pmatrix} \delta\omega_z \\ \delta\omega_x \\ \delta\omega_y \end{pmatrix} \quad (6.4)$$

Then the design matrix for the angular rate measurements can be formed as

$$H_{gyro} = \begin{pmatrix} 0 & 0 & 0 & c(\varphi)c(\theta) & -s(\theta) & 0 & 1 & 0 & 0 \\ 0 & 0 & 0 & s(\varphi)c(\theta) & c(\varphi) & 0 & 0 & 1 & 0 \\ 0 & 0 & 0 & -s(\theta) & 0 & 1 & 0 & 0 & 1 \end{pmatrix} \quad (6.5)$$

A random walk model is used to predict the angular rates and gyro biases in the Kalman filter. Therefore, the transition matrix  $\Phi$  can be derived from the dynamics model as

$$\phi = \begin{pmatrix} 1 & 0 & 0 & dt & 0 & 0 & 0 & 0 & 0 \\ 0 & 1 & 0 & 0 & dt & 0 & 0 & 0 & 0 \\ 0 & 0 & 1 & 0 & 0 & dt & 0 & 0 & 0 \\ 0 & 0 & 0 & 1 & 0 & 0 & 0 & 0 & 0 \\ 0 & 0 & 0 & 0 & 1 & 0 & 0 & 0 & 0 \\ 0 & 0 & 0 & 0 & 0 & 1 & 0 & 0 & 0 \\ 0 & 0 & 0 & 0 & 0 & 0 & 1 & 0 & 0 \\ 0 & 0 & 0 & 0 & 0 & 0 & 0 & 1 & 0 \\ 0 & 0 & 0 & 0 & 0 & 0 & 0 & 0 & 1 \end{pmatrix} \quad (6.6)$$

The process noise of the dynamic model in the Kalman filter, which is represented by the  $\mathbf{Q}$  matrix, has to be precisely modeled in order to achieve the high accuracy estimation of the attitude parameters. The mathematical expression of the process noise is

$$\mathbf{Q} = \begin{pmatrix} \frac{\sigma_{\dot{\psi}}^2}{3} dt^3 & 0 & 0 & \frac{\sigma_{\dot{\psi}}^2}{2} dt^2 & 0 & 0 & 0 & 0 & 0 \\ 0 & \frac{\sigma_{\dot{\theta}}^2}{3} dt^3 & 0 & 0 & \frac{\sigma_{\dot{\theta}}^2}{2} dt^2 & 0 & 0 & 0 & 0 \\ 0 & 0 & \frac{\sigma_{\dot{\phi}}^2}{3} dt^3 & 0 & 0 & \frac{\sigma_{\dot{\phi}}^2}{2} dt^2 & 0 & 0 & 0 \\ \frac{\sigma_{\dot{\psi}}^2}{2} dt^2 & 0 & 0 & \sigma_{\dot{\psi}}^2 & 0 & 0 & 0 & 0 & 0 \\ 0 & \frac{\sigma_{\dot{\theta}}^2}{2} dt^2 & 0 & 0 & \sigma_{\dot{\theta}}^2 & 0 & 0 & 0 & 0 \\ 0 & 0 & \frac{\sigma_{\dot{\phi}}^2}{2} dt^2 & 0 & 0 & \sigma_{\dot{\phi}}^2 & 0 & 0 & 0 \\ 0 & 0 & 0 & 0 & 0 & 0 & \sigma_{w_x}^2 & 0 & 0 \\ 0 & 0 & 0 & 0 & 0 & 0 & 0 & \sigma_{w_y}^2 & 0 \\ 0 & 0 & 0 & 0 & 0 & 0 & 0 & 0 & \sigma_{w_z}^2 \end{pmatrix} \quad (6.7)$$

As discussed in Chapter Five, the variance of attitude rates in the above equation depends largely on the dynamic constraint in the Kalman filter. The numerical value of the variance of the gyro bias estimated here represents the stability of the bias drift.

A quality control system based on innovation sequences, which has been successfully implemented in the unaided GPS attitude determination system in Chapter Five is also employed in the filtering process for GPS/gyro integration. With the introduction of angular rate measurements from rate gyros in the Kalman filter, a more robust estimation of the attitude rates can be obtained, which improves the sensitivity of error detection of the quality control system as well.

During GPS outages, no antenna vector solutions are available and the attitude parameters are estimated solely from the rate gyro data. The rotation of the platform can be determined

by integrating the estimated attitude rates over the sampling rate. With the knowledge of the initial orientation of the platform since the last GPS outage, the three Euler angles are calculated as

$$\begin{pmatrix} \psi \\ \theta \\ \varphi \end{pmatrix}_{K+1} = \begin{pmatrix} \psi \\ \theta \\ \varphi \end{pmatrix}_K + dt \cdot \begin{pmatrix} \dot{\psi} \\ \dot{\theta} \\ \dot{\varphi} \end{pmatrix} \quad (6.8)$$

The attitude rates are computed directly from the gyro data after compensating for the gyro biases using

$$\begin{pmatrix} \dot{\psi} \\ \dot{\theta} \\ \dot{\varphi} \end{pmatrix} = \begin{pmatrix} 0 & \frac{s(\varphi)}{c(\theta)} & \frac{c(\varphi)}{c(\theta)} \\ 0 & c(\varphi) & -s(\varphi) \\ 1 & s(\varphi)t(\theta) & c(\varphi)t(\theta) \end{pmatrix} \begin{pmatrix} \omega_y - \delta\omega_y \\ \omega_x - \delta\omega_x \\ \omega_z - \delta\omega_z \end{pmatrix} \quad (6.9)$$

From this equation, one can see that the estimation of attitude rates is related not only to the rate gyro measurements, but to the gyro bias and attitude parameter estimation as well.

The performance of attitude estimates during GPS outage also rests on the length of the GPS outages. Since there is no GPS data to update the gyro bias online during the outage interval, the gyro bias estimates are kept fixed and degraded due to bias drift over time. The compensation for the gyro biases is less effective with an increase of the GPS outage period, which leads to a drift in the attitude parameters as well.

## 6.6 Gyro aiding ambiguity resolution

In the GPS/gyro integrated attitude determination system, the attitude parameters are continuously obtainable during the navigation process. In the case of resolving double

difference ambiguities, the apriori knowledge of the platform orientation can be used to specify the search region as a small cube near the location of the secondary antenna instead of the entire spherical search space. The use of external attitude information significantly improves the reliability of the ambiguity resolution since the smaller search region makes the ambiguity identification process much easier (Lu 1994). This is especially true when low-cost GPS sensors are involved. The carrier phase measurements from such units are noisier than those from high-performance GPS receivers and the smaller number of candidate ambiguity sets can largely prevent incorrect ambiguities set from being identified in the search process.

Once the double difference ambiguities are correctly determined at the beginning of the mission, the attitude parameters can be obtained from either the integrated Kalman filter solution or the gyro-only solution at each epoch. With the knowledge of the antenna array configuration, the inter-antenna vector 3D components in the local level frame can be calculated based on the approximate attitude information as

$$\begin{pmatrix} x_{ll} \\ y_{ll} \\ z_{ll} \end{pmatrix} = \mathbf{R}_b^{ll} \begin{pmatrix} x_b \\ y_b \\ z_b \end{pmatrix} \quad (6.10)$$

where

$\mathbf{R}_b^{ll}$  is the rotation matrix from the body frame to the local level and is the transpose of  $\mathbf{R}_{ll}^b$ .

After transforming the antenna vector from the local level into the earth-fixed frame, the coordinates of the secondary antenna in WGS-84 with respect to the primary antenna can easily be estimated. As shown in Figure 6.6, the search space for the secondary antenna can be defined as a cube with the origin at the estimated secondary antenna location and the size given by the estimation uncertainty. All the double difference ambiguity combinations that fall in this region are then formed and tested in identification tests in the ambiguity resolution procedure. The estimated relative location of the secondary antenna can be further used as an extra constraint to select the correct ambiguity set.

One challenge that may occur when implementing the cubic search method is the determination of the side length. If the cube is set to give a fairly small search region, the limited candidate combinations lead to a quick ambiguity search, but there is an increased risk that systematic errors may cause the correct ambiguity set to fall outside of the search zone. In the case that a large size is selected, the expanded search region has a good possibility of including the correct ambiguity set; however, the increased candidate ambiguity combinations make the ambiguity search process less reliable and slower due to the large measurement errors using low-cost GPS sensors (Schleppé 1996). In this project, the size of the cube is determined by the standard deviation of attitude estimates multiplied by a certain expansion factor. The expansion factor here is conservatively selected as five in order to allow for severe systematic multipath and antenna phase centre variation effects on attitude estimation accuracy.

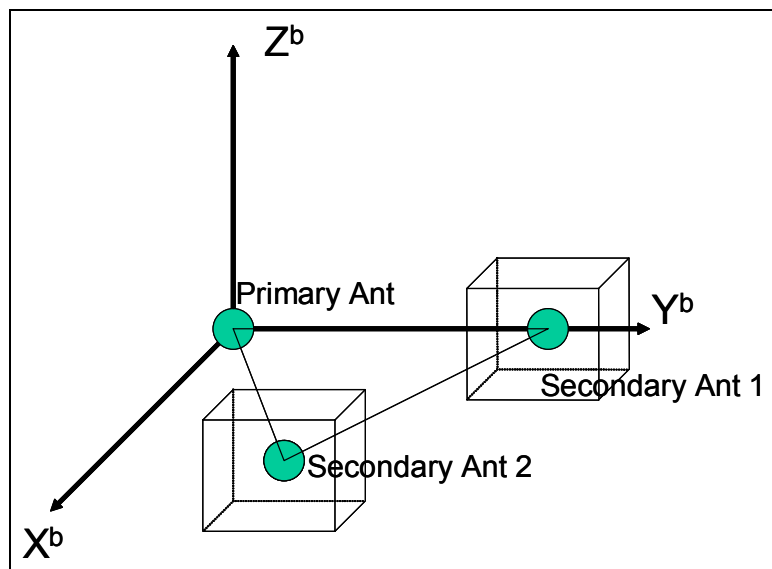


**Figure 6.6: Cubic search region method**

The gyro-aided ambiguity resolution scheme is very powerful as it can largely reduce the candidate ambiguities compared to the sphere region definition. A stationary test was conducted to investigate the efficiency of the cubic search method using two CMC Allstar receivers. The double difference ambiguities were intentionally reset every 120 seconds to obtain the statistics of time to fix ambiguities. The ambiguity fixing ratio was set to three and the MTTFA is zero in HeadRT+<sup>TM</sup>. With an inter-antenna vector of one metre, the number of ambiguity combinations that fall in the sphere is about 1400. The number decreases to 12-20 using the cube definition with a side of 20 cm. As shown in Figure 6.7, with such a small number of candidate combinations, all the ambiguity sets can be correctly determined within one second. However, using the sphere search region, some of the ambiguities take more than five seconds to resolve and the success rate of determining the correct one is 97%.

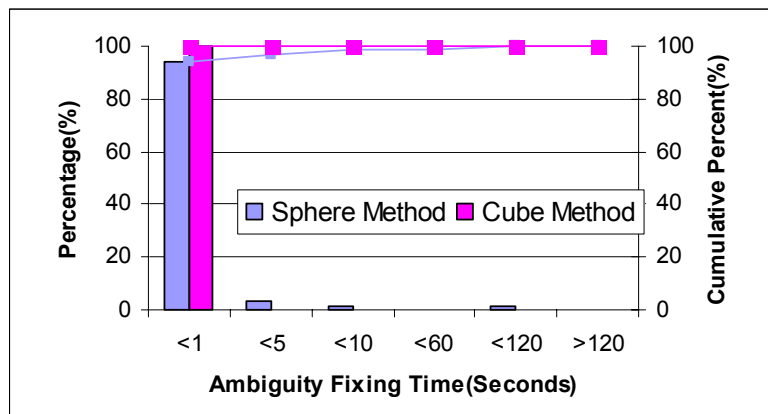


**Figure 6.7: Time to fix ambiguity using different search regions using 10 Hz data**

## 6.7 Static test

The purpose of the test is to examine the performance of the low-cost integrated system, especially the low-cost rate gyros, in static mode. The integrated methodology and the filtering algorithm described in the previous sections for attitude estimation are also investigated under this benign condition.

### 6.7.1 Test description

The static test for the low-cost integrated attitude system was conducted on October 31<sup>st</sup>, 2002. The GPS sensors used in the test were three CMC Allstar receivers. Three low-cost AT575-70 antennas were deployed in an L-shape in the horizontal plane with inter-antenna distances of 0.8 and 0.6 metres as shown in Figure 6.8. The three orthogonally-placed Murata ENV-05D-52 rate gyros were rigidly mounted in an aluminum box to sense the angular velocity of the platform body frame. The low-cost attitude determination system shown in Figure 6.9 was placed on the roof of Engineering Building at the University of Calgary. Due

to the reflections from a nearby concrete wall and a metal tower adjacent to the location of antennas, the location of this test was considered a high multipath environment.

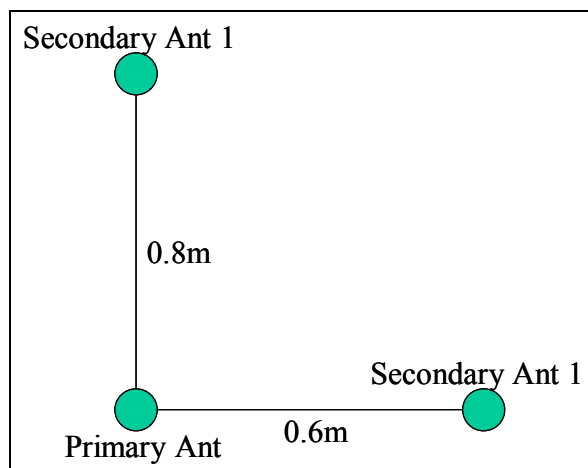


**Figure 6.8: Antenna configuration in static test**

The overall test lasted 45 minutes. The number of satellites and DOP values during the test are depicted in Figure 6.10. In most cases, there were eight satellites above the masking angle and the large E1-DOP during the test led to the low accuracy of attitude estimation in pitch and roll directions. All the raw data from the integrated system were logged into the computer and then processed to estimate the attitude parameters in post mission mode.

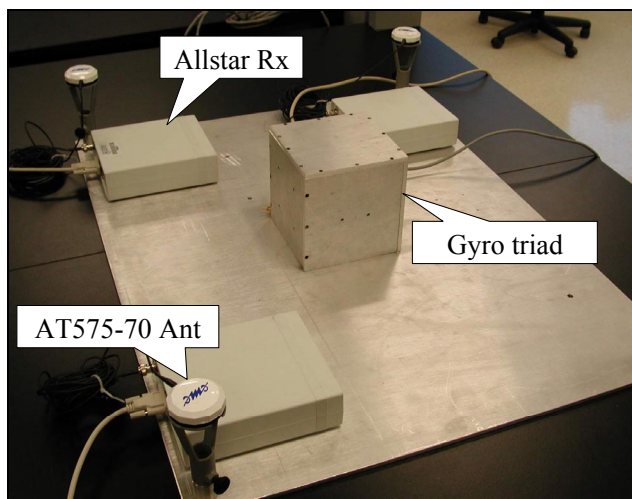


**Figure 6.9: GPS/gyro attitude platform**

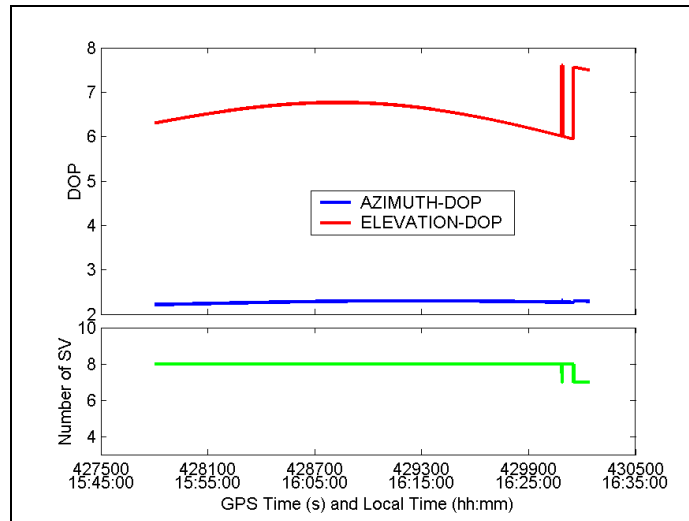


**Figure 6.10: Satellite number and DOPs in static test**

### 6.7.2 Static test results

First, the data from CMC Allstar receivers were processed in the Kalman filter based HeadRT+™ described in Chapter Five. The estimated attitude parameters and the attitude rates are shown in Figure 6.11 and 6.12, and the statistics of those estimates are listed in Table 6.2 and 6.3 respectively. The attitude parameter estimates show the low frequency variation, which is due to the effect of multipath and antenna phase centre variations. The Kalman filter had a positive effect on reducing the random receiver noise in the carrier phase, but did not work on the low frequency multipath and antenna phase centre variations. However, the filter process could not entirely remove the high noise level in the attitude estimates, as the short inter-antenna distances did not dilute the receiver noise effect on attitude estimates. The estimated attitude rates from the Kalman filter using GPS data only have a random noise behavior and the RMS values of three rates were 0.06, 0.09 and 0.09

deg/sec respectively. As the platform remained stationary during the test, the estimated non-zero attitude rates were estimation errors, which are caused mainly by the receiver noise.

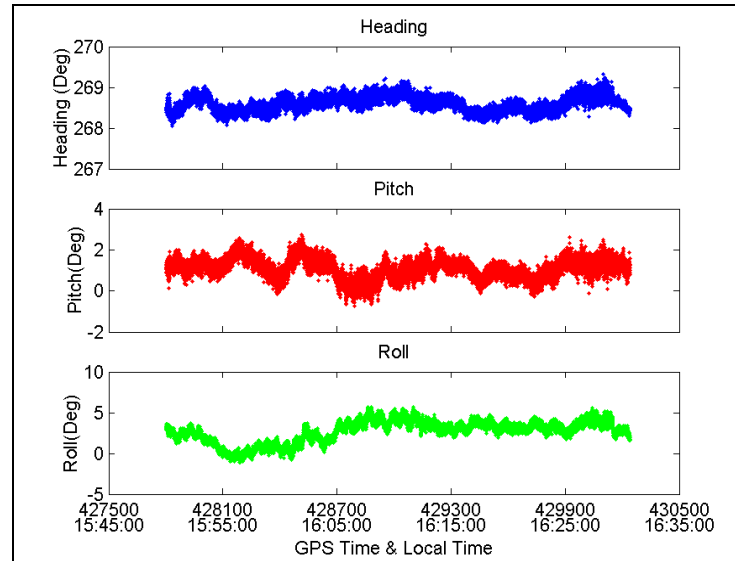


**Figure 6.11: GPS attitude estimates in static test**

**Table 6.2: GPS attitude estimate statistics –Static test (Unit: degrees)**

	Heading	Pitch	Roll
Mean	268.60	1.08	2.68
STD	0.19	0.53	1.37

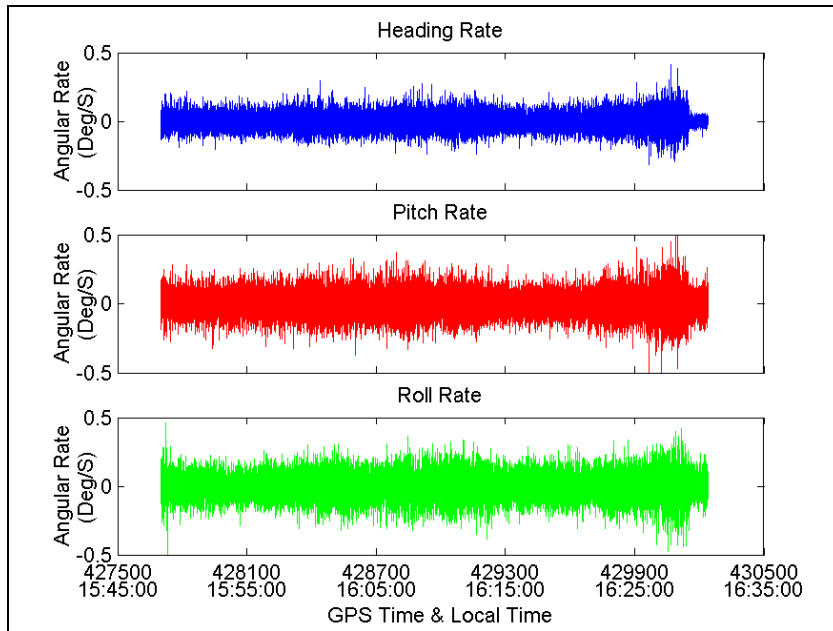


**Figure 6.12: GPS attitude rate estimates in static test**

**Table 6.3: Attitude rate estimate statistics using GPS only (Unit: deg/s)**

	Heading Rate	Pitch Rate	Roll Rate
Mean	0.00	0.00	0.00
RMS	0.06	0.09	0.09

The measurements from the rate gyros were then integrated with the GPS data in the modified GPS/gyro integration Kalman filter. During the process, it was found that the gyro bias estimates were not stable due to the high noise level in the angular rate measurements even after gyro data downsampling to 10 Hz. A smoothing process with a window length of 20 seconds was introduced to decrease the noise effect on these estimates since gyro bias always drifts smoothly over time.

Even though the Murata gyroscope suffers severely from a large drift of gyro bias over time, it has a good accuracy in the attitude velocity measurement over very short intervals.

Therefore, the use of gyro measurements can decrease the noise of the attitude estimates. As a result, the estimated attitude component noise level, shown in Figure 6.13, is significantly smaller than when using GPS data only. However, since the rate gyros can only sense angular rates and the integrated attitude errors from gyro data-only grow rapidly with time, the absolute attitude parameters are primarily derived from GPS. As the attitude statistics in Table 6.4 show, the low frequency variations due to multipath and phase centre variations cannot be removed using rate gyro aiding, as anticipated. This is why the standard deviations given in Table 6.4 are quite similar to those given in Table 6.2.

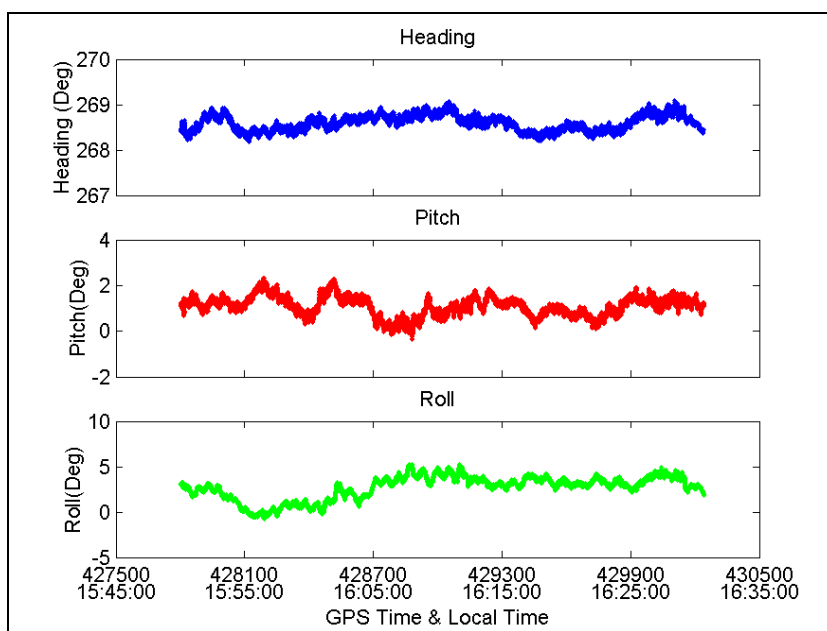


**Figure 6.13: Integrated system attitude estimates in static test**

**Table 6.4: Integrated system attitude estimate statistics in static test (Unit: degrees)**

	Heading	Pitch	Roll
Mean	268.60	1.08	2.67
STD	0.17	0.43	1.32

The attitude rate estimates from the integrated system are shown in Figure 6.14 and the corresponding statistics are listed in Table 6.5. During the test, the attitude rates have a zero mean and random noise behaviour. The magnitude of the attitude rates here are always within 0.2 deg/sec, and the RMS values for angular velocity in heading, pitch and roll are 0.03, 0.04 and 0.04 deg/sec accordingly, which are much lower than those from the GPS-only solution. With the aid of rate gyro measurements, the attitude rate estimates have been improved by nearly 50 %.

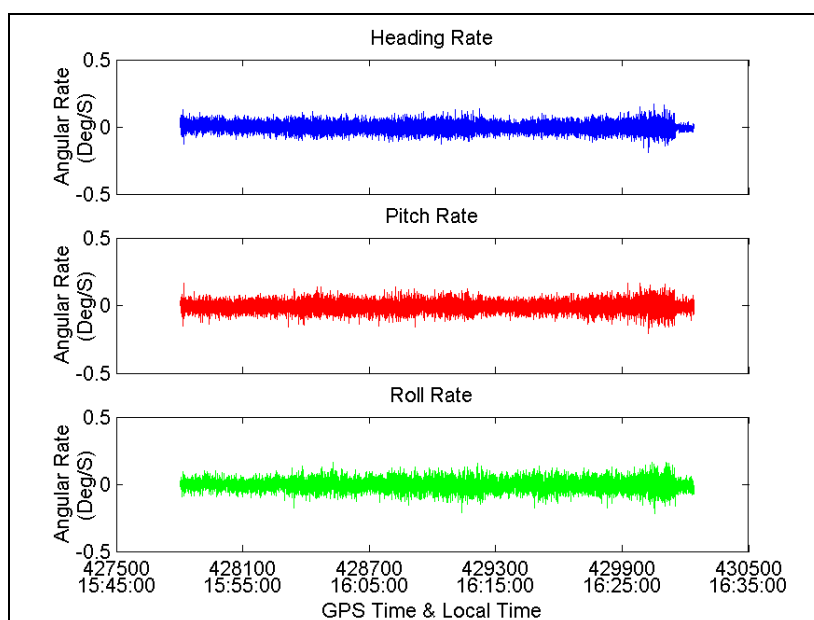


**Figure 6.14: Integrated system attitude rate estimates in static test**

**Table 6.5: Integrated system attitude rate estimate statistics (Unit: deg/s)**

	Heading Rate	Pitch Rate	Roll Rate
Mean	0.00	-0.01	0.00
RMS	0.03	0.03	0.03

The gyro coasting capability during GPS outages is heavily dependent on the estimation of the gyro biases in the Kalman filter. Therefore precise estimation of the gyro bias is always

required for this low-cost GPS/gyro integrated attitude determination system. In this test, as the platform was kept stationary, the variations of voltage output were solely due to the drift of the gyro biases and measurement noise. Figure 6.15 shows the variation pattern of gyro output that has been scaled into angular rate and the estimated gyro bias from the Kalman filter. The blue lines represent the variation patterns of the actual gyro biases contaminated with noise, and the red lines represent the corresponding estimates from the Kalman filter. After smoothing with a window of 20 seconds, the noise in the three estimated gyro biases has been successfully decreased and tightly coincide with the true values. It also can be seen that in the case of the pitch gyro, there is a sudden jump in voltage output, which may be caused by the instability of the power supply. Since the smoothing process is implemented to estimate the gyro bias, the abnormal output leads to a larger gyro bias estimation error.

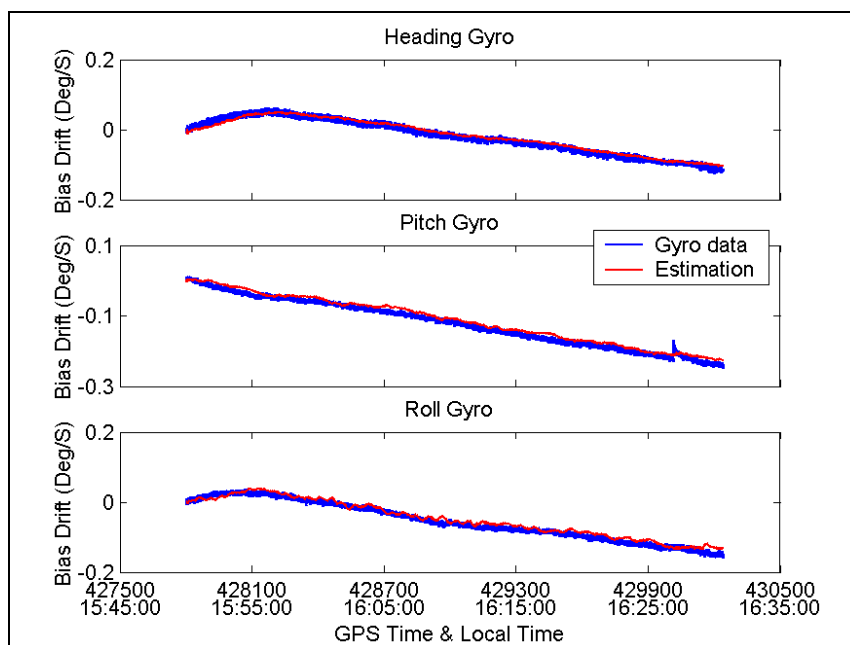


**Figure 6.15: Gyro bias estimation**

With the aid of rate gyros, the accuracy as well as the reliability of the attitude rate estimates in the Kalman filter is significantly improved. The enhancement of attitude rate estimation increases the accuracy of the innovation sequence testing and therefore leads to smaller Minimum Detectable Blunders (MDB) in the reliability analysis. The statistical external reliability, which represents the effect of potential maximum undetected errors on the estimated parameters, has been enhanced as well. In Figure 6.16, the blue lines show the maximum undetected attitude estimation errors due to the limitation of MDB using the GPS data only and the red lines indicate the corresponding values for the integrated system. By introducing the rate gyro measurements, the external reliability of attitude parameters improves distinctly. The measurement redundancy provided by the rate gyros is therefore quite significant. Note that the improvement in roll is more apparent than that in the other two dimensions, mainly because the accuracy of roll parameters from GPS is inferior to the heading and pitch estimates. When the angular velocity measurements are available from low-cost rate gyros, the improvement in roll rate is therefore much more significant than in the other two dimensions. Referring to the satellite information in Figure 6.10, it can also be seen that the error detection capability is correlated with the number of satellite observables. The variation of the external reliability in the last part of test is still dependent on the satellite constellation during that time.

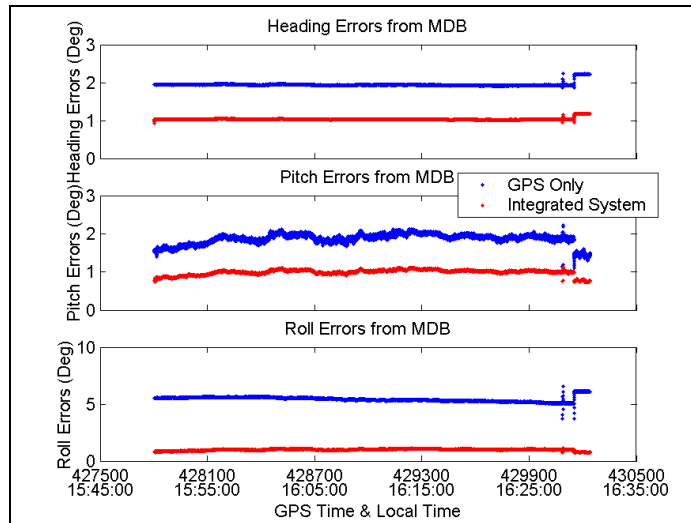


**Figure 6.16: External reliability in static test**

In order to examine the coasting capability of rate gyros when no GPS solutions are available, five GPS outages with different lengths ranging from 20 to 60 seconds were simulated in this data set. The start epochs and durations of GPS outages are listed in Table 6.6. During these GPS outages, the attitude parameters were directly estimated using the angular rate measurements from the rate gyros. The attitude estimates during the entire test are shown in Figure 6.17. During the outages, the attitude rate estimates are biased due to the inaccuracy in gyro bias compensation, and this led to a drift in the attitude parameters. Compared with the attitude results from the integrated system without GPS outages, the differences shown in Figure 6.18, which are indicative of the estimated errors due to the free run of the gyroscopes, are within one degree over 60 seconds for heading and pitch. The roll differences are slightly larger and grow to more than two degrees in one 60-second outage. The accuracy of gyro bias estimates, as well as the length of the outages affects the coasting performance of the rate gyros. In this test, the roll difference for the first 60-second outage (second gap in Figure 6.18) is larger than the attitude drift in the second 60-second outage (fifth gap), which

indicates that the gyro bias estimate in the fifth gap is somehow better than during the second gap.

**Table 6.6: GPS outages during static test in GPS time (Unit: second)**

Outages	Start Epoch	End Epoch	Duration
1 <sup>st</sup>	428000	428020	20
2 <sup>nd</sup>	428500	428560	60
3 <sup>rd</sup>	429100	429120	20
4 <sup>th</sup>	429300	429340	40
5 <sup>th</sup>	429700	429760	60

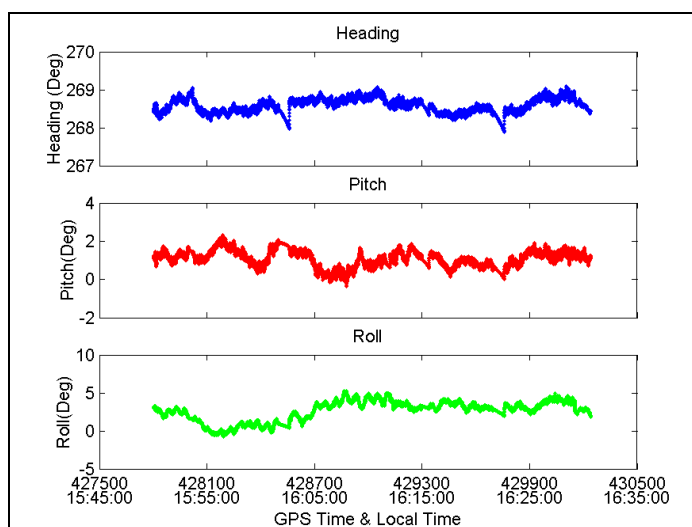


**Figure 6.17: Attitude estimates with GPS outages**

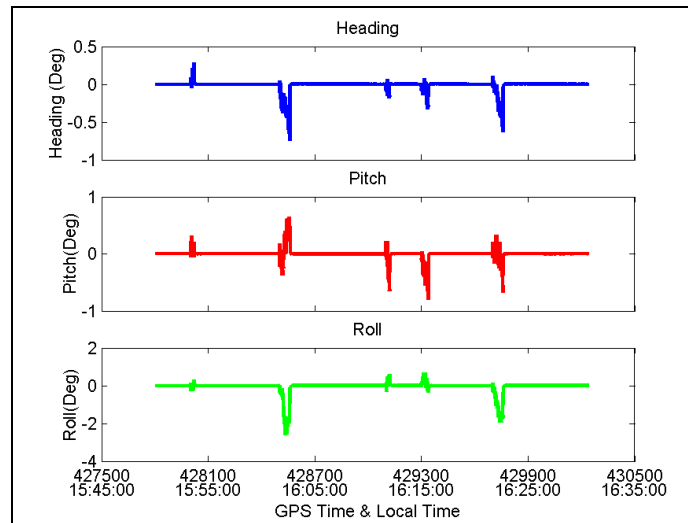


**Figure 6.18: Attitude differences**

## 6.8 Kinematic test

After achieving satisfactory results in the static test, a kinematic test with the low-cost integrated system was conducted with a 2001 Dodge Grand Caravan test vehicle to assess the performance under higher dynamic conditions. The test description and results are shown below.

### 6.8.1 Kinematic test description

The kinematic test was carried out on Jan 29<sup>th</sup>, 2003. The test area consisted of selected streets near the University of Calgary. In order to achieve measurement redundancy for GPS attitude estimation, a fourth GPS unit was added to the system. The baseline lengths for the three inter-antenna vectors were 0.6, 0.8 and 1.0 metre, respectively. A medium-performance GPS/INS system, namely the NovAtel BlackDiamond™, was used with the SAINT™ (Satellite and Inertial Navigation Technique) software developed by the University of Calgary (Petovello 2003) during the test to provide independent and accurate reference

values for attitude parameters. The standard deviations of the attitude estimates from SAINT™ software were always within three arc minutes during the test. Also, a high-performance GPS multi-antenna attitude system using NovAtel Beeline™ receivers and 501 antennas was used to allow further comparisons using different GPS receiver grades. Due to installation limitations, the attitude platforms were not perfectly parallel and the misalignments between the attitude systems were always within 1-2 degrees. The antenna and receiver setups on the test caravan are shown in Figure 6.19 and 6.20.



**Figure 6.19: Antenna setup in kinematic test**

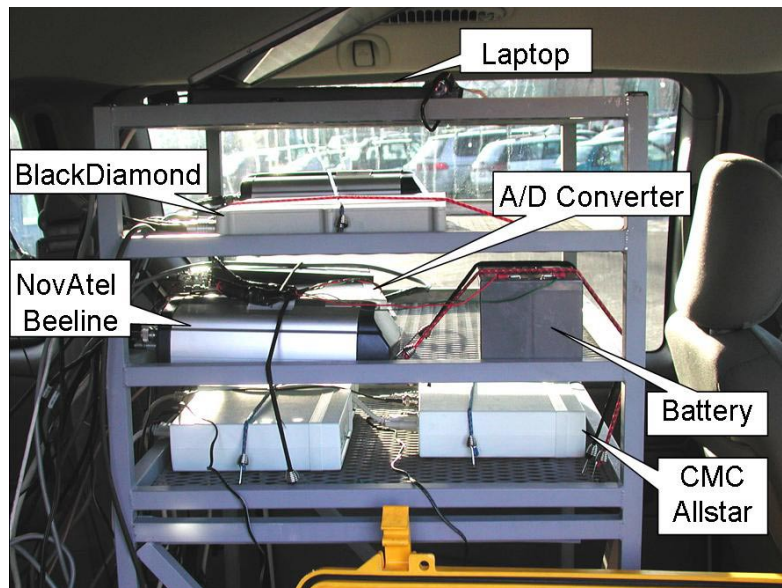


**Figure 6.20: Hardware layout in the vehicle**



the systems. According to the cascade property of rotation (Wertz 1978), the attitude parameters with respect to Body Frame A can be transformed into those with respect to Body Frame B using the following equation if the misalignment angles between A and B are known:

$$\mathbf{R}_b^l = \mathbf{R}_b^a \cdot \mathbf{R}_a^l \quad (6.11)$$

where  $\mathbf{R}_b^a$  represents the rotation matrix from Body frame B to A, which is a function of the misalignment angles.

At the end of the test, the vehicle was kept in stationary mode for about 5 minutes. Therefore it was possible to average the attitude results during this period to obtain the best estimation of the misalignment angles between the attitude platforms. The following steps were taken to determine the misalignment angles: First, the average attitude parameters from different attitude determination systems were calculated during the static mode to reduce the effect of multipath and phase centre variations as well as receiver noise. Then, the averaged attitude parameters were used in Equation 6.12 to calculate the misalignment angles. After that, the estimated attitude parameters from HeadRT+™ were rotated by the misalignment angles. The converted attitude results were then compared with the reference provided by SAINT™ to calculate the estimation errors.

$$\mathbf{R}_a^b = \mathbf{R}_a^l \cdot \mathbf{R}_l^b = \mathbf{R}_a^l \cdot (\mathbf{R}_b^l)^T \quad (6.12)$$

### 6.8.3 Test results

After the data collection, the GPS data from the two grades of GPS sensors were independently fused with the gyro data in the modified HeadRT+<sup>TM</sup>, as discussed in Section 6.5. The attitude results from the integrated system during the dynamic mode were then compared with the references from the SAINT<sup>TM</sup> system. The number of satellites was no less than seven, which provided good geometry during the test run.

The attitude parameters estimated from the SAINT<sup>TM</sup> are shown in Figure 6.22. The standard deviations of the attitude parameters are always within three arc minutes for heading and 0.5 arc minutes for pitch and roll.

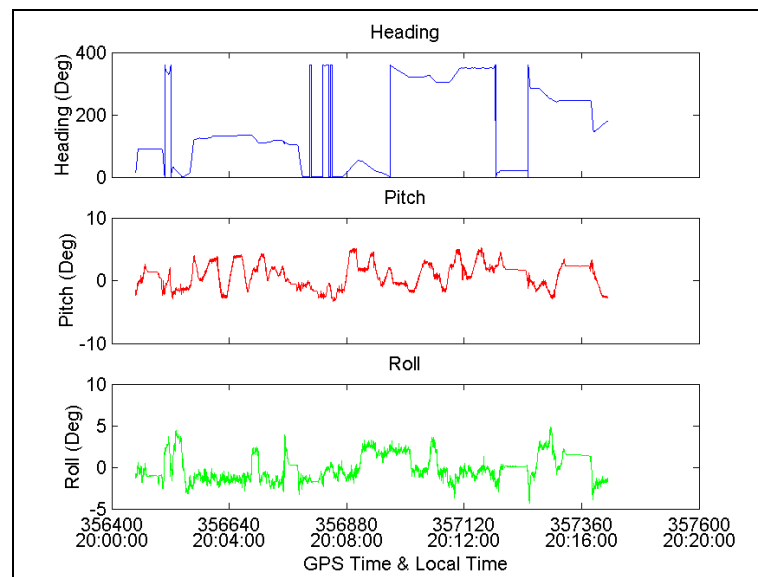


**Figure 6.22: Attitude reference in kinematic test**

During the data processing phase, the carrier phase measurements from the Beeline<sup>TM</sup> units were found to be quite good, and the true double difference ambiguities were solved instantaneously at the start of the test. No cycle slips occurred or were detected and the

integer ambiguities for the three antenna vectors were correctly fixed during the entire test run. The attitude results from the Beeline™ based integrated system are shown in Figure 6.23. After misalignment angle compensation, the estimated attitude parameters were then compared with the reference results from the SAINT™. The estimated attitude errors are then shown in Figure 6.24 and the resulting statistics can be found in Table 6.7. The small mean values of attitude estimates indicate that estimation accuracy is only affected by the small measurement errors introduced by multipath and antenna phase centre variations. The RMS for heading error is 0.37 degrees and the corresponding values for pitch and roll are about 0.52 and 0.85 degrees, respectively. Taking the short inter-antenna distances into account, the estimation accuracy is satisfactory.

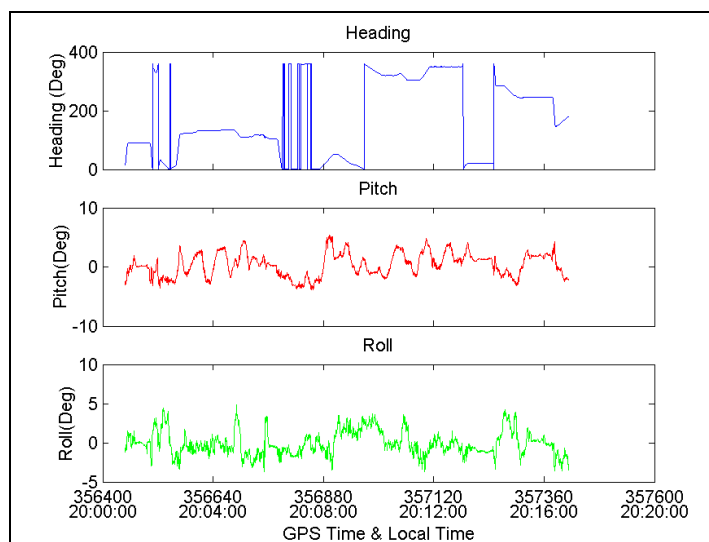


**Figure 6.23: Integrated system attitude estimates -Kinematic test using Beeline™ units**

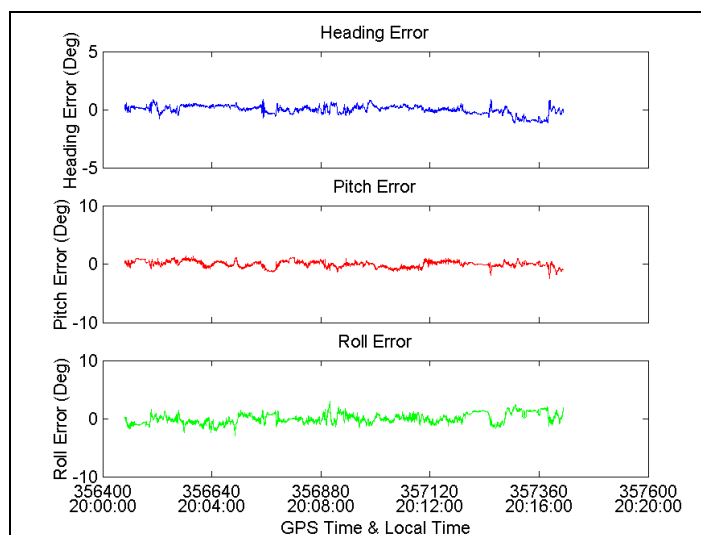


**Figure 6.24: Attitude estimation errors –Kinematic test using Beeline™ units**

**Table 6.7: Attitude estimation error statistics - Kinematic test using Beeline™ units**

Unit: degrees	Heading	Pitch	Roll
Mean	-0.01	-0.01	0.00
RMS	0.37	0.52	0.85
Max (abs)	1.15	2.53	2.98

The gyro bias estimation in the Beeline™ based integrated system is shown in Figure 6.25. As the continuous accurate attitude estimates are available with this system, these gyro biases from the centralized Kalman filter should be precisely estimated. Such estimates will be used as the reference when examining the gyro bias estimation in the low-cost integration solution.

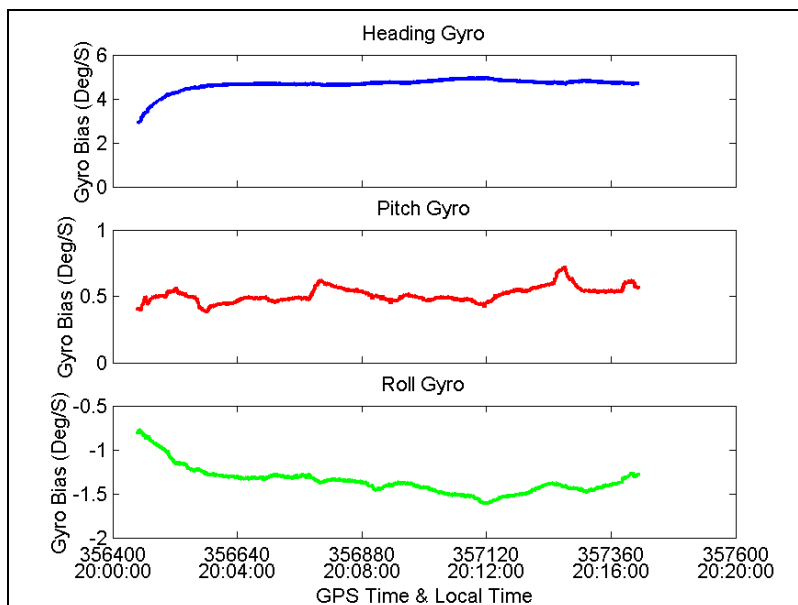


**Figure 6.25: Gyro bias estimation--Kinematic test using Beeline™ units**

As may be expected, carrier phase measurements using the low-cost CMC receivers and AT575-70 antennas are more affected by multipath and antenna phase centre variations as well as cycle slip occurrences. In this test, it was found that the double difference residuals reached 7-8 cm even though the integer ambiguities were correctly determined. Such noisy carrier phase measurements not only result in a poor estimation accuracy of attitude parameters, but also can lead to difficulties in ambiguity resolution and cycle slip detection. Under high dynamics, some small cycle slips with the magnitude of half or one cycle were found in the carrier phase measurements. Figure 6.26 shows the double difference phase of antenna vectors in the kinematic test. The sudden change of phase combination with a magnitude of 0.1 m is caused by a half cycle slip. The large carrier phase measurement errors due to antenna effects in kinematic condition make the residual check for cycle slip detection too sensitive if the tolerance selected is as small as the default criteria in HeadRT+™ used for the Beeline™ system. However, choosing a higher threshold for the residual check is

very risky as it may lead to a wrong ambiguity combination passing through the ambiguity distinguishing process as well as the insensitivity of small cycle slips. In this test, the tolerances used in the residual check were 5.5 cm for a single DD residual and 3.5 cm for a group in order to reject any incorrect ambiguity set since the rate gyros can ensure availability in the case of no GPS solutions. As a result of choosing small thresholds, the fixed double difference ambiguities were frequently identified as erroneous, and ambiguity resolution restarted very often for the large double difference phase residuals. Even though false alarms have occurred, they do not affect the attitude estimation performance provided the correct double difference ambiguities can be resolved again instantaneously. However, when the sphere search volume was used in ambiguity resolution, the entire search process took 10-20 seconds to determine the integer ambiguity sets, 20 % of which were identified as erroneous by the quality control system. This kind of long time to fix ambiguities resulted in large estimation errors in the attitude parameters because the coasting capability of rate gyros degraded due to vibration in high dynamics. Compared with the sphere volume method, the cube search region significantly reduced the search volume and the number of candidate ambiguities, which resulted in fast and reliable ambiguity resolution. In this test, the integer ambiguities could be correctly selected in less than one second in 91% of the cases.

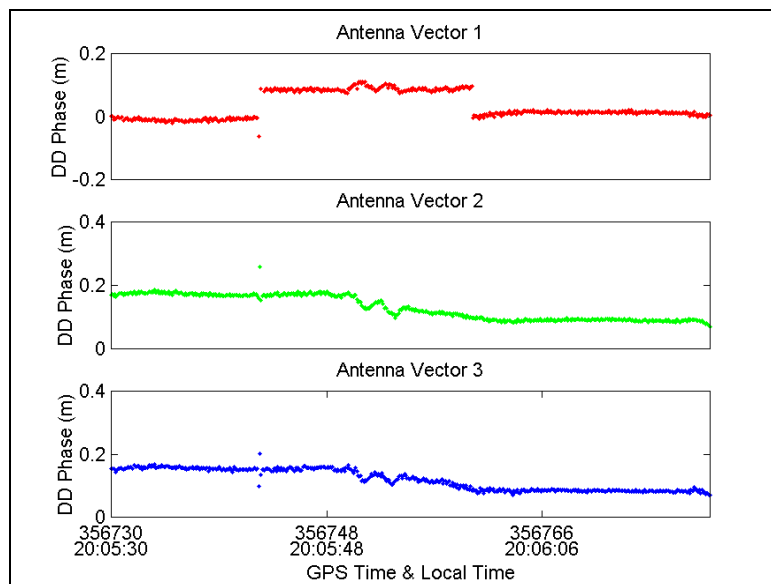


**Figure 6.26: DD phase in kinematic test using Allstar units**

Figure 6.27 shows the attitude parameters estimated using CMC Allstar units integrated with rate gyros. Compared with the attitude results using high-end Beeline™ units, the performance are much poorer, as anticipated. Using phase measurements from low-cost CMC Allstar sensors, the GPS inter-antenna vector solutions are not always available. In this test, 88.4 % of the attitude solutions are estimated from GPS/gyro measurements and the other 11.6% are obtained from rate gyro measurements only. The low availability of GPS vector solutions is caused by the large carrier phase measurement errors, such as multipath and antenna phase centre variations and the tight threshold used for the residual test. The longest coasting period using gyro data only is 12.9 s, which leads to a 2-degree error in each attitude component. The gyro coasting capability degrades compared with the performance in the static test, because the low-cost gyros suffer from vibration and jerk introduced by platform motion.

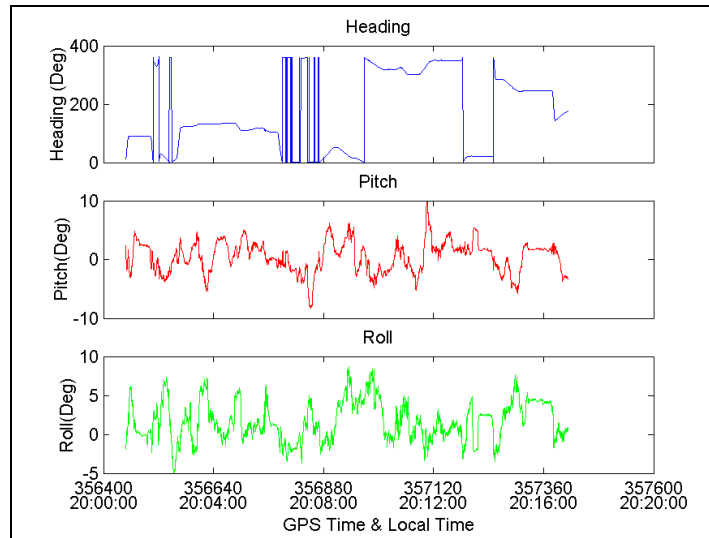


**Figure 6.27: Integrated system attitude estimates - Kinematic test using Allstar units**

The differences between attitude estimates from the low-cost integrated system after the misalignment compensation and the attitude reference obtained from SAINT™ are shown in Figure 6.28, and the corresponding statistics are listed in Table 6.8. Compared with the corresponding statistics of Beeline™ based attitude solutions, the RMS values grow to 0.73, 1.46 and 1.74 degrees for heading, pitch and roll. Even though most of the attitude errors are within a two-sigma limit, the maximum heading, pitch and roll differences reached 3.38, 5.50 and 7.26 degrees, respectively. These large estimation errors are mainly due to low frequency carrier phase measurement errors introduced by multipath and antenna phase variations. Cycle slip occurrences can be successfully identified using the phase prediction method, residual check as well as the innovation sequences since the dramatic changes in residuals or vector solutions due to cycle slips are easy to detect by the above methods. However, the quality control system based on innovation sequence is insensitive to low frequency antenna phase centre variations and multipath. Using a smaller tolerance in the residual check may

have an impact on rejecting GPS antenna vector solutions contaminated by strong multipath and large antenna phase centre variations in attitude estimation; however the resulting lower availability of GPS solutions can lead to larger errors in the attitude parameters, as the rate gyro errors grow quickly without GPS update.

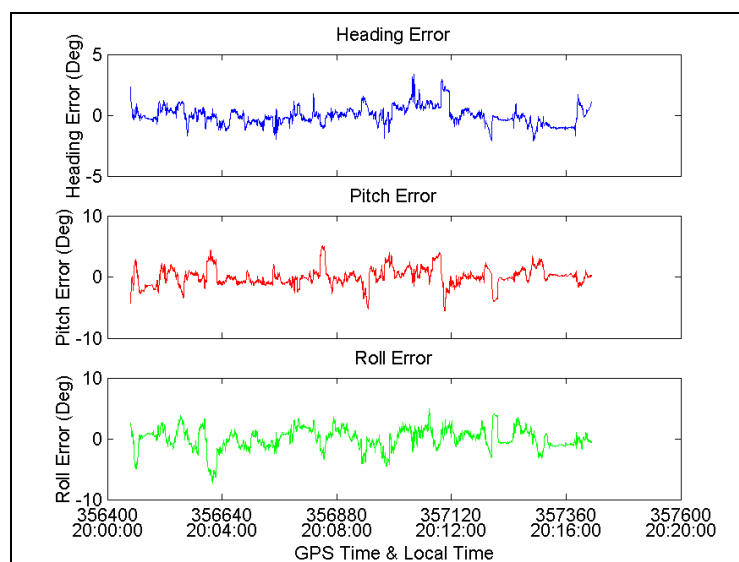


**Figure 6.28: Attitude errors using the integrated Allstar based attitude system**

**Table 6.8: Integrated attitude estimation error statistics of kinematic test using Allstar units**

Unit: degrees	Heading	Pitch	Roll
Mean	-0.04	0.03	-0.01
RMS	0.73	1.46	1.74
Max	3.38	5.50	7.26

The gyro bias estimation from the Allstar based integration system is shown in Figure 6.29. Compared with the gyro bias estimates from Beeline<sup>TM</sup> based attitude system, the estimates have similar drifting trends but are not as smooth as those from the integrated solution using the Beeline<sup>TM</sup> units. The differences in gyro bias estimates between the two attitude systems are mainly caused by inaccurate attitude estimation and the low availability of GPS vector

solutions in the Allstar based integrated system. The poor estimation of gyro biases in the low-cost integrated system therefore leads to significant estimated attitude parameter drifts during the GPS outages.

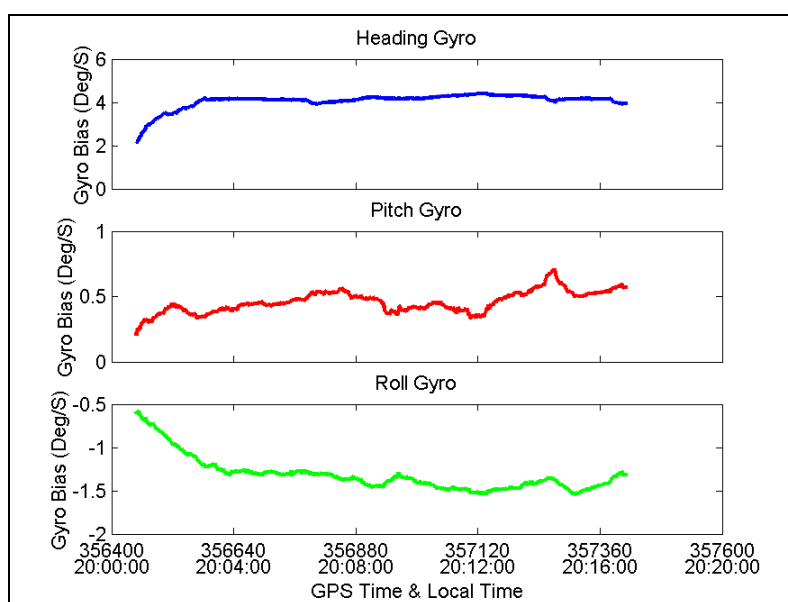


**Figure 6.29: Gyro bias estimation from Allstar based integration system in kinematic test**

## **CHAPTER 7**

### **CONCLUSIONS AND RECOMMENDATIONS**

In this research, the performance of a low-cost GPS based attitude determination system was extensively investigated. The concept of attitude determination using multiple closely spaced GPS antennas was reviewed. The error sources in carrier phase measurements and other factors that affect attitude estimation have been examined with the help of a Spirent STR-4760 hardware simulator. Low-cost CMC Allstar receivers were used in the attitude determination system and the impact of low-cost receivers and antennas on attitude estimation has been explored at length. The estimation error introduced by the misalignment between the low-cost receiver clocks has been assessed in static mode. Some reliability improvement measures, namely using a higher data rate, angular constraints and a quality control system in a Kalman filter, have been tested to improve the reliability of the low-cost attitude determination system under kinematic conditions. Due to the limitations of the standalone GPS low-cost attitude system, three Murata rate gyros were used to sense the angular velocity of the platform. A centralized Kalman filter has been developed to fuse the data of the low-cost GPS/gyro integrated system. The integrated attitude system was tested both in static mode and under kinematic conditions to gauge the performance under different dynamics.

Based on the results and findings obtained from the above work, the following specific conclusions can be drawn:

1. The low-cost CMC Allstar receiver has fairly good receiver noise performance in a benign environment. Without multipath and antenna phase centre variation effects, the attitude estimation from the Allstar receivers can achieve performance similar to those of high performance NovAtel OEM4 receivers. In high dynamics, the low-cost receiver suffers from cycle slip occurrences.
2. The antennas have significant effects on the accuracy of attitude estimation, as the main error sources are the multipath as well as antenna phase centre variations in GPS attitude determination. Multipath usually is the dominant error source that plagues the performance of low-cost attitude determination systems. In order to mitigate this error source, a clear antenna site with no reflector in the vicinity should be selected to avoid the high multipath environment, whenever possible. Antenna phase centre variations are highly dependent on antenna type. The calibration of this error source for the low-cost antennas is very complicated in that it is nearly impossible to isolate antenna phase centre variations from the carrier phase multipath error under normal field operating conditions.
3. Using low-cost GPS sensors, the reliability of ambiguity resolution in attitude determination is severely degraded due to the noisier carrier phase measurements and

- cycle slip occurrences. The use of higher data rate measurements can improve ambiguity resolution as well as dynamic modeling in the Kalman filter. The angular constraint test can effectively detect erroneous ambiguity combinations and wrong inter-antenna vector solutions. The quality control system based on the innovation sequences in the Kalman filter estimation can effectively identify incorrect antenna vector solutions. Due to the high carrier phase measurement errors and the change in the number of valid estimated inter-antenna vectors, the above measures have limitations in the low-cost GPS alone system.
4. The employment of low-cost piezoelectric vibrating gyros in the low-cost attitude system enhances the overall attitude estimation performance. With the aid of continuous angular rate measurements, the high frequency noise in attitude estimates can be reduced, since the low-cost rate gyros have satisfactory short-term accuracy after smoothing. Another advantage of the integrated system is the coasting ability of rate gyros. During GPS outages, the rotation of the platform can be determined by integrating the sensed angular rate measurements over time and the absolute attitude output can be maintained. Since the direct measurements of angular velocity are available, the prediction process in the Kalman filter is enhanced compared with the GPS-only system, which improves error detection capability in the quality control system.

5. Compared to the sphere search region definition, the specific cube search volume based on attitude information decreases the number of candidate ambiguity combinations. The reliability of ambiguity resolution as well as the time to fix ambiguities can be improved with fewer candidate ambiguity combinations.
6. Small cycle slip occurrences are very difficult to detect in the low-cost attitude determination data. Since the CMC Allstar receiver does not output raw phase velocity (i.e. Doppler) measurements, the phase prediction method is ineffective to detect small cycle slips with a magnitude of half or one cycle. With the existence of large measurement errors due to multipath and antenna phase centre variations as well as increased receiver noise, the large double difference residuals lead to numerous false alarms resulting from the residual check in cycle slip detection algorithm.
7. As gyro biases drift randomly, the long-term accuracy of the low-cost rate gyro degrades significantly with time. The absolute attitude parameters are mainly estimated from the GPS carrier phase measurements. The low frequency multipath and antenna phase centre variation effects on attitude estimation cannot be removed with the aid of low-cost rate gyros.
8. The performance of gyro coasting is highly correlated with the estimation of gyro biases as well as with the lengths of GPS outages. In order to achieve the best estimation of gyro biases, highly accurate carrier measurements from GPS sensors are

required. The limitations of the low-cost GPS units used herein lead to the ineffectiveness of the ambiguity resolution process. Without the update of GPS solutions, the gyro bias estimation degrades accordingly, which ultimately results in a poor bridging capability.

More work needs to be done to improve the performance of low-cost GPS-based attitude determination systems. Based on the above work, the following are recommendations for future research in this area:

1. The quality of carrier phase measurements from CMC Allstar receivers has to be investigated in high dynamics. Using the GSS simulator, only the impact of the high-dynamic GPS signals on tracking loops can be examined. When the low-cost receiver experiences high velocity or acceleration, performance degradation of the oscillator is expected. The impact of the above factor on carrier phase measurements is not fully investigated here..
2. The investigation of carrier phase multipath mitigation in kinematic conditions is highly recommended for attitude determination. With the use of low-cost antennas, carrier phase measurements severely suffer from multipath. The accuracy and reliability of GPS-based attitude systems can be significantly improved if the carrier phase multipath can be mitigated. In addition, calibration of the antenna phase centre variations should be investigated.

3. The implementation of a real time GPS/gyro integration system should be carried out. The major modification in the attitude software would be raw data conversion and synchronization in real time.
4. Investigation into the use of other types of MEMS-based rate gyros in the low-cost integrated attitude system is recommended. With well-modeled gyro bias estimation, the performance of attitude determination of an integrated system could be significantly improved.
5. The use of Doppler measurements in attitude determination should be investigated as some low cost receivers output such measurements. The inclusion of Doppler can enhance the estimation of attitude rate in Kalman filter and improve the accuracy of GPS-only and GPS/Gyro attitude system.
6. A larger inter-antenna spacing configuration should be tested for this low-cost integrated system. With the extension of inter-antenna distances, estimation accuracy using GPS measurements can be effectively upgraded, which will enhance accuracy performance.
7. The low-cost integrated attitude determination system should be further tested in different environments and dynamics. As expected, the low-cost attitude system

tested herein shows a lot of promise. Considering the stronger multipath and lower dynamics in marine applications, the performance of this low-cost attitude determination system in this special environment should be extensively investigated.

## REFERENCES

- Alban, Santiago (2002) An Inexpensive and Robust GPS/INS Attitude System for Automobiles, Proceedings of ION GPS03, Portland, OR, Institute of Navigation
- Axelrad, P. and L.M. Ward (1994) On-Orbit GPS Based Attitude and Antenna Baseline Estimation, ION National Technical Meeting, San Diego, CA, Institute of Navigation
- Bernelli-Zazzera, F. and Campana, R. (1999) Adaptive Kalman Filtering for Multipath rejection in GPS Based Attitude Determination, AIAA Conference AAS 99-167.
- Braasch, M.S. (1996) GPS Multipath Model Validation, Proceedings of IEEE PLANS96, Atlanta, April 22-26, pp. 276-278.
- Braasch, M. and F. van Graas (1991) Guidance Accuracy Considerations for Real Time GPS Interferometry, Proceedings of ION GPS91 Conference, Albuquerque, New Mexico, the Institute of Navigation, pp. 373-386.
- Brown, R.G. and P.Y.C. Hwang (1992) Introduction of Random Signals and Applied Kalman Filter, Second Edition, John Wiley & Sons, Inc., New York.

Campana, R. and Marradi, L., (1999) GPS Attitude Determination by Adaptive Kalman Filtering, Proc. of ION GPS99, 14-17 September, 1999, Nashville, TN, pp. 1979-1988.

Cannon, M.E., J.K. Ray, and J. Deschamps (2000) Attitude Determination Using Multipath Mitigation on Multiple Closely-Spaced Antennas. Proceedings of GPS 2000, Salt Lake City, The Institute of Navigation, Alexandria, VA, pp.2201-2208.

Chen, D. and Lachapelle, G. (1994) A Comparison of the FASF and Least-Squares Search Algorithms for Ambiguity Resolution On The Fly, Proc. of the International Symposium on Kinematic Systems in Geodesy, Geomatics and Navigation, KIS94, Banff, Alberta, August 30-September 2, 1994.

Cohen, C.E. (1992) Attitude Determination Using GPS, Ph.D. Thesis, Stanford University, Dec. 1992.

Cohen, C.E. (1996) Global Positioning System: Theory and Application, Chapter 19: Attitude Determination, Volume 163, Progress in Astronautics and Aeronautics, pp. 519-538.

- Cohen, C.E. and Parkinson, B.W. (1991), Expanding the Performance Envelope of GPS-Based Attitude Determination, Proc. ION GPS-91, Albuquerque NM, 1991, pp. 1001-1012.
- Comp, C. (1993) Optimal Antenna configuration for GPS Based Attitude Determination, Proceedings of the six International Technical Meeting of ION GPS93, Salt Lake City, Utah, Institute of Navigation, pp.773-779.
- Dierendonck, A.J., Fenton, P. and Ford, T. (1992), Theory and Performance of Narrow Correlator Pacing in a GPS Receiver, Navigation, Journal of the Institute of Navigation, Vol. 39, No. 3, pp. 265-83, 1992.
- Dumaine, M. (1996) High Precision Attitude Using Low Cost GPS Receivers, Proceeding of ION GPS96, Kansas City, September 17-20, Institute of Navigation, pp.1029-1035.
- El-Mowafy, A. (1994) Kinematic Attitude Determination From GPS, Ph.D. Thesis, UCGE Reports, Number 20074, University of Calgary, Calgary, Alberta, Canada, <http://www.geomatics.ucalgary.ca/links/GradTheses.html>.
- Euler, H. and Hill, C. (1995) Attitude Determination: Exploiting all Information for Optimal Ambiguity Resolution, Proceedings of the Eighth International Technical Meeting, GPS95, Palm Spring, California, Institute of Navigation, pp.1751-1757.

Frei, B. and Beutler, G. (1990) Rapid Static Positioning Based on the Fast Ambiguity Resolution Approach "FARA": Theory and First Results, *Manuscripta Geodaetica*, Vol 15, November 6, pp.325-356.

Georgiadou, Y. and Kleusberg, A. (1988) On Carrier Signal Multipath Effects in Relative GPS Positioning, *Manuscripta Geodetica*, Springer-Verlag., Vol. 13, No. 3, pp 172-179.

Global Simulation Systems (2000) STR Series Multichannel Satellite Navigation Simulator – Reference Manual, Aspen Way, Paignton, Devon TQ4 7QR.

Gomez, S. (2000) Attitude Determination and Attitude Dilution of Precision (ADOP) Results for International Space Station Global Positioning System (GPS) Receiver, Proc. of ION GPS 2000, Salt Lake City, UT, 19-22 September, 2000, pp.1995-2002.

Hatch, R. (1989) Ambiguity Resolution in the Fast Lane, Proceedings of the Second International Technical Meeting of the Satellite Division of the Institute of Navigation, ION GPS-89, Colorado Springs, Colorado, September 26-29, 1989, pp45-52.

Hatch, R. (1991) Instantaneous Ambiguity Resolution, Proceedings of IAG Symposium No.107 on Kinematic systems in Geodesy, Surveying and Remote Sensing, Springer Verlag, New York.

Hayward, R., Gebre-Egziabher, D., Schwall, M., Powell, D. and Wilson, J. (1997) Inertially Aided GPS Based Attitude Heading Reference System (AHRS) for General Aviation Aircraft, Proc. of ION GPS 97, Kansas City, MO, September, 1997, pp.289-298.

Hofmann-Wellenhof, B., Lichtenegger and H., Collins, J.(2001) Global Positioning System: Theory and Practice, Fifth edition, Springer, Wien New York.

Hoyle, V., Lachapelle, G., M.E. Cannon and Wang, C. (2002) Low-Cost GPS Receivers and their Feasibility for Attitude Determination, Proc. of GPS NTM02, The Institute of Navigation, San Diego, CA, pp.226-234.

Jefferson,D. and Y. Bar-Sever. (2000) Accuracy and Consistency of Broadcast GPS Ephemeris Data. Proceedings of ION GPS2000 Conference, Salt Lake City, Utah, Institute of Navigation, pp.391-395.

Lachapelle, G., Liu, C., Lu, G., Townsend, B., Cannon, M.E. and Hare, R. (1993) Precise Marine DGPS Positioning Using P Code and High Performance C/A Code Technologies, Geomatica, Canadian Institute of Geomatics, Ottawa, Vol.47, No.2, pp.117-128

Lachapelle, G., M.E. Cannon and G. Lu (1992) High-Precision GPS Navigation with Emphasis on Carrier-Phase Ambiguity Resolution, Marine Geodesy, Vol. 15, pp.253-269.

Leick, A. (1995) GPS Satellite Surveying, Second edition, John Wiley and Sons, Inc., New York, 560 pp.

Lu, G. (1991) Quality Control for Differential Kinematic GPS Positioning, M.Sc. Thesis, UCGE Report, No. 20042, Department of Geomatics Engineering, University of Calgary, Alberta, Canada, <http://www.geomatics.ucalgary.ca/links/GradTheses.html>.

Lu, G. (1994) Development of a GPS Multi-Antenna System for Attitude Determination, Ph.D. thesis, UCGE Reports, Number 20073, Department of Geomatics Engineering, University of Calgary, Alberta, Canada, <http://www.geomatics.ucalgary.ca/links/GradTheses.html>.

Mader, G. (1998) Calibration of GPS Antennas, NOAA, NOS, NGD, GRD, WWW-Server: <http://www.grdl.noaa.gov/grd/gps/projects/antcal>

Marconi Electronics (2000) Allstar User's Manual, P/N 220-600944-0XX

Markley, F.L. (1993) Attitude Determination from Vector Observations: a Fast Optimal Matrix Algorithm, The Journal of the Astronautical Sciences, Vol. 41, No. 2, 1993, pp. 261-280.

Mitra, P. and Enge, P. (2001) Global Positioning System: Signals, Measurements, and Performance, Ganga-Jamuna Press, Lincoln, Massachusetts, ISBN:0-9709544-0-9

Motta, L.(2003) Coriolis Force <http://scienceworld.wolfram.com/physics/CoriolisForce.html>

Murata (2000) Technologies Used for Ceramic Bimorph Gyroscopes,

<http://www.murata.com/articles/9089.html>

Nakamura, T. (1990) Vibration Gyroscope Employs Piezoelectric Vibrator, JEE, September, 1990.

Olynik, M. (2002) Temporal Characteristics of GPS Error Sources and Their Impact on Relative Positioning, M.Sc. Thesis, UCGE Report 20162, Department of Geomatics Engineering, University of Calgary, Calgary, Alberta, Canada, <http://www.geomatics.ucalgary.ca/links/GradTheses.html>.

Parkinson, W.W. and Enge P.K. (1996) Global Positioning system: Theory and Applications, Vol. 2, American Institute of Aeronautics and Astronautics, Inc., Washington DC, pp. 3-55.

Petovello, M. (2003) Real-time Integration of a Tactical-Grade IMU and GPS for High-Accuracy Positioning and Navigation, Ph.D. thesis, UCGE Report No. 20173, Department of Geomatics Engineering, University of Calgary, Calgary, Alberta, Canada, <http://www.geomatics.ucalgary.ca/links/GradTheses.html>.

Phelts, R.E. and Enge, P. (2000), The Multipath Invariance Approach for Code Multipath Mitigation, Proc. ION GPS2000, Salt Lake City, UT, 2000, pp.2376-2384.

Pruszynski, C.J., Ulmer, K.W. and Phelps, C.W. (2001), Tactical Far Target Location Using Position and Azimuth from a P(Y) Code GPS Attitude Determination System, Proc. ION GPS01, Salt Lake City, UT, 2001, pp. 2937-2945.

Raquet, J. (1998) Development of a Method for Kinematic GPS Carrier-Phase Ambiguity Resolution Using Multiple Reference Receivers, Ph.D. Thesis, UCGE Report, No. 20116, Department of Geomatics Engineering, University of Calgary, Alberta, Canada, <http://www.geomatics.ucalgary.ca/links/GradTheses.html>.

Raquet, J. (2001) GPS Receiver Design, ENGO699.64 Lecture Notes, Department of Geomatics Engineering, University of Calgary, Calgary, Alberta, Canada.

Ray, J. (2000) Mitigation of GPS Code and Carrier Phase Multipath Effects Using a Multi-Antenna System, Ph.D. thesis, UCGE Reports, Number 20136, University of Calgary, Calgary, Alberta, Canada, <http://www.geomatics.ucalgary.ca/links/GradTheses.html>.

Ray, J. (2002) Advanced GPS Receiver Theory, ENGO699.73 Lecture Notes, Department of Geomatics Engineering, University of Calgary, Calgary, Alberta, Canada.

Savage, P. (1978) Strapdown Sensors NATO AGGAARD Lecture Series No. 95.

Schleppé, J. (1996) Development of a Real-Time Attitude System Using a Quaternion Parameterization and Non-Dedicated GPS Receivers, M.Sc. Thesis, UCGE Reports, Number 20096, University of Calgary, Calgary, Alberta, Canada, <http://www.geomatics.ucalgary.ca/links/GradTheses.html>.

Schmitz, M., G. Wübbena, G. Boettcher, G. Seeber, V. Böder, F. Menge (2002). Absolute Receiver Antenna Calibrations with a Robot. Presentation at IGS Workshop "Towards Real-Time", April 8-11, 2002, Ottawa, Canada.

Seeber, G. (1993) Satellite Geodesy, Walter de Gruyter and Co., Berlin, pp. 531.

Shuster, M.D. and Oh, S.D. (1981) Three Axis Attitude Determination from Vector Observations, Journal of Guidance, Control and Dynamics, Vol. 4, No. 1, 1981, pp.70-77.

Skone, S. (1999) Wide Area Ionosphere Grid Modelling in the Auroral Region, Ph.D. Thesis, University of Calgary, Calgary, Alberta, Canada, <http://www.geomatics.ucalgary.ca/links/GradTheses.html>.

Spilker, J. (1996) Global Positioning System: Theory and Application, Chapter 13: Tropospheric Effects on GPS, Volume 163, Progress in Astronautics and Aeronautics, pp. 517-546

Stephen, J. (2000) Development of a Multi-sensor GNSS Based Vehicle Navigation System, M.Sc. thesis, UCGE Reports, Number 20140, Department of Geomatics Engineering, University of Calgary, Alberta, Canada, <http://www.geomatics.ucalgary.ca/links/GradTheses.html>.

Teunissen, P.J.G. and Salzman, M.A. (1988) Performance Analysis of Kalman Filters, Reports of the Faculty of Geodesy, Delft University of Technology, Delft, The Netherlands.

Townsend, B., et al (1995), Performance Evaluation of the Multipath Estimating Delay Lock Loop, Navigation, Journal of Navigation, Vol. 42, NO. 3, pp.503-14, 1995.

Ueno, M., Santerre, R. and Babineau, S. (1997) Impact of Antenna Configuration on GPS Attitude Determination, Proc. of the 9<sup>th</sup> World Congress of International Association of Institute of Navigation (IAIN97), Amsterdam, The Netherlands, November, 1997.

Vinnins M., & L.D. Gallop (1997) GPS as a Method of Heading Determination in a Short Baseline Application in the Canadian Arctic. Proceedings of International Symposium on Kinematic Systems in Geodesy, Geomatics and Navigation - KIS97 (Banff, June 3-6), Dept of Geomatics Engineering, The University of Calgary, pp.389-394.

Wahba, G. (1965) A Least Squares Estimate of Spacecraft Attitude, SIAM Review, Vol. 7, No.3, 1965.

Wang, C. and Lachapelle, G. (2002) GPS Attitude Determination Reliability Improvement Using Low Cost Receivers, Proc. of ION GPS02 Conference, Portland, OR, The Institute of Navigation, pp.1064-1074.

Wertz, J.R. (1978) Spacecraft Attitude Determination and Control, Kluwer Academic Publishers, The Netherlands, 1978.

Wong, L. (1979) Mathematics Hand Book, Advanced Education Express, Beijing, China, 1979.

**APPENDIX A:**  
**DOUBLE DIFFERENCE RESIDUALS OF SELECTED SATELLITE PAIRS**

The double difference residuals for different time misalignments are intentionally offset by -1 cm in the following plots.

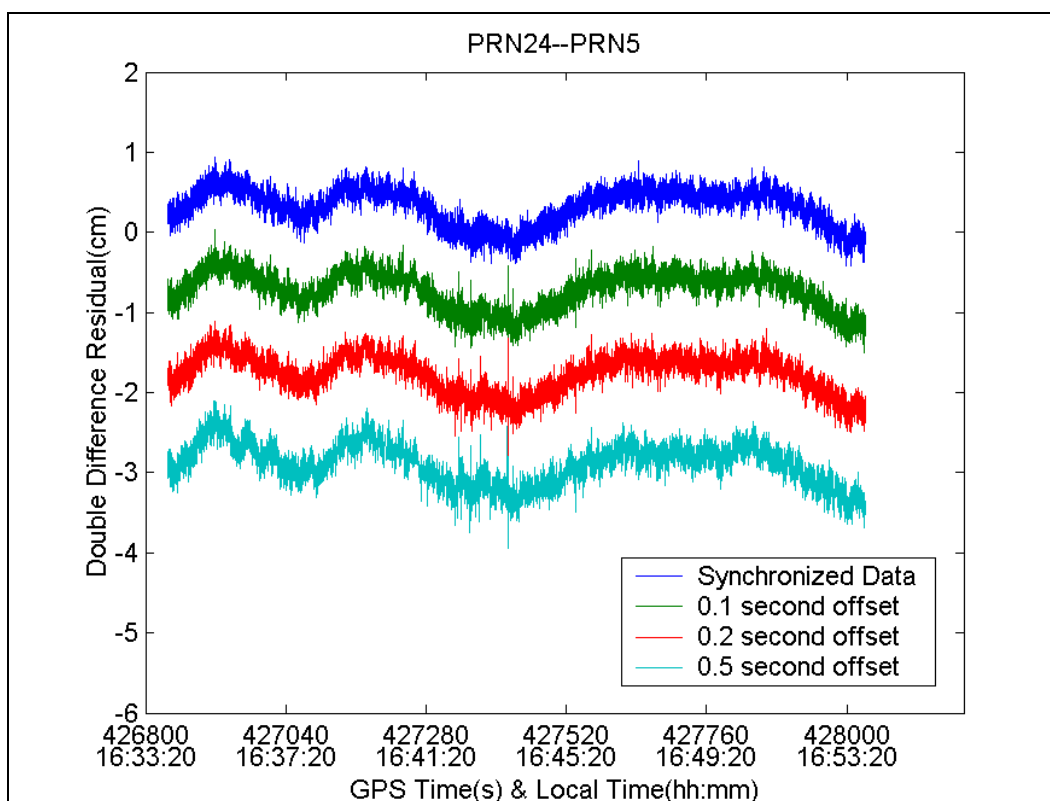


**Figure A.1: Double difference residuals for PRN24--PRN5**

**Table A.1: Statistics of double difference residuals (PRN 24-- PRN 5)**

	Mean (cm)	STD (cm)	RMS (cm)	MIN (cm)	MAX (cm)
Synchronized	0.3	0.2	0.4	-0.4	0.9
0.1 s offset	0.3	0.2	0.4	-1.0	1.0
0.2 s offset	0.2	0.2	0.3	-1.4	0.9
0.5 s offset	-0.1	0.3	0.3	-0.9	0.9

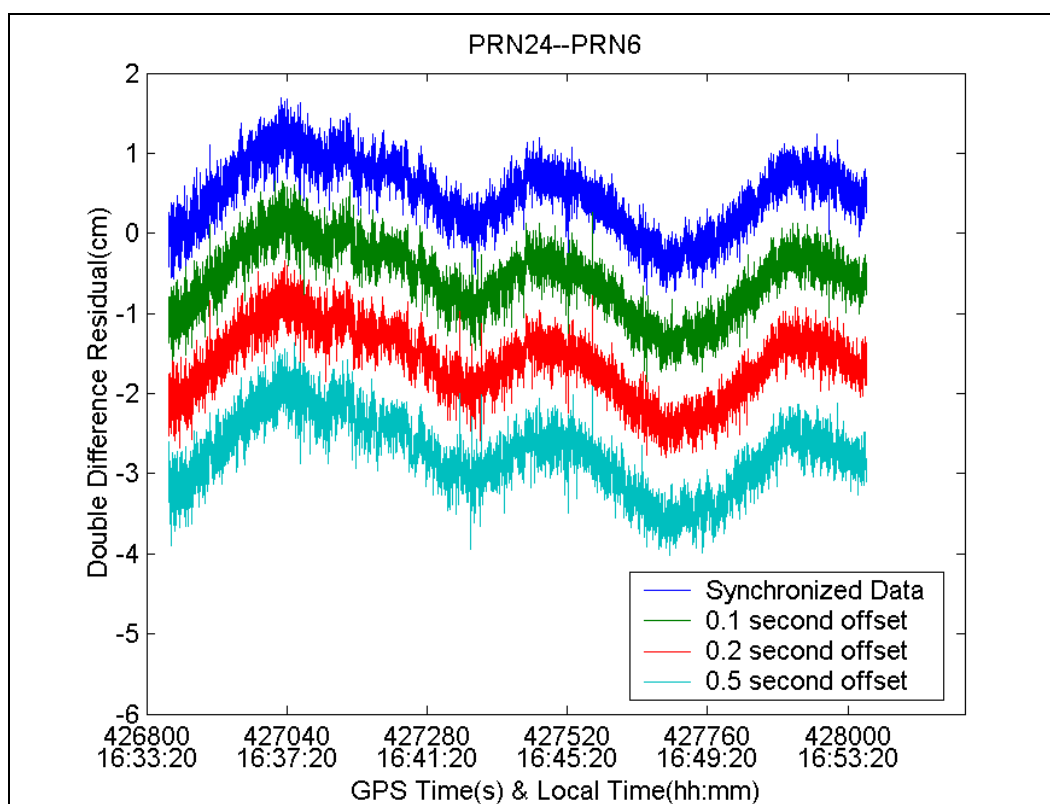


**Figure A.2: Double difference residuals for PRN24--PRN6**

**Table A.2: Statistics of double difference residuals (PRN 24-- PRN 6)**

	Mean (cm)	STD (cm)	RMS (cm)	MIN (cm)	MAX (cm)
Synchronized	0.5	0.4	0.6	-0.8	1.7
0.1 s offset	0.4	0.4	0.6	-0.9	1.7
0.2 s offset	0.4	0.4	0.6	-0.8	1.7
0.5 s offset	0.2	0.5	0.5	-1.0	1.6

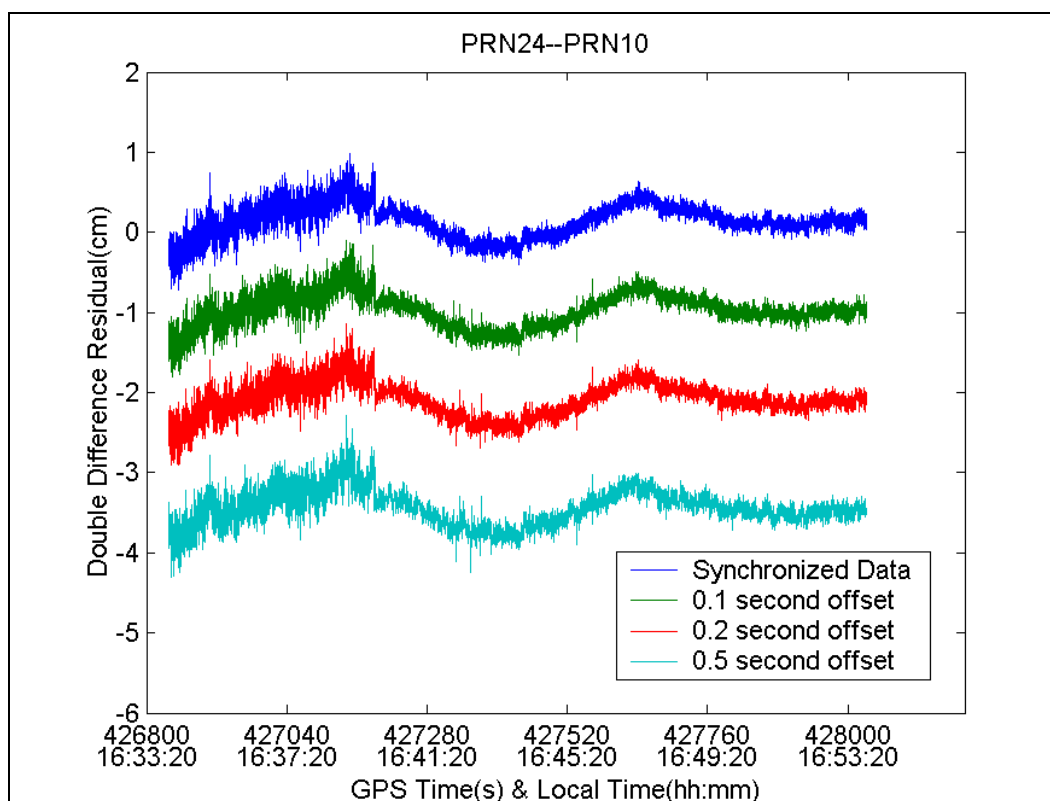


**Figure A.3: Double difference residuals for PRN24--PRN10**

**Table A.3: Statistics of double difference residuals (PRN 24-- PRN 10)**

	Mean (cm)	STD (cm)	RMS (cm)	MIN (cm)	MAX (cm)
Synchronized	0.1	0.3	0.3	-0.7	1.7
0.1 s offset	0.0	0.2	0.2	-0.8	1.7
0.2 s offset	-0.1	0.2	0.2	-0.9	1.7
0.5 s offset	-0.4	0.5	0.6	-1.3	1.6

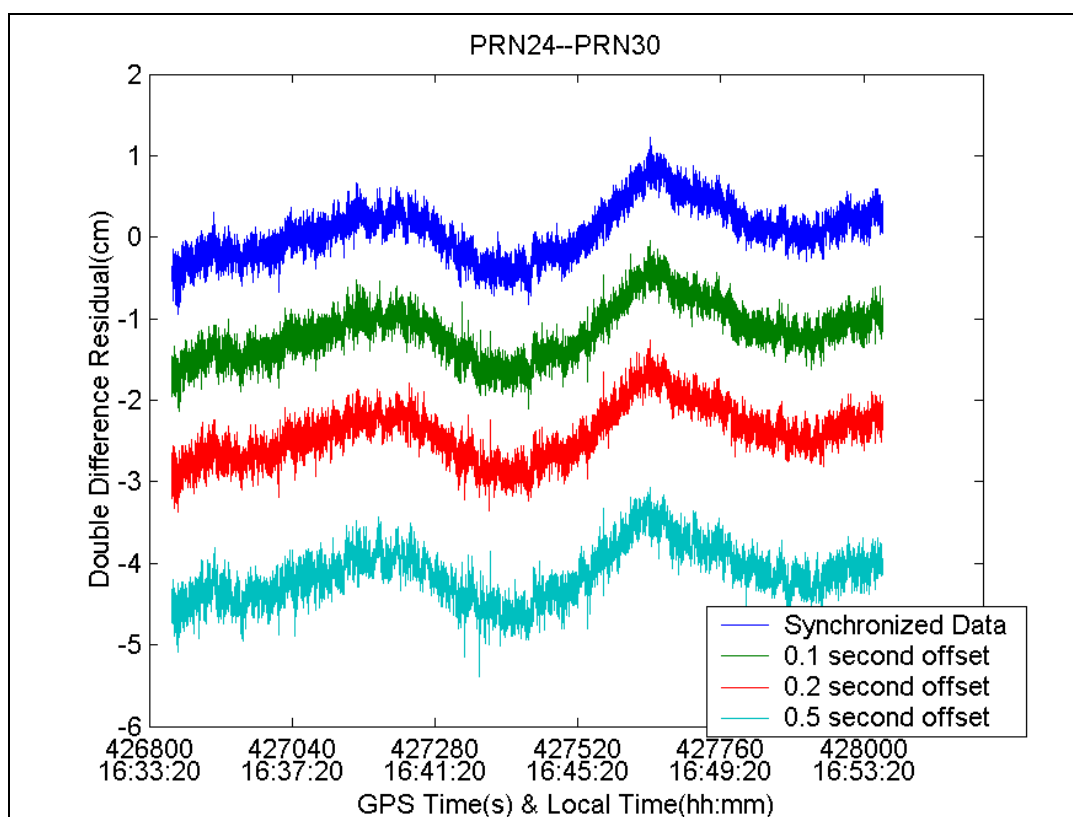


**Figure A.4: Double difference residuals for PRN24--PRN30**

**Table A.4: Statistics of double difference residuals (PRN 24-- PRN 30)**

	Mean (cm)	STD (cm)	RMS (cm)	MIN (cm)	MAX (cm)
Synchronized	0.1	0.3	0.3	-0.9	1.2
0.1 s offset	-0.2	0.3	0.4	-1.1	1.0
0.2 s offset	-0.4	0.3	0.5	-1.4	0.7
0.5 s offset	-1.1	0.3	1.2	-2.4	-0.1